

*ENGINEERING EVALUATION AND CONTROL OF
TOXIC AIRBORNE EFFLUENTS*

Volume II

RESEARCH AND DEVELOPMENT OF METHODS FOR THE ENGINEERING
EVALUATION AND CONTROL OF TOXIC AIRBORNE EFFLUENTS

LIBRARY-AIR RESOURCES BOARD

R.L. Bell, B.J. Morrison, and D.R. Shonnard

Department of Chemical Engineering
University of California, Davis

Submitted in Partial Fulfillment of
California Air Resources Board
Contract No. A6-051-32
June 1988

Picture on cover reprinted from Gas Cleaning for Air Quality Control, edited by J.M. Marchelle and J.J. Kelly, 1975, p.127, by courtesy of Marcel Dekker, Inc.

CONTENTS

I. TRANSPORT OF VOLATILE ORGANIC COMPOUNDS

1.0	Introduction	1
2.0	Model Development	4
3.0	Required Parameters and Data	11
4.0	Experimental Procedure	23
5.0	Results and Discussions	36
6.0	Conclusions	45
	References	46
	Nomenclature	47
	Appendix A: Transport Equation for Mass Transfer	53
	Appendix B: Numerical Solution to Mass Transfer Problem	58
	Appendix C: Transport Equation for Heat Transfer	61
	Appendix D: Numerical Solution to Heat Transfer Problem	66
	Appendix E: Emissions Model Computer Program	69
	Appendix F: Wind Data	75
	Appendix G: Temperature Data	76
	Appendix H: Residence Time Model Computer Program	78

FIGURES:

Figure 1.	Schematic Diagram of Three-Phase System	7
Figure 2.	Crude Oil Viscosity Correlation	13
Figure 3.	Data versus Predicted Viscosity	13
Figure 4.	Residence Time of Crude Oil	22
Figure 5.	Schematic Diagram of Meterological Station	24
Figure 6.	Solar Radiation Data and Prediction	25
Figure 7.	Solar Radiation Data and Prediction	25
Figure 8.	Ambient Temperature Data and Prediction	27
Figure 9.	Ambient Temperature Data and Prediction	27
Figure 10.	Thermocouple Float	28
Figure 11.	Map of Sump 36-W	29
Figure 12.	Temperature Profile During Upset Condition	30
Figure 13.	Measured Temperature Profile	31
Figure 14.	Predicted Temperature Profile	31
Figure 15.	Measured Temperature Profile	32
Figure 16.	Predicted Temperature Profile	32
Figure 17.	Residence Time Distribution	35
Figure 18.	Temperature Profile through Oil Pad	37
Figure 19.	Concentration Profile through Oil Pad	37
Figure 20.	Mass Flux over Time	38
Figure 21.	Total Emissions over Time	38
Figure 22.	Average Emissions over Time	39
Figure 23.	Emissions for Each Psuedocomponent	41
Figure 24.	Diurnal and Seasonal Emission Estimates	42
Figure 25.	Log-normal Distribution Function	44
Figure 26.	Emission Estimates for Various RTD	44

TABLES

Table 1.	Identified Compounds in the VOC	5
Table 2.	Pseudocomponents in the VOC	6
Table 3.	Viscosity of 36-W Crude Oil	12
Table 4a.	Wagner Equation Coefficients	15
Table 4b.	Physical Properties of the Pseudocomponents	15
Table 5.	Initial Concentration of the Pseudocomponents	16
Table 6.	Cloud Cover Correction	20
Table 7.	Oil Pad Depth Measurements	33

II. VOLATILE ORGANIC COMPOUND EMISSIONS FROM SOIL	
1.0 Introduction	83
2.0 Laboratory Simulator Design and Performance	85
2.1 Description of Experimental Procedure	89
2.2 Diffusion Cell Mixing	91
3.0 Experimental Objectives	95
4.0 Results of Initial Experiments	97
4.1 VOC Emission Rates From Gasoline Contaminated Soils	97
4.2 Soil Transport Parameter, D_{app}	100
4.3 Toxic Component Identification	101
4.4 Soil Moisture Effect on Emission Rates	105
5.0 Mathematical Predictions of VOC Emission Rates From Gasoline Contaminated Soils.	106
5.1 Mathematical Model of Diffusion/Adsorption of Gasoline Components in a Soil Under a Diurnal Temperature Cycle.	109
5.1-1 Model Formulation	109
5.1-2 Model Predictions	113
5.1-3 Analytical Solution: Isothermal Case	113
5.1-4 Numerical Solution: Nonisothermal Case	114
5.1-5 Effect of Diurnal Soil Temperature Cycle	116
5.1-6 Multicomponent Emission Rate Predictions	121
5.2 Conclusions	123
5.3 Future Considerations For Models.	124
Appendix I. Derivation of the Continuity Equation for a Gasoline Component in Dry Soil.	125
Appendix II. D_{app} and Henry's Law Constant for Adsorption of Gasoline Component A onto soil.	129
References	131
Nomenclature	133

FIGURES:

Figure 1.	Experimental apparatus: air pretreatment section.	86
Figure 2.	Experimental apparatus: diffusion cell.	88
Figure 3.	Experimental apparatus: data acquisition section.	88
Figure 4.	Soil moisture vs. suction pressure for soil samples.	92
Figure 5.	Evaluation of mixing in the headspace above the soil column.	92
Figure 6.	Gas phase mass transfer coefficient, k_g , above moist soil.	94
Figure 7.	Gas phase mass transfer coefficient, k_g , above dry soil.	94
Figure 8.	Ranges of soil temperature, SMC, and sweep air RH considered in experiments on emissions from gasoline contaminated soils.	96
Figure 9.	Emission rates of VOC from gasoline contaminated dry soil. $\langle C \rangle_0 = 1000$ ppm. $\langle T_s \rangle = 41^\circ\text{C}$.	98
Figure 10.	Environmental conditions in the diffusion cell.	98
Figure 11.	Best fit of penetration model to data.	99
Figure 12.	Comparison of penetration model with data.	99
Figure 13.	Gas chromatography - mass spectroscopy analysis of unleaded gasoline.	103
Figure 14.	Mass spectrum of a xylene isomer.	103
Figure 15.	Mass spectrum of toluene.	104
Figure 16.	Mass spectrum of benzene.	104
Figure 17.	Comparison of penetration model with data for N_A vs. time.	115
Figure 18.	Comparison of penetration model with data for M_A vs. time.	115
Figure 19.	Effect of soil temperature on N_A predictions using the penetration model.	117
Figure 20.	Effect of soil temperature on M_A predictions using the penetration model.	117
Figure 21.	Effect of a diurnal soil temperature cycle on N_A using a penetration model starting at sunrise.	118

Figure 22.	Effect of a diurnal soil temperature cycle on M_A using a penetration model starting at sunrise.	118
Figure 23.	Effect of a diurnal soil temperature cycle on N_A using a penetration model starting at sunset.	120
Figure 24.	Effect of a diurnal soil temperature cycle on M_A using a penetration model starting at sunset.	120

TABLES

Table 1.	Summary of experimental results for emission rates from gasoline contaminated soil.	101
Table 2.	Prevalence of benzene, toluene, and xylene isomers in unleaded gasoline.	102
Table 3.	Representative compounds in unleaded gasoline.	105
Table 4.	Transport processes for contaminant chemicals through soils.	108
Table 5.	Physical and chemical properties of importance in the penetration model.	108

ACKNOWLEDGEMENTS

The Authors would like to extend special thanks to Adrian Jund and Steve Richardson for their ingenious inventions as well as their creative troubleshooting abilities. Dan Jones of the Facility for Advanced Instrumentation and Bob Okamoto and Don Fitzell of the CARB were sources of endless assistance and information on the subject of analytical chemistry, especially in relation to gas chromatography and mass spectrometry. The authors also acknowledge the assistance of Mr. Joseph A. Pantalone, the contract manager at CARB and thank him for his support and to Mr. Dean Simeroth for his suggestions and encouragement of this project.

This report was submitted in fulfillment of Contract Number A6-051-32: Research and Development of Methods for the Engineering Evaluation and Control of Toxic Airborne Effluents by Richard L. Bell of the Department of Chemical Engineering at the University of California, Davis, under the sponsorship of the California Air Resources Board.

DISCLAIMER

The statements and conclusions in this report are those of the contractor and not necessarily those of the California Air Resources Board. The mention of commercial products, their source or their use in connection with materials reported herein is not to be construed as either an actual or implied endorsement of such products.

SUMMARY

Volume II

RESEARCH AND DEVELOPMENT OF METHODS FOR THE ENGINEERING EVALUATION AND CONTROL OF TOXIC AIRBORNE EFFLUENTS

Part I. TRANSPORT OF VOLATILE ORGANIC COMPOUNDS

Nearly all of the oil production in the Southern Central Valley of California now depends on secondary recovery by steam injection. As a result the wells produce about 8 times as much water as oil. The water/oil mixture has been separated by gravity in impoundments, called sumps, which may be as large as 150 ft. long by 50 ft. wide. The crude oil forms a "pad" which floats on the surface of the water and moves from the inlet to the outlet where it is decanted. During its transit through the sump very complex flow patterns are formed which are related to complex fluid mechanical behavior referred to as Lagrangian turbulence. The surface of an impoundment is open and consequently the volatile organic compounds (VOC) are free to escape to the atmosphere. The rate at which the VOC escapes depends on the specific molecules which are escaping, the viscosity and temperature of the crude oil and the wind velocity and air temperature.

The purpose of this program has been to study the rate at which VOCs are transported to the atmosphere from crude oil sumps. This has involved field studies in which atmospheric conditions have been monitored, the movement and temperature of the crude oil have been measured and samples have been taken for laboratory analysis. In a previous report (*RESEARCH AND DEVELOPMENT OF METHODS FOR THE ENGINEERING EVALUATION AND CONTROL OF TOXIC AIRBORNE EFFLUENTS* Vol. II Contract No. A4-159-32) we have discussed results from several aspects of the study leading to this report. An extensive sampling program was conducted to determine the constituents in the crude oil which make up the VOCs. The boiling range of the VOCs was shown to extend to about 200 °C depending on the residence time of the sump. Within this

range 68 compounds were unambiguously identified. This provided a basis for selecting model or pseudo compounds for the mathematical modeling study. The work on molecular diffusivity of the VOC type compounds in high viscosity liquids provided the basis for estimating this parameter. Finally the analytical model was the precursor to the more complete and exact predictive numerical model reported here. Field measurements of VOC emissions, taken by the California Air Resources Board (CARB), have been used to validate the model in this report. Because the transport rates are highly temperature dependent it was also necessary to include a heat balance in the calculations, which accounted for heat transfer with the atmosphere, solar insolation and the temperature of the underlying water layer.

The mathematical model is based on the assumption that the oil pad is unmixed in the vertical direction. This assumption was checked in the field by measuring vertical temperature profiles in the pad and water layer below. The profiles showed no evidence of vertical mixing. A second important assumption is that the oil/water interface is isothermal because of the thermal capacitance of the underlying water layer. Again the field temperature measurements verified this assumption. The heat and mass transfer coefficients between the atmosphere and the sump were estimated from existing correlations. The solar radiation, wind direction and velocity, wet and dry bulb temperature and relative humidity were measured using the UCD portable meteorological station. The long wave radiation was calculated from existing formulae. The heat and mass balances were solved simultaneously, using a finite difference method, on a VAX computer.

It was first determined that the latent heat effects at the surface due to volatilization of the VOC were insignificant compared to the sensible heat effects and had a negligible effect on the surface temperature. This resulted in a significant reduction in the computer time required for a calculation. The calculated temperature profiles were very similar, both spatially

and temporally, to those measured in the field. This ability to accurately predict temperatures made it possible to include the temperature effects on the transport parameters.

An important element in the modelling was to include the effect of the residence time distribution of the oil in the sump. The field observations were that the flow patterns were of the Lagrangian turbulence type which are characteristic of viscous free surface flows. The theory of Lagrangian turbulence is at best inadequate for predicting flows *a priori* in a system such as a sump. Regardless of the mechanism generating a spread of residence times, it was anticipated, based on experience, that the residence time curve would be approximately log-normal about the mean. The mean residence times had been estimated using markers in the oil and from volumetric throughput and pad thickness data. Therefore the effects of the residence time distribution could be estimated by setting the mean based on data and assuming a variance. The calculated effect of residence time was on the order of 15% going from plug flow to very dispersed flow. This is due to the fact that after the initial formation of the pad and the concentration profile in the pad, the transport rate is low and increasing the exposure time does not notably change the total amount transported. This is consistent with the previously reported observation that the emissions can be reduced per volume of throughput by making the pad thicker.

One of the main objectives of this study was to explore theoretical verification of the CARB flux chamber method of measuring emissions. Because of the time required to make a single observation with the flux chamber, measurements at different locations on a sump were separated by hours and sometimes days. The presence of changing flow patterns raised the question of whether data obtained over such long time intervals remained correlated. The fact that the theoretical results exhibit an insensitivity to residence time suggested that the temporal distribution of the measurements was probably not a problem. The range of emissions predicted for the sump in question was 600 to

1200 pounds per day based on best and worse case estimates. These values bracket the value of 1000 pounds per day measured by CARB. These results clearly indicate that: 1) the emissions measured by CARB are in full agreement with theory , and 2) the theoretical model can be used for emission estimates in place of or in conjunction with measurements from oil sumps. Finally, it is anticipated that the methods developed for sumps can be used for estimating emissions from other liquid impoundments containing volatile constituents.

Part II. VOLATILE ORGANIC COMPOUND EMISSIONS FROM SOILS

There are approximately 20,000 leaking underground gasoline storage tanks in California. These tanks represent a severe threat to groundwater in their vicinity. Remediation of this threat first requires that the tanks be excavated for replacement and that the surrounding soil be removed and treated for removal of the gasoline. The treatment processes take several forms. However, regardless of the process being used there is a period during which the soil is exposed to the atmosphere. Because of the mass of gasoline involved, contamination of the atmosphere with VOCs from this source can be large. This problem is a special case of the much larger problem of loss of hazardous and toxic VOCs wastes from landfills, toxic waste sites, National Priorities List (Superfund) sites and landfarming of petroleum wastes. In the June 1987 report (Contract #A4-159-32, Volume II), a review of the general problem of VOC emissions from soils was presented. The important distinguishing characteristics of the problem presently being studied are that the gasoline is comprised of essentially all VOC components, consequently their concentrations are high, and that the VOC tends to evaporate in a relatively short time period. As a result, bacterial degradation of VOCs may not be sufficiently rapid to be an important factor. Studying this problem, while important in its own right, is also a logical starting point for understanding the more global application.

The transport process is one which depends on molecular diffusion through the pores of the soil. The process is mediated by "sorption" partitioning among the solid, humus, liquid and gas phases in the soil. The values for the partition coefficients are not well known and estimations are usually performed using the octanol/water partition coefficient. Because so little precise information about partition coefficients is known it was decided to design a gravimetric sorptometer around an existing electro-balance. This unit is not complete but will contribute to the continuing project. Another important factor in the partitioning process is soil moisture content. The sorptive capacity of the soil for VOC is substantially reduced as water loading is increased. In the presence of soil water, VOC molecules are displaced from the soil surface because of preferential adsorption of water. Thus more VOC molecules must exist in the soil vapor space, which in turn leads to increased diffusion and rates of emission to the atmosphere.

A cell designed to measure the flux of VOC from a soil sample has been constructed. Soil containing a preset amount of VOC is placed in the cell. A special system designed to mix and compress reproducible samples is used for filling the cell. Air of a controlled temperature and humidity is passed through an annular space above the soil sample. Soil moisture is controlled by the humidity of the air and the water suction applied to the soil column. The headspace is well mixed using a variable speed impeller. The mass transfer coefficient between the soil sample and the air in the headspace can be controlled by the speed of the impeller. The concentration in the gas leaving the headspace is analyzed for total hydrocarbon with a continuous FID detector. The analog output from the detector is passed to an analog-to-digital converter and then to a computer for data storage and analysis.

The results to date show that the process is more complex than simple "penetration" type transport through soil. There appear to be at least two shifts in mechanism which may be

related to kinetically controlled adsorption or transport in micro-capillaries. An "apparent" diffusivity which includes the complex phenomena which mediate soil transport can be defined. These have been calculated for the runs which have been completed, and are reported in Volume II for approximate calculations. The transport rates have been measured in both dry and wet soil and show that the presence of water in the soil changes the transport rate by nearly an order of magnitude, in keeping with similar studies of pesticide transport.

I. TRANSPORT OF VOLATILE ORGANIC COMPOUNDS

1.0 INTRODUCTION

Oil fields in the Bakersfield-Kern County area are now being produced by steam flood or secondary recovery, and on a volumetric basis about 8 times more water than oil is produced. The oil/water mixture is separated by gravity in large open impoundments referred to as sumps. Accurate methods for measuring and predicting the loss to the atmosphere of volatile organic compounds (VOC) from these sumps has been a focus of study both for the California Air Resources Board (CARB) and the Department of Chemical Engineering at the University of California Davis (UCD).

UCD has developed a comprehensive program for studying VOC emissions which includes field tests, laboratory experiments and mathematical modeling. It was apparent from the outset that unlike aqueous (low viscosity) impoundments, a high viscosity layer of crude oil formed on the surface of the water in the crude oil sumps. It was hypothesized that the highly viscous layer could be assumed to be vertically unmixed which has been subsequently shown to be true by temperature profile measurements. A mathematical model of single component isothermal transport from the oil was developed based on this assumption. The effect of heat transfer due to convection, radiation, and heat of vaporization effects has been investigated. The single component model has been extended to the multicomponent case and the effect of residence time in the sump added. The model will be applicable not only to crude oil impoundments but to any impoundments in which the liquid can be considered vertically unmixed.

The work presented in the following section is a summary of the study of VOC transport from crude oil impoundments (sumps) during the 1986-1987 contract period (A4-159-32).

Since the theoretical approach we adopted was based on component-by-component predictions, it was essential that we determined which components or classes of components were present in the volatile fraction of the crude oil. A procedure was developed in the laboratory for quantitative distillation of the fraction of crude oil which contained the VOC. During the initial contract period (A2-157-32) we had a contract with Hewlett Packard which included the loan of a gas chromatograph with a mass spectrometer detector (GCMS). This instrument was used to determine the peak areas present in the sump inlet and outlet samples. By comparing the VOC peak areas, a very clear picture of the relative loss of each component (peak) was obtained. The peaks were identified by first comparing the mass spectra of the peak with the National Bureau of Standards reference library stored in the GCMS computer library. This gave the 10 most probable compounds. These compounds were then screened using boiling point criteria and finally the compound spectra were compared visually with the published NBS mass spectra. Although the GCMS was returned to Hewlett Packard in August 1985, the analysis of the data has been a significant effort during the present contract year. We now have certain identification of 67 different molecular species or isomers.

Based on the analyses of inlet and outlet samples the relative loss of the individual VOC components has been estimated and from this an estimate of the total loss of VOC has been obtained. These estimates are substantially the same as those obtained by CARB using the "flux box" method.

The conditions in the sump (temperature, composition, residence time) and in the atmosphere (temperature, solar radiation, wind) which determine the rate of loss of VOC are continually changing daily and seasonally. The data which were obtained early in the study represented a "snapshot" of this dynamic system.

The theoretical model is viewed as a tool for extrapolating these snapshots to a more global basis. Consequently, a major field effort during the '86 - '87 contract period was to conduct a 5 day continuous monitoring and sampling test of sump 36W. This was coordinated with a scheduled CARB test of the same sump. Inlet and outlet samples were obtained every 4 hours and continuous sump temperatures and meteorological data were obtained. These data were collected to determine the magnitude of diurnal variations and the effect they have on emissions. An extremely important result of this test was to confirm the assumption that the oil layer is vertically unmixed and the boundary condition that the temperature at the oil/water interface is virtually constant.

2.0 MODEL DEVELOPMENT

Pollutant movement in the environment is a complex process that can be described by transport equations. In order to solve the equations, simplifying assumptions must be made to both the equations and the boundary conditions. Both mass and heat transfer occur in the VOC evaporation process. A concentration gradient exists between the oil and air which provides a driving force for mass transfer. In addition, a temperature gradient exists between the oil and air due to the elevated temperature of the oil entering the sump and the much cooler ambient air temperature. The temperature difference between the oil and air of up to 60°C drives the heat transfer. Diffusion is the dominant mass transport mechanism in the oil. Since diffusion is strongly affected by temperature it is necessary to consider temperature effects on emissions. The two transport problems are described below.

Mass Transfer

Crude oil from Kern County is quite viscous. The residual fraction of crude - containing no VOCs - is modeled as a single component of high molecular weight and is the solvent species. An individual solute species of the VOC will behave together with the solvent as a binary pair since the solute species are present in small amounts. We can use a pseudocomponent approach to estimate the properties of the solute species. Pseudocomponents are compounds that represent a group of compounds with similar physical properties. The pseudocomponent approach requires a number of real or pseudocomponents to be selected and their relative amounts estimated. We have positively identified 68 compounds in the VOC from crude oil taken from three different sumps in Kern county (13). In order to describe the evaporation of this multicomponent mixture of VOC, we characterize it by three pseudocomponents. This method was patterned after the work of Yang et al (16). Yang suggested that the compounds be grouped according

Table 1: Compounds Identified in the VOC

NAME OF COMPOUND IDENTIFIED	GC RETENTION TIME (MIN)				INLET PEAK AREAS			
	BOIL T (C)	M CRIST	31X	36W	M CRIST	31X	36W	36V
2-METHYLBUTANE (ISOPENTANE)	27.8	5.199	---	---	---	---	---	---
2,2-DIMETHYLBUTANE	49.7	6.484	---	---	80279	---	---	86897 123555
2,3-DIMETHYLBUTANE	58.0	7.403	---	---	680554	---	---	317327
2-METHYLPENTANE	60.3	---	---	7.539	---	---	---	---
3-METHYLPENTANE	63.3	8.101	---	8.121	35651	---	---	87939
HEXANE	68.7	8.860	---	8.866	---	---	---	---
2,2-DIMETHYLPENTANE	79.2	10.222	---	---	115780	---	---	288216
METHYLCYCLOPENTANE	71.8	10.390	10.325	10.382	---	---	---	---
2,4-DIMETHYLPENTANE	80.5	10.585	---	---	232107	---	---	---
2,2,3-TRIMETHYLBUTANE	80.9	10.968	---	10.956	201184	---	---	---
BENZENE	80.1	---	---	11.919	---	---	---	---
3,3-DIMETHYLPENTANE	86.1	12.326	---	---	141020	---	---	241464
CYCLOHEXANE	80.7	12.617	12.541	12.637	16065	38512	21459	---
2-METHYLBUTANE	96.0	13.268	---	13.262	57303	---	57303	---
2,3-DIMETHYLPENTANE	88.8	13.441	13.353	13.420	870324	26255	58325	---
1,1-DIMETHYLCYCLOPENTANE	87.5	---	13.594	---	---	---	---	---
3-METHYLBUTANE	83.9	13.669	---	---	71516	---	---	---
3-METHYLBUTANE	91.9	13.975	13.900	13.981	33709	17790	92965	---
1-CIS-3-DIMETHYLCYCLOPENTANE	90.8	14.777	14.460	14.543	352184	63857	40748	---
1-TRANS-3-DIMETHYLCYCLOPENTANE	91.7	14.536	14.701	14.77	203641	78782	47674	---
1-TRANS-2-DIMETHYLCYCLOPENTANE	91.9	---	14.939	15.021	197401	66597	---	---
2,2,3-TRIMETHYLBUTANE	109.8	15.141	---	---	35323	---	---	---
HEPTANE	98.4	---	---	16.129	---	---	256045	---
METHYLCYCLOHEXANE	100.9	18.042	17.994	18.062	44279	436576	129427	---
1,1,3-TRIMETHYLCYCLOPENTANE	104.9	---	18.279	18.346	86082	37634	---	---
ETHYLCYCLOPENTANE	103.5	---	19.144	19.233	86594	---	---	---
2,5-DIMETHYLBUTANE	105.1	19.329	---	---	---	---	---	---
2,4-DIMETHYLBUTANE	108.4	19.539	19.447	---	488289	27717	---	---
1-TRANS-2-CIS-4-TRIMETHYLCYCLOPENTANE	109.3	20.202	20.084	20.126	1969937	204532	61558	---
1-TRANS-2-CIS-3-TRIMETHYLCYCLOPENTANE	110.4	20.909	20.840	---	438278	374831	---	---
3-METHYL-2,4-HEXADIENE	110.4	---	---	21.25	---	---	78415	---
TOLUENE	110.6	---	21.522	21.615	103165	103165	338678	---
2,3,4-TRIMETHYLPENTANE	113.5	21.679	21.133	---	---	---	20697	---
2,3-DIMETHYLBUTANE	115.6	---	---	22.405	---	---	---	---
1,1,2-TRIMETHYLCYCLOPENTANE	113.7	---	22.408	---	440134	120501	---	---
2-METHYL-3-ETHYLPENTANE	118	22.831	22.728	22.84	68374	26568	213569	---
1,1,3,3-TETRAMETHYLCYCLOPENTANE	117.7	---	22.998	23.008	---	---	356721	---
4-METHYLHEPTANE	117.7	23.273	23.142	23.242	53563	---	---	---
3-METHYLHEPTANE	118.9	23.427	23.356	23.925	195651	---	---	---
1-TRANS-4-DIMETHYLCYCLOHEXANE	119.4	24.365	24.047	24.342	310563	549732	---	---
3-METHYLHEXANE	120.0	23.762	---	---	221824	---	---	---
1,1-CIS-3-TRANS-4-TETRAMETHYLCYCLOPENTANE	121.6	24.148	---	---	2020449	---	---	---
1,1-DIMETHYLCYCLOHEXANE	119.6	24.977	24.881	24.981	221278	43504	---	---

13025145 5370529 30654312

to the hydrocarbon types and the number of carbons. Table 1 lists the compounds identified in the VOC. Table 2 shows the breakdown of components and their approximate relative amounts in the VOC. A characteristic compound for each group is chosen based on its representation in terms of physical properties of that group.

Table 2: Pseudocomponents in Kern County Crude Oil VOC

Description	Pseudocomponent	Weight %
Paraffin C5-C8	n-heptane	32
Cycloparaffin C6-C9	1,1,3-trimethylcyclopentane	65
Aromatic C6-C9	toluene	3

Mass transfer through oil is described by the mass continuity equation with molecular diffusion as the primary transport mechanism in the crude oil. We assume that molecular diffusion occurs only in the vertical direction. Figure 1 is a schematic diagram of the three-phase system. Chemical equilibrium is assumed to exist at each interface. There is no flux of VOC at the water/oil interface. However, at the air/oil interface a concentration gradient exists and continuity of flux is required. We define the initial concentration of species A in the oil as C_{A0} . A complete derivation of the mass transfer equation and boundary conditions is presented in Appendix A. The governing differential equation describing mass transfer and the boundary conditions are given by

$$\frac{\partial C_A}{\partial t} = \frac{\partial}{\partial z} \left(D_{AS} \frac{\partial C_A}{\partial z} \right) \quad (1)$$

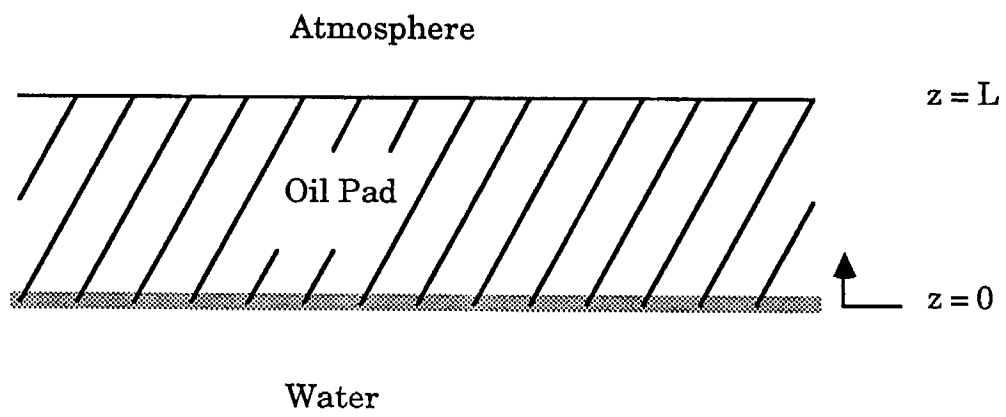


Figure 1: Schematic Diagram of the Three Phase System

$$\text{IC} \quad C_A = C_{A0} \quad \text{at} \quad t = 0 \quad (2)$$

$$\text{BC 1} \quad \frac{\partial C_A}{\partial z} = 0 \quad \text{at} \quad z = 0 \quad (3)$$

$$\text{BC 2} \quad -D_{AS} \frac{\partial C_A}{\partial z} = K_G \tilde{H} C_A \quad \text{at} \quad z = L \quad (4)$$

where C_A is the molar concentration of solute species A, D_{AS} is the diffusion coefficient of A in solvent S, z is depth, and t is time. Identical equations are written for each volatile species in the oil. This set of equations has been solved analytically in a previous report (13) in which case the diffusion coefficient was taken to be a constant.

In this study the equation was solved numerically using an implicit Crank-Nicolson finite difference technique. Finite differences are used to approximate differential increments of concentration in time and space coordinates. Finite difference solutions also allow one to change the value of the coefficients, in this case the diffusion coefficient, throughout the domain of the problem. Details of the numerical method are given in Appendix B.

Heat Transfer

It may be important to know both the surface temperature of the oil and the temperature profile in the oil in order to determine the diffusion coefficients. Heat and mass transfer are coupled by two paths in this problem: first, through the temperature effect on the diffusion coefficient; second, through the change in the heat of vaporization at the surface due to the change in composition at the surface. Both of these effects will be explored in detail.

Conduction is the major mechanism of energy transport in the oil. We assume that the oil/water mixture enters the sump at some temperature T_0 and the water remains constant at this temperature for the length of time it resides in the pool. We further assume that temperature is constant across the oil/water interface. This assumption may not work if the oil layer is very thin but it suits our purposes in this problem. The oil/air interface is subject to convection, longwave and shortwave radiation, and the compositional effect on the heat of vaporization. A complete derivation of the heat transfer equation and the boundary conditions is given in Appendix C. The heat transfer process is described by

$$\frac{\partial T}{\partial t} = \alpha \frac{\partial^2 T}{\partial z^2} \quad (5)$$

$$\text{IC} \quad T = T_0 \quad \text{at} \quad t = 0 \quad (6)$$

$$\text{BC 1} \quad T = T_0 \quad \text{at} \quad z = 0 \quad (7)$$

$$\text{BC 2} \quad -k \frac{\partial T}{\partial z} = h(T - T_\infty) + \sum_{i=1} N_i \Delta H_{\text{vap}} - Q_{\text{rad}} \quad \text{at} \quad z = L \quad (8)$$

where α is thermal diffusivity, k is thermal conductivity, h is the heat transfer coefficient, T_∞ is ambient air temperature, ΔH_{vap} is the heat of vaporization, and Q_{rad} is net radiation flux toward the interface. An analytical solution to this equation was not possible to formulate due to the complex boundary condition at the surface. We again used an implicit Crank-Nicolson finite difference technique to solve the equation numerically. The numerical solution is presented in Appendix D.

Simultaneous Solution

The finite difference method allows one to solve the differential equations at many different times by stepping forward or incrementing time. We can solve for the temperature profile and with this calculate the diffusivity at each point in the domain. Then the concentration profile can be determined and from it the instantaneous flux of material to the air and the total emissions. Time is incremented and the process is repeated. An iterative process is used between the two solutions at each time step to correct the heat of vaporization term. The FORTRAN code is listed in full in Appendix E.

3.0 REQUIRED PARAMETERS AND DATA

Several physical parameters are needed before the mass transfer and heat transfer equation sets can be solved. Some of these values can be measured, some are calculated, and some come from the literature. The methods used to obtain each parameter are described here.

Six physical properties are required in the mass transfer solution: D_{AS} , \bar{H} , C_{A0} , C_{B0} , C_{C0} , and K_G . The subscripts A, B, and C refer to each specific solute species pseudocomponent in the multicomponent mixture.

Diffusion Coefficient

We use a method of estimating diffusivities of solutes in crude oil that relies upon the work of others in high viscosity solvents. The Stokes-Einstein theory for liquid phase diffusion predicts that the diffusion coefficient will be directly proportional to temperature and inversely proportional to viscosity. Wilke and Chang (15) extended the theory and observed a direct proportionality on the square root of the molecular weight of the solvent and an inverse proportionality of the solute molar volume to the 0.6 power.

$$D_{AS} \propto \frac{M_s^{1/2} T}{\eta V_A^{0.6}} \quad (9)$$

Hiss and Cussler (3) investigated diffusion of hydrocarbons in solvents of high viscosity. Without a molecular weight correction they determined that at constant temperature the diffusion coefficient was inversely proportional to viscosity to the 2/3 power. We adopt the same dependence on temperature and molar volume as Wilke-Chang but use the Hiss-Cussler viscosity dependence as shown below

$$D_A \propto \frac{T}{\eta^{2/3} V_A^{0.6}} \quad (10)$$

We have measured the viscosity of crude oil as a function of temperature for several samples of 36W crude. 36W is a primary sump in the Chevron Cymric oil field in Kern County. The viscosity data are listed in Table 3. A correlation of viscosity and temperature is determined from these by a linear regression of the data and is given by

$$\eta = \exp \left[\frac{8105}{T} - 22.76 \right] \quad (11)$$

where η is viscosity in poise, and T is temperature in K .

Table 3: Viscosity of 36-W Crude Oil

Sample	Viscosity (poise)	Temperature (°C)
Inlet 3/28/86 @2:30	123.0	20.0
	92.5	25.1
	55.9	30.6
	31.7	37.6
Outlet 3/28/86 @2:30	137.0	19.8
	74.7	26.7
	41.8	33.6
	19.7	42.7
Inlet 3/28/86 @15:00	124.5	21.2
	94.9	25.4
	50.9	32.5
	27.6	41.3
Outlet 3/28/86 @15:00	137.5	19.6
	78.9	26.4
	34.8	34.0
	19.0	41.6

Figure 2 shows the crude oil viscosity correlation and Figure 3 shows the measured versus the predicted viscosity. With this viscosity correlation and Hiss-Cussler data for n-hexane we can use this equation to predict the diffusivity of any VOC in crude oil. With only the $V^{0.6}$ correction the diffusivity of other components can be calculated.

FIGURE 2: VISCOSITY CORRELATION

CYMRIC OIL FIELD CRUDE

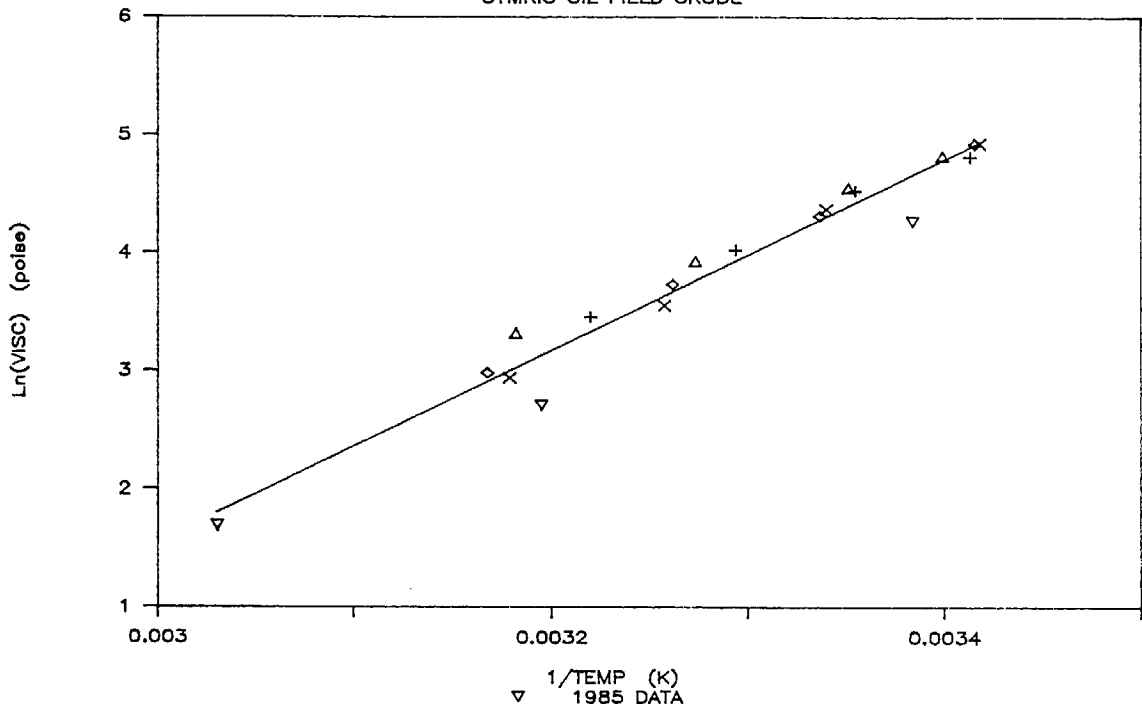
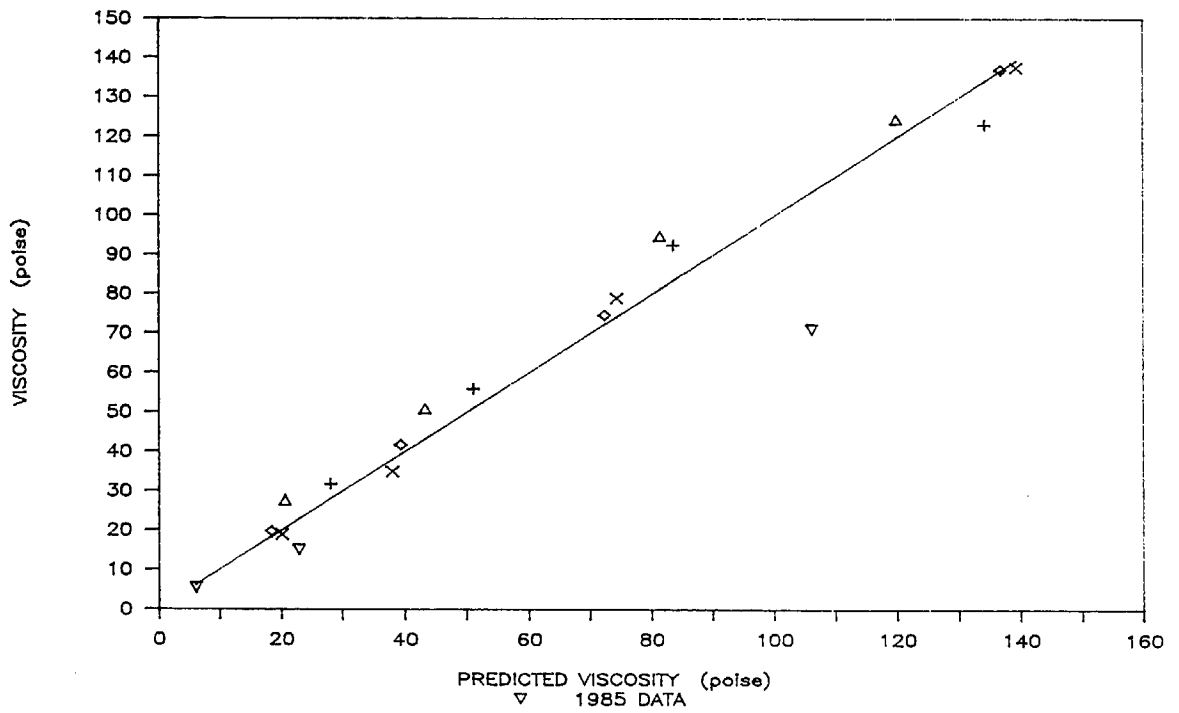


FIGURE 3: DATA vs PREDICTED VISCOSITY



Henry's Law Constant

The parameter \tilde{H} in the mass transfer equation is equal to (Hc_L/c_G) where H is the Henry's Law coefficient, and c_L and c_G are the total molar concentrations in the liquid and gas phases respectively. If we assume that the air behaves as an ideal gas and the oil behaves as an ideal liquid, we can write the vapor-liquid equilibrium equation as

$$y_i P = x_i p_i^{\text{sat}} \quad (12)$$

The Henry's Law constant for a species of low concentration in equilibrium between the vapor and liquid phases is

$$H = \frac{y_i}{x_i} \quad (13)$$

Combining Equations 12 and 13 we get the expression

$$H = \frac{p_i^{\text{sat}}}{P_i} \quad (14)$$

p_i^{sat} is calculated from the Wagner equation (11)

$$\ln (p_i^{\text{sat}}/P_c) = (1-x)^{-1} \{Ax + Bx^{1.5} + Cx^3 + Dx^6\} \quad (15)$$

where

$$x = 1 - \frac{T}{T_c}$$

The Wagner coefficients are given in Table 4a and critical temperature and pressure, boiling point and molecular weight for our selected components are given in Table 4b.

Table 4a: Coefficients for Use in the Wagner Equation to Calculate Vapor Pressure

Pseudocomponent	A	B	C	D
n-heptane	-7.67468	1.37068	-3.5362	-3.20243
1,1,3-trimethylcyclopentane	-6.97215	1.62353	-4.90587	2.76293
toluene	-7.28607	1.38091	-2.83433	-2.79168

Table 4b: Physical Properties of Pseudocomponents

Pseudocomponent	MW	T _b (K)	T _c (K)	P _c (bar)
n-heptane	100.205	371.6	540.3	27.4
1,1,3-trimethylcyclopentane	112.216	378.0	569.5	28.3
toluene	92.141	383.8	591.8	41.0

Gas Side Mass Transfer Coefficient

For surface impoundments Ehrenfeld (2) recommends the mass-transfer coefficient correlation developed by Mackay and Matsugu (5)

$$K_G = 0.0292 u^{0.78} x^{-0.11} Sc^{-0.67} \quad (16)$$

where u is windspeed in meters per hour, x is pool diameter in meters, and Sc is the Schmidt number which is about 2.3 for gases at the required temperature.

Initial Concentration

A sample of the crude, when distilled to 220°C, yielded a cut of 3.85% by mass. We previously determined (13) that about 73% of the cut is potential VOC, so the potential VOC is 2.81% of the crude. The volume-average specific gravity is 0.837. Therefore, there exists 2.35×10^4 grams of potential VOC per cubic meter of oil. The initial concentration of each pseudocomponent is estimated and listed in Table 5.

Table: 5 Initial Concentration of Pseudocomponents

Pseudocomponent	Molar Concentration (gram VOC/m ³ oil)
n-heptane	7.99×10^4
1,1,3-trimethylcyclopentane	14.6×10^4
toluene	0.940×10^4

Heat Transfer Parameters

Five parameters are required in the heat transfer equation:

$$\alpha, k, h, Q_{\text{rad}}, \text{ and } \Delta H_{\text{vap}}$$

Thermal Diffusivity

Vargaftik (14) gives the thermal diffusivity for many different oils. The heavier oils have a value of about $9 \times 10^{-8} \text{ m}^2/\text{s}$ at warm temperatures, between 40° and 60°C.

Thermal Conductivity

For petroleum fractions and oil mixtures, Cragoe's equation for thermal conductivity (9) can be used

$$k = \frac{0.0677}{S} [1 - 0.0003(T_F - 32)] \frac{Btu}{hrFt^\circ F} \quad (17)$$

where S is specific gravity and T_F is in $^\circ F$.

Heat Transfer Coefficient

A heat transfer coefficient can be calculated for flat terrain with the equation

$$h = \frac{k^2 \rho_c u_{10}}{z_a \ln\left(\frac{z_a}{z_o + 1}\right)} \quad (18)$$

where z_o is determined from a logarithmic velocity profile (7).

The impoundment studied in this report could not be considered situated in open, flat terrain since it was built into a hill and was covered by a net. For this reason we assume that the windspeed at the surface is lower than would be predicted by a logarithmic wind velocity profile. For flow over a flat plate at nearly stagnant conditions, the relationship given by Bolz and Tuve (1) predicts a value of $h = 10 \text{ W/m}^2 \text{ K}$.

Heat of Vaporization

The heat of vaporization was calculated from the Watson correlation (11).

$$\Delta H_{\text{vap}} = \Delta H_{\text{vap}(bp)} \left(\frac{1 - T_r}{1 - T_{r(bp)}} \right)^{0.38} \quad (19)$$

where $\Delta H_{\text{vap}(bp)}$ is ΔH_{vap} of a compound at its boiling point, T_r is the reduced temperature of the compound, T/T_c , and $T_{r(bp)}$ is the reduced temperature of the compound at its boiling point, $T_{(bp)}/T_c$.

Radiation

The three components in the radiation term are longwave radiation, both incoming and outgoing, and shortwave radiation. Incoming longwave radiation is estimated with the equation (7).

$$Q_{LW} = \epsilon \sigma T_{sky}^4 \quad (20)$$

$$T_{sky} = 0.0552 T_{\infty}^{1.5}$$

T_{∞} = ambient temperature, K

ϵ = longwave emissivity (assumed to be 1)

σ = Stefan-Boltzmann constant = $5.669 \times 10^{-8} \text{ W/m}^2\text{K}^4$

The outgoing black-body radiation is given by (12)

$$Q_B = \epsilon \sigma T_s^4 \quad (21)$$

T_s = surface temperature

Shortwave solar radiation can be calculated with Equation (10)

$$Q'_s = S \left(\frac{\bar{d}}{d}\right)^2 \cos(\bar{z}) \quad (22)$$

where S is the solar constant, 1376 W/m^2 , \bar{z} is the zenith angle of the sun to the earth, d is the instantaneous distance from the earth to the sun, and \bar{d} is the mean distance from the earth to the sun. The ratio of \bar{d} to d is close to unity and is taken to be 1 for this problem.

$$\cos \bar{z} = \sin \phi \sin \delta + \cos \phi \cos \delta \cos \bar{h} \quad (23)$$

where ϕ is the latitude, 35°N or 0.611 radians in Bakersfield, \bar{h} is the hour angle (0° at solar noon, -90° at sunrise and 90° at sunset), and δ is the declination of the sun in radians given by

$$\delta = 0.006918 - 0.399912 \cos d_0 + 0.070257 \sin d_0 - 0.006758 \cos 2d_0 + 0.000907 \sin 2d_0 - 0.002697 \cos 3d_0 + 0.001480 \sin 3d_0 \quad (24)$$

where $d_0 = 2\pi m/365$ and m is the Julian day.

The total solar radiation is then

$$Q_s = b Q'_s$$

or

$$Q_s = b S \cos \bar{z} \quad (25)$$

where $b = 1-A$ and A is the albedo of the oil. The albedo of fresh asphalt is 0.09 (4) and we will assume that this is also the albedo of crude oil.

The total radiation is

$$Q_{\text{rad}}^0 = \sigma [(0.0552T_\infty^{1.5})^4 - T_s^4] + 0.9 S \cos z \quad (26)$$

Cloud cover will affect the amount of radiation at the earth's surface. A modification to the calculated radiation is made

$$Q_{\text{rad}} = Q_{\text{rad}}^0 (1 - \bar{k}n) \quad (27)$$

where n is the cloud cover in tenths, and k can be found in Table 6.

Table 6: Cloud Cover Correction (12)

Cloud Type	Height (m)	$1-\bar{k}$
Cirrus	12200	0.84
Cirrostratus	8390	0.68
Altostratus	3660	0.34
Altostratus	2140	0.2
Stratocumulus	1220	0.12
Stratus	460	0.04
Nimbostratus	92	0.01
Fog	0	0

Ambient temperature can be approximated with a sine function. An even better way of estimating ambient temperature is to use a Fourier series. McCutchan (5) fit a four term Fourier series to data which had been collected in Southern California in mountainous terrain. This equation is

$$\begin{aligned}
 T = & -0.32815 + 0.96592T_{\text{avg}} - 0.43503T_{\Delta} \cos \frac{\pi t}{12} \\
 & -0.14453T_{\Delta} \sin \frac{\pi t}{12} + 0.09995T_{\Delta} \cos \frac{\pi t}{6} \\
 & -0.02450T_{\text{avg}} \sin \frac{\pi t}{6}
 \end{aligned} \tag{28}$$

where T_{avg} is the daily mean temperature, T_{Δ} is the daily range of temperature and t is the local time. The ambient temperature at a specified time now can be substituted into the radiation calculation. The inputs to the radiation equation are average daily temperature, daily range of temperature, day of year, time of day, cloud cover correction, and surface temperature. The surface temperature is not known, but is calculated with the solution to the heat transfer equation, so an iterative process is required.

Residence Time

Flow patterns in the sump have been observed to be complex and subject to change as the inlet conditions change. Parts of the sump are stagnant while others are quite active and subsequently channel most of the crude oil to the outlet. We can borrow from chemical reactor theory and include the effect of a residence time distribution on the total VOC emissions.

Measurements in nature of physical properties frequently exhibit a log-normal distribution. The log-normal distribution does not allow any negative observations and it is skewed so the tail drops off gradually. A log-normal residence time distribution is used in the emissions model. The frequency function (F) for this distribution is expressed as

$$df = \frac{1}{\sqrt{2\pi} \ln\sigma_g} \exp \left[- \frac{(\ln t - \ln \text{CMT})^2}{2(\ln\sigma_g)^2} \right] dt \quad (29)$$

where CMT is the count median time and σ_g is the geometric standard deviation. CMT is the time below which half of the residence times lie and above which half of the residence times lie. The frequency function integrated over all time is equal to unity. Total VOC emissions are found by integrating the product of the frequency function and the integrated mass flux over all time

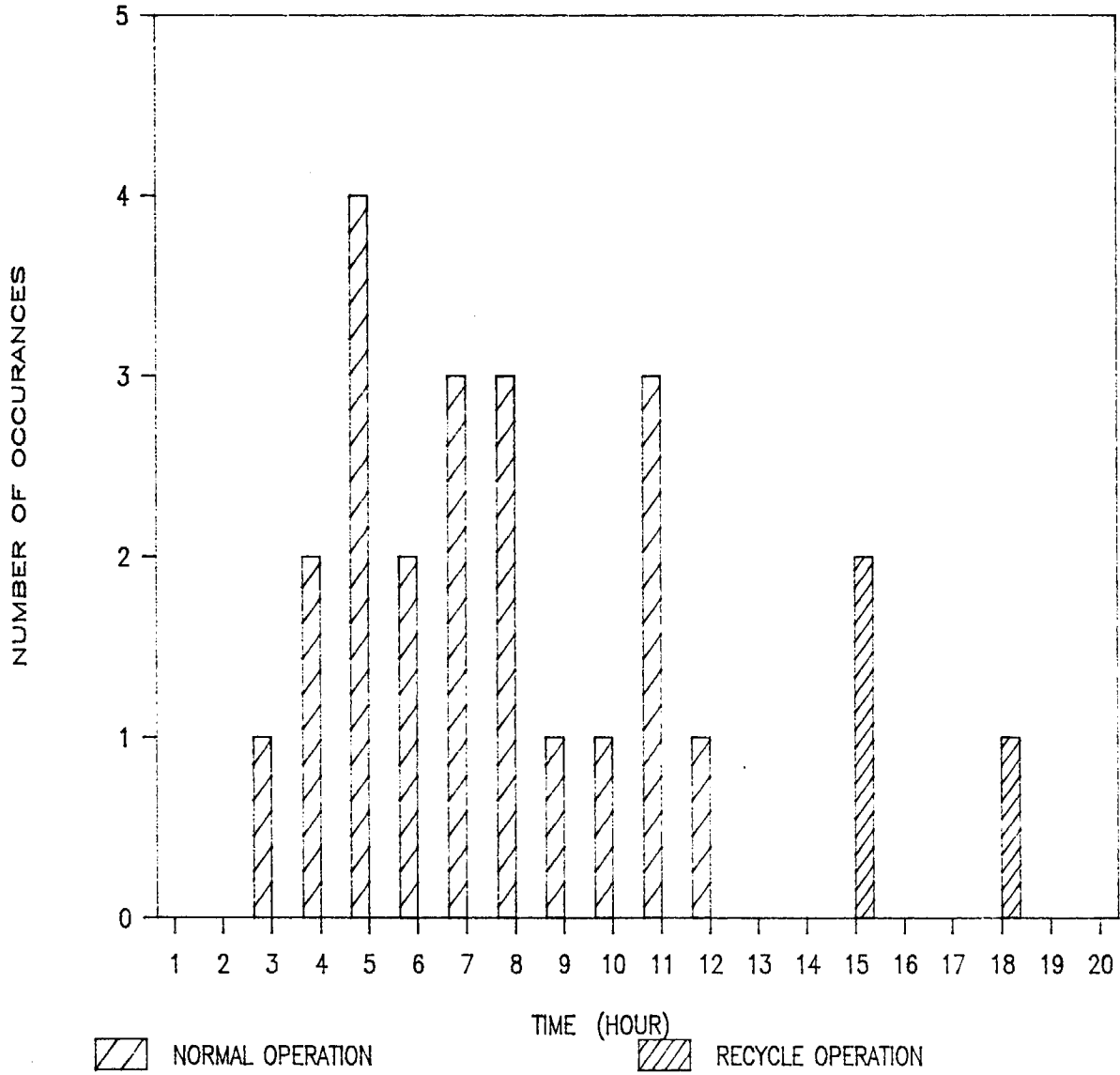
$$\int_0^t \left[\int_0^t \text{Flux}(t) dt \right] F(t) dt = \text{total emissions as } t \rightarrow \infty \quad (30)$$

The count median residence time was calculated with data from an operator's log book of sump 36W. The data included the volumetric flowrate and oil depth over a one month period. Residence time was calculated by dividing the volume of oil in the sump by the flowrate. These values are shown graphically in Figure 4. If a log-normal distribution of the data is assumed, we can calculate a CMT of 6.25 hours and a σ_g of 1.60.

The residence time distribution is discussed in the following section.

FIGURE 4: RESIDENCE TIME

BASED ON PRODUCTION FIGURES



4.0 EXPERIMENTAL PROCEDURE

A series of three field trips was made to the Kern County Chevron Cymric oil field sump 36W by the UCD research team. The trips were made in March 1986, February 1987, and March 1987. The purpose of these trips was to gather experimental data for use in the model and to collect oil samples.

The central piece of equipment used in the field tests was a Campbell Scientific model 21X datalogger which stored data from many different inputs. In addition, we used the following equipment for weather and temperature measurements: a wind direction vane; up to three anemometers for wind speed; a silicon pyranometer for solar radiation; a thermistor and relative humidity probe; and up to 30 Type T thermocouples for temperatures. Figure 5 shows the equipment schematically. The datalogger was programmed to take a reading from each instrument every minute and calculate and record the average of the readings every 15 minutes. In addition, the datalogger was programmed to convert readings from the instruments into familiar units, e.g. thermocouple voltages into degrees centegrade.

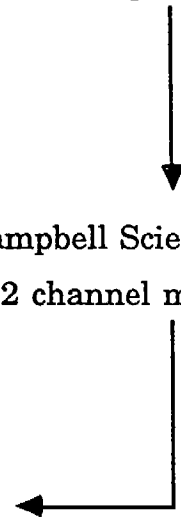
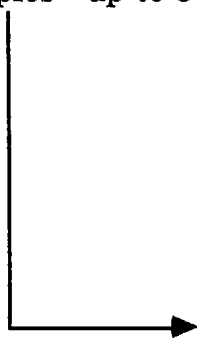
Wind speed and direction were measured at 2.4 m on the instrument tripod and at 2.25 m above the oil on the bridge. During the March 1987 trip windspeed was also measured at 10 m above the ground. The data was smoothed over a one hour period using a simple moving average. Plots of the data are found in Appendix F. Plots of relative humidity as a function of time are also included in this appendix.

Solar radiation data is compared to the predicted values of Equation 22 and shown in Figure 6 and 7. We see that the calculated values match fairly close the measured values.

Anemometer - up to 3 different heights
Wind Direction Vane
Ambient Temperature Probe
Relative Humidity Probe
Silicon Pyranometer
Thermocouples - up to 8

Thermocouples - up to 32

Campbell Scientific AM-32
32 channel multiplexer



Campbell Scientific 21-X
Datalogger

Short Haul Answer Modem

Short Haul Call Modem

IBM PC



Figure 5: Schematic Diagram of Meteorological Station

FIGURE 6: DATA AND PREDICTED SOLAR RADIATION

February 21, 1987

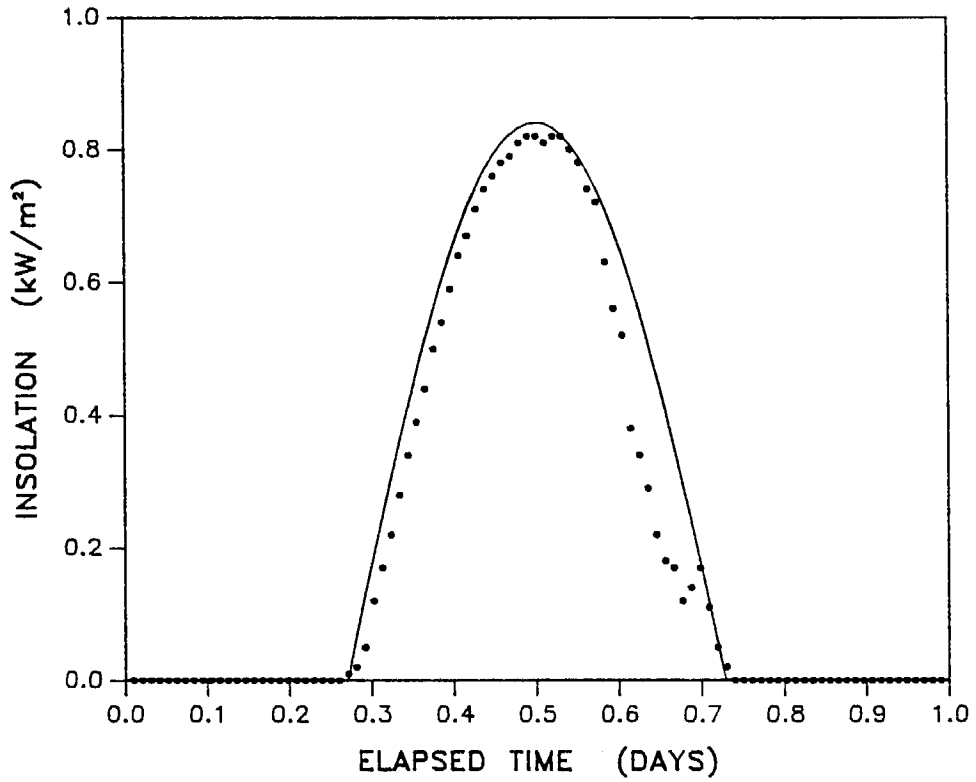
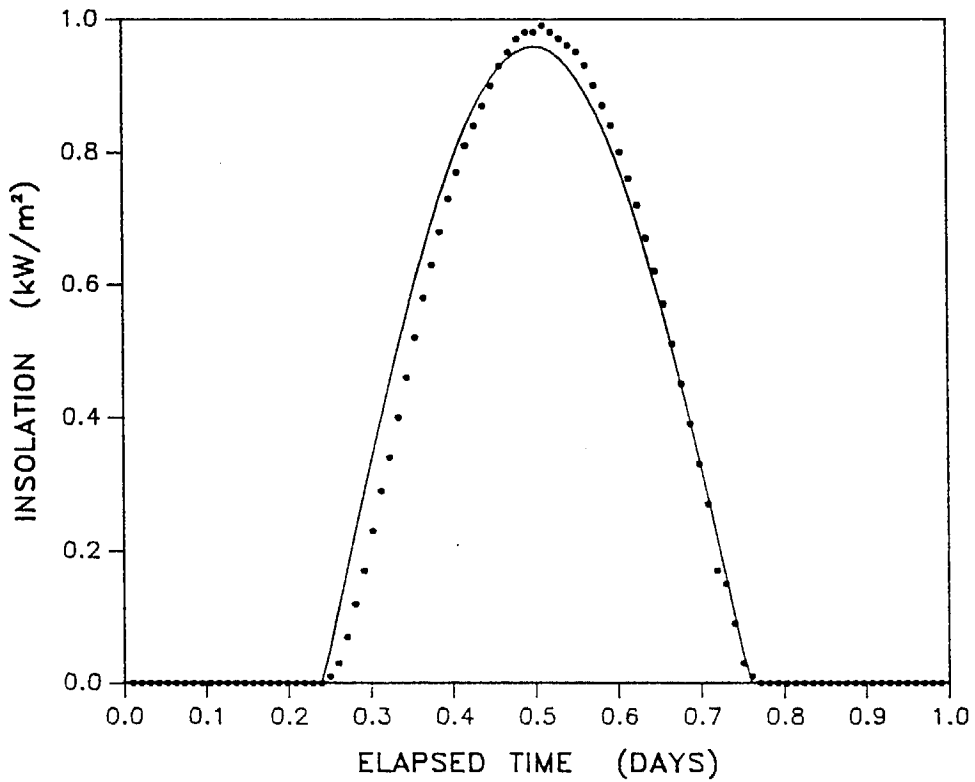


FIGURE 7: DATA AND PREDICTED SOLAR RADIATION

March 31, 1987



Figures 8 and 9 show ambient temperature data compared to the predicted values of Equation 25. The equation adequately predicts the ambient temperature measured at 2.4 m.

In March 1987 an experiment was set up to determine the temperature of the oil at various depths in different locations in the sump. Floats were built of 1 inch PVC pipe as shown in Figure 10. Four of the floats were fitted with five thermocouples each and placed in the sump as shown in Figure 11. Two floats were just upstream of the bridge and two were 70 feet downstream of the bridge. The thermocouples were placed at depths of 1, 2, 3, 6, and 10 inches. Halfway through the experiment, the thermocouples at the 2 inch depth on the floats nearest the bridge were moved to just below the surface. Thermocouples were also placed at 1 and 5 inch depths near the oil inlet and at a three inch depth at the outlet. One thermocouple was placed in the outlet pipe to measure the bulk average outlet oil temperature. The temperature data was smoothed with a simple moving average over a 2 hour period to reduce the noise. Appendix G contains plots of temperature data. The temperature data supports the assumption of constant temperature made for the boundary condition at the oil/water interface in the heat transfer model. Data recorded during an operations upset in March 1986 is shown in Figure 12. Oil was being recycled from the outlet back into the sump and the depth of the oil pad grew to over 2 feet. The temperature is shown to stay constant over time and at the same value for depths of 7 inches and 19 inches.

Experimentally determined temperature profiles can now be compared to the theoretical model. The heat transfer model was run by itself for this comparison. Figures 13 and 15 show the measured profiles as temperature versus time at various depths. Figures 14 and 16 show the predicted temperature profiles in the same format. Note that we changed the depth of the oil pad in the

FIGURE 8: DATA AND PREDICTED AMBIENT TEMPERATURE

February 21, 1987

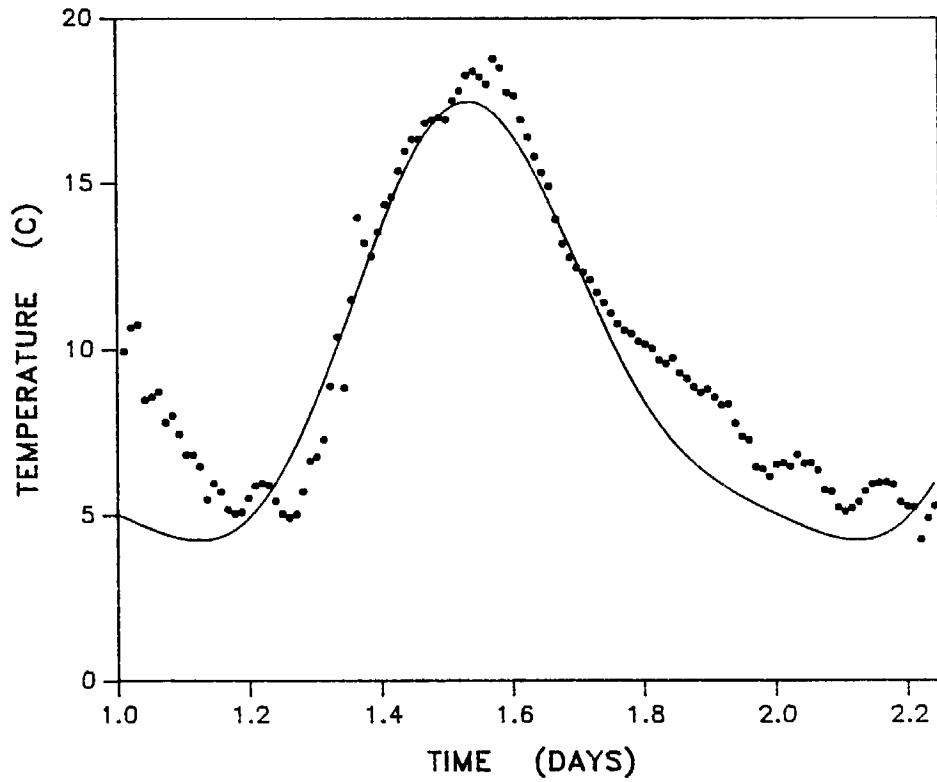
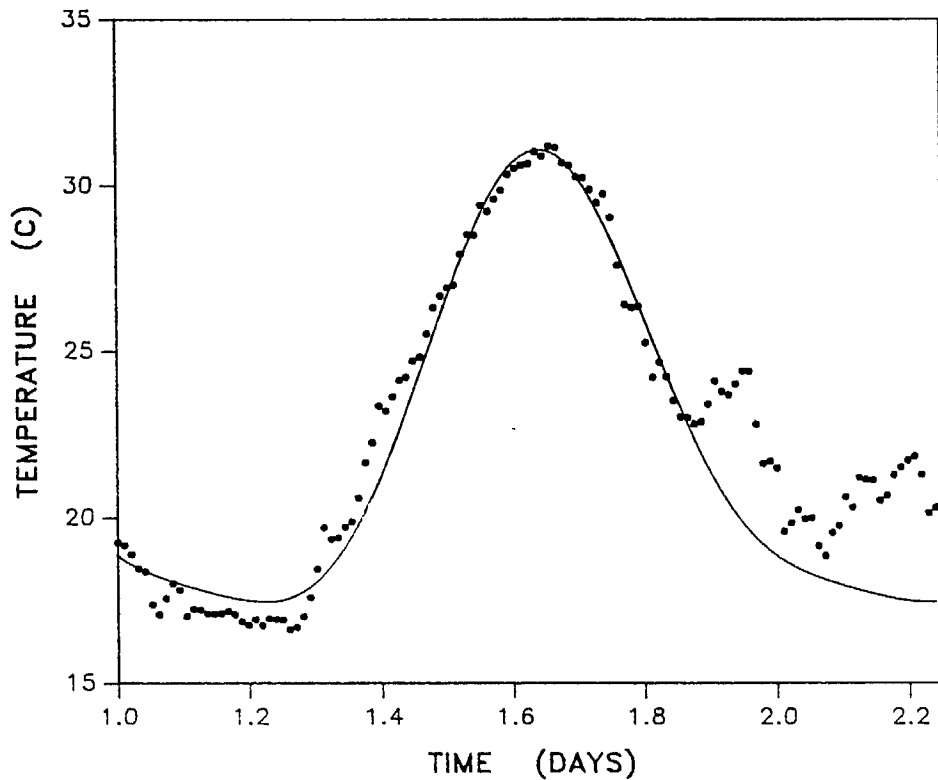


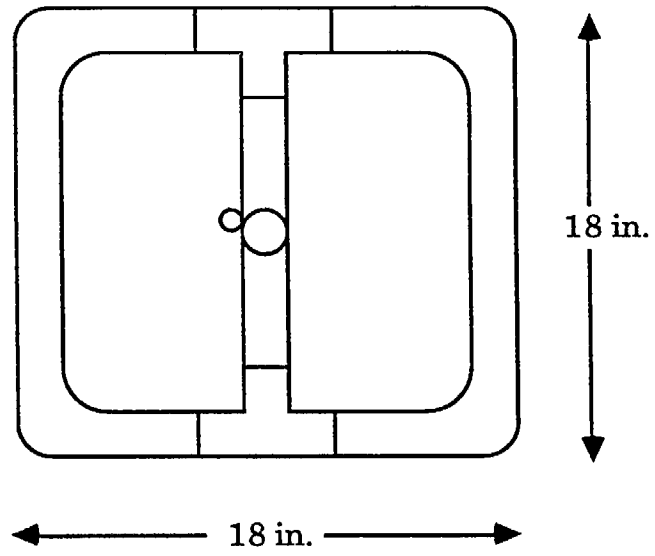
FIGURE 9: DATA AND PREDICTED AMBIENT TEMPERATURE

March 31, 1987



Midnight = 1.0, Noon = 1.5

Top View



Side View

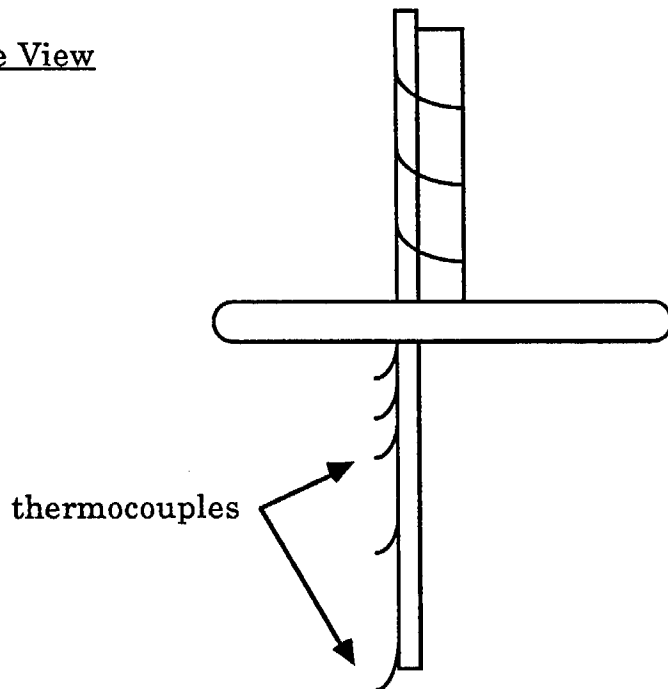
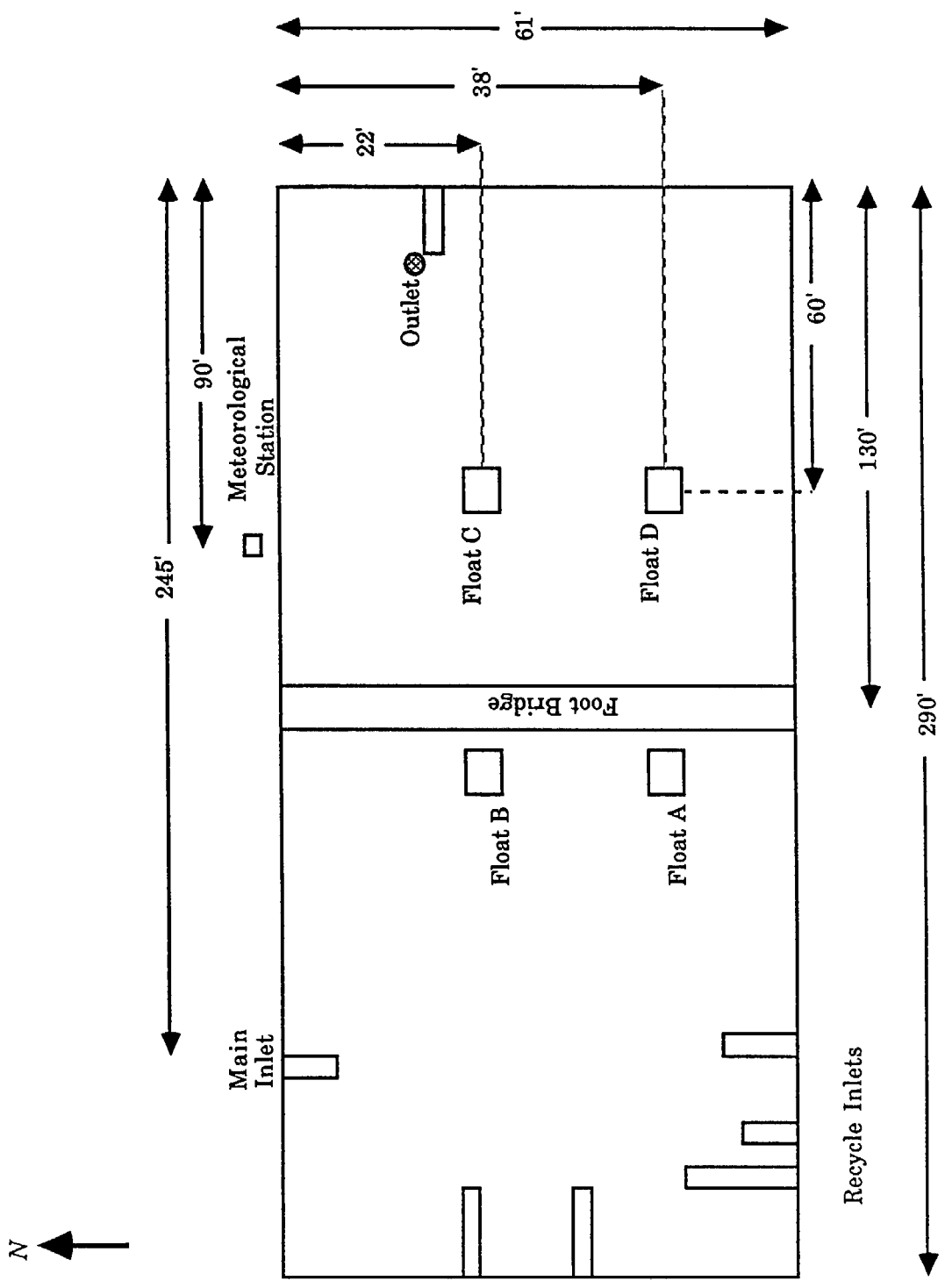


Figure 10: Thermocouple Float



not to scale

Figure 11: Map of Sump 36W

FIGURE 12: TEMPERATURE PROFILE

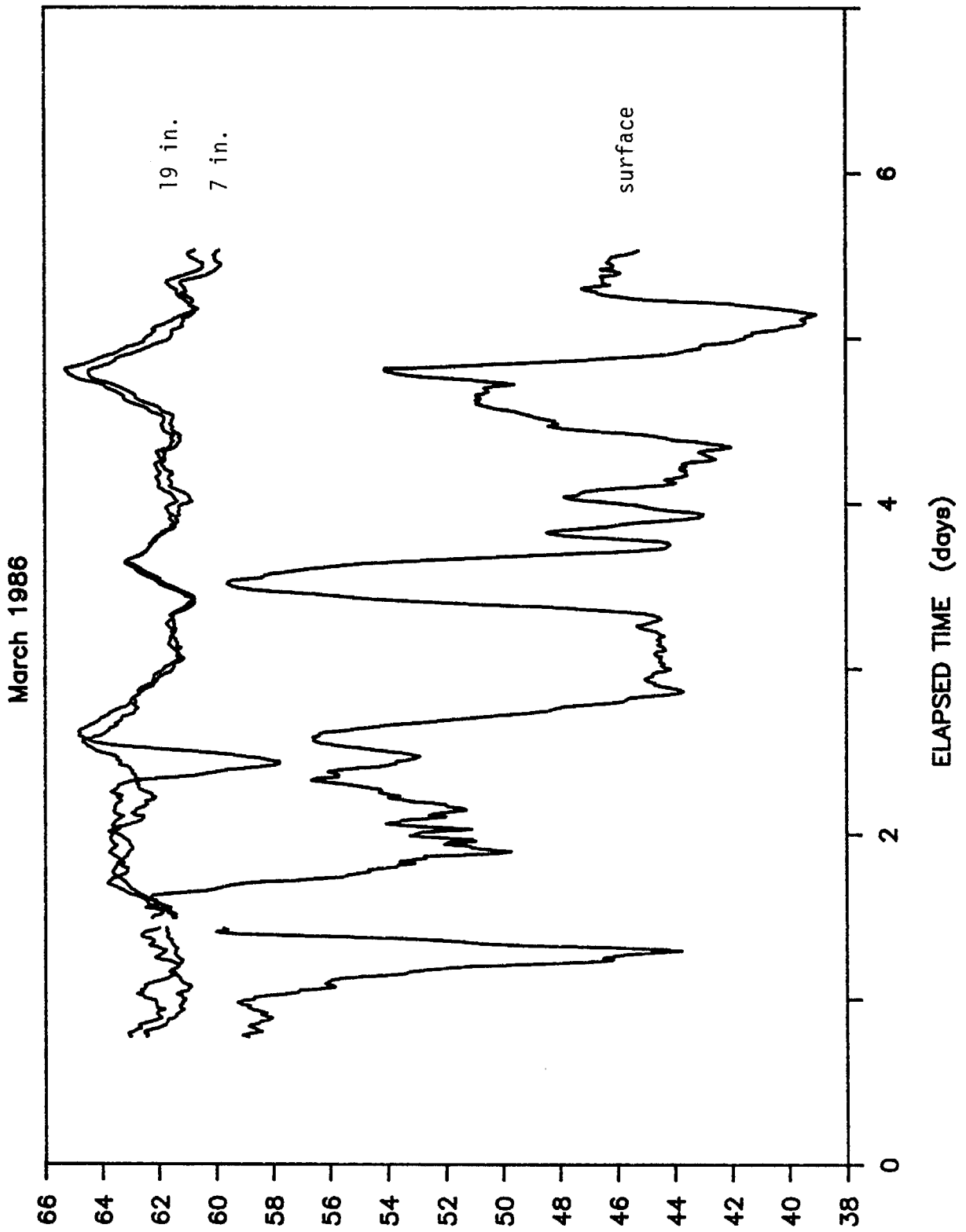


FIGURE 13: TEMPERATURE PROFILE

36W FLOAT B - MARCH 1987

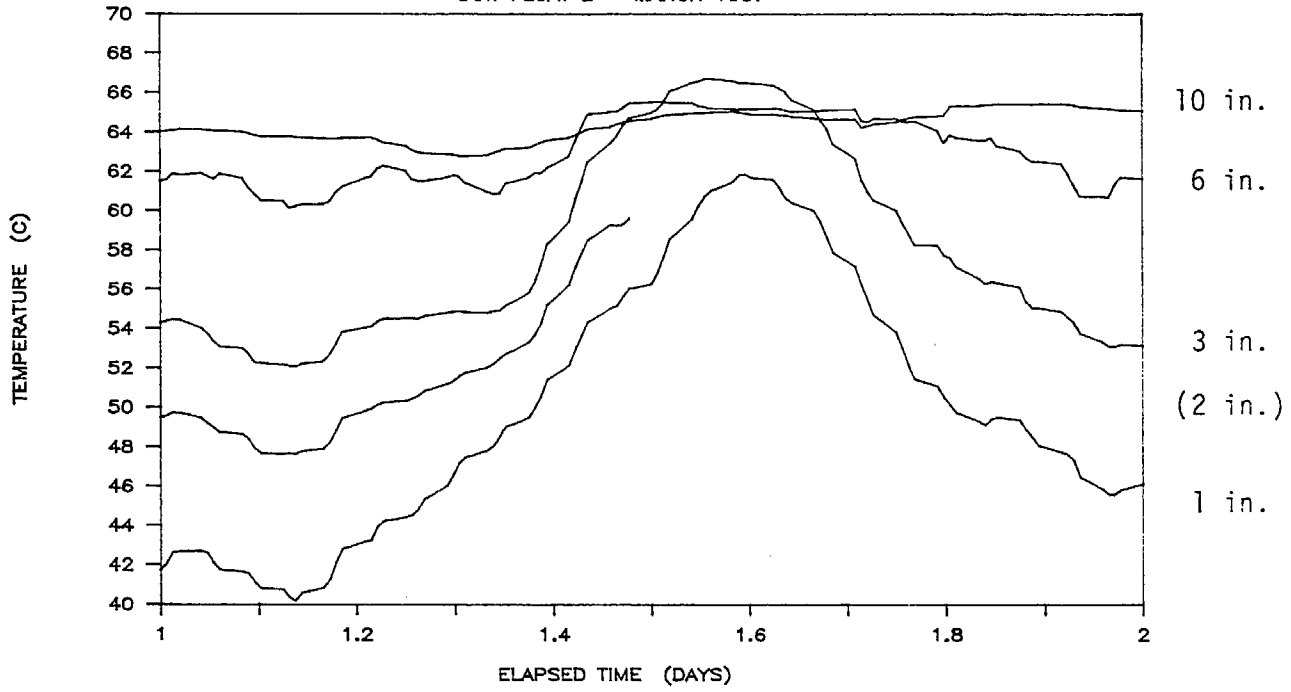


FIGURE 14: TEMPERATURE PROFILE

OIL PAD 0.2 m

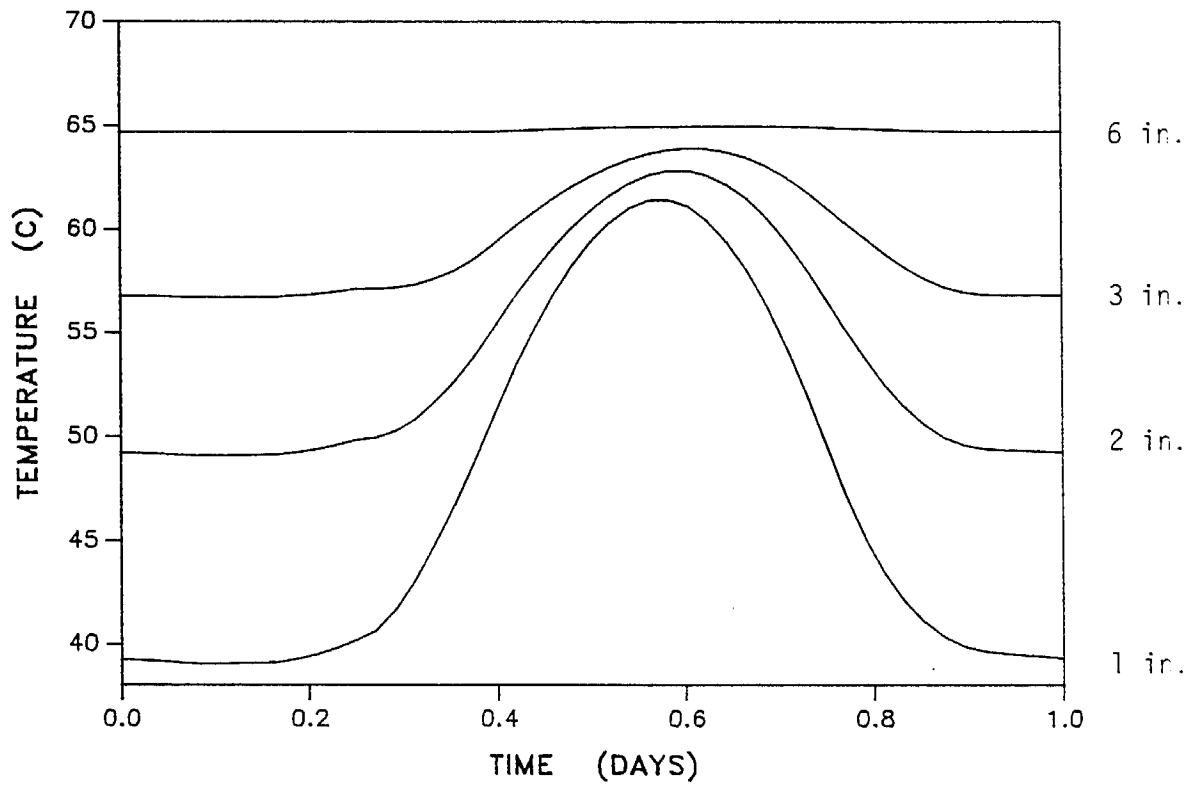


FIGURE 15: TEMPERATURE PROFILE

36W FLOAT C - MARCH 1987

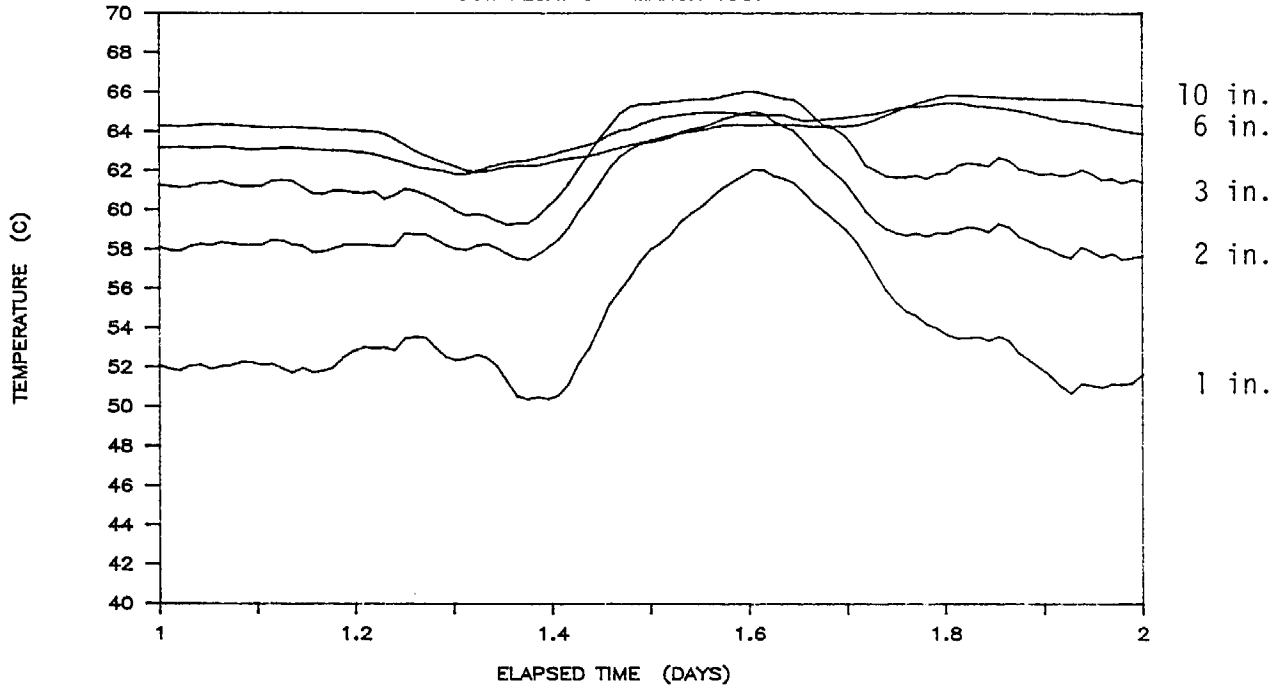
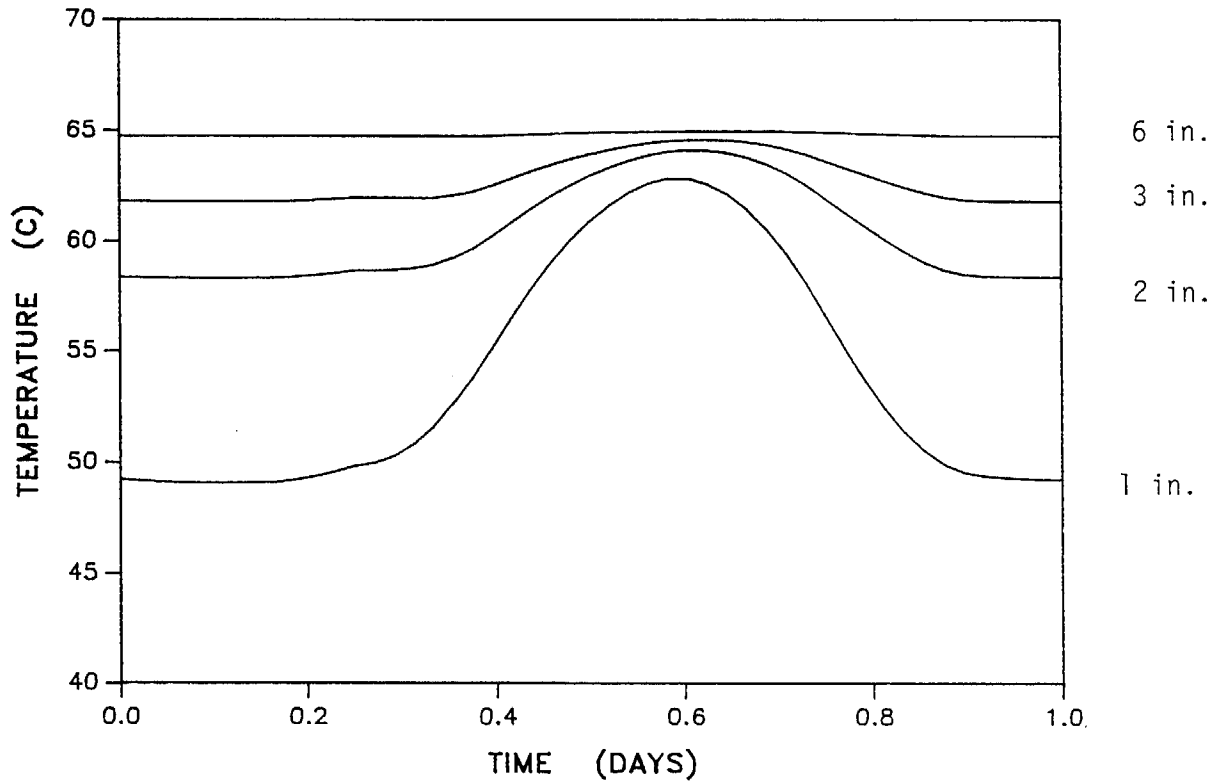


FIGURE 16: TEMPERATURE PROFILE

OIL PAD 0.15 m



two modeled cases. This change was based on the experimentally measured oil pad thickness. Oil pad thickness was determined by measuring the electrical resistance between a reference point in the water and a series of points above the reference. Twelve conductors, spaced one inch apart, were attached to a vertical pole mounted on a float similar to the thermocouple float. The bottom conductor, always in the water, served as the ground or reference point and the remaining eleven conductors were connected, via an eleven position switch, to the positive terminal of the resistance meter. With respect to the reference conductor, the conductors in the water phase detect only small changes in resistance while those in the oil phase detect very high resistances. By noting where the extreme change in resistance occurs, we determined the depth of the interface within one inch. Experimental depth measurements are given below in Table 7.

Table 7: Depth Measurements

Normal Operation

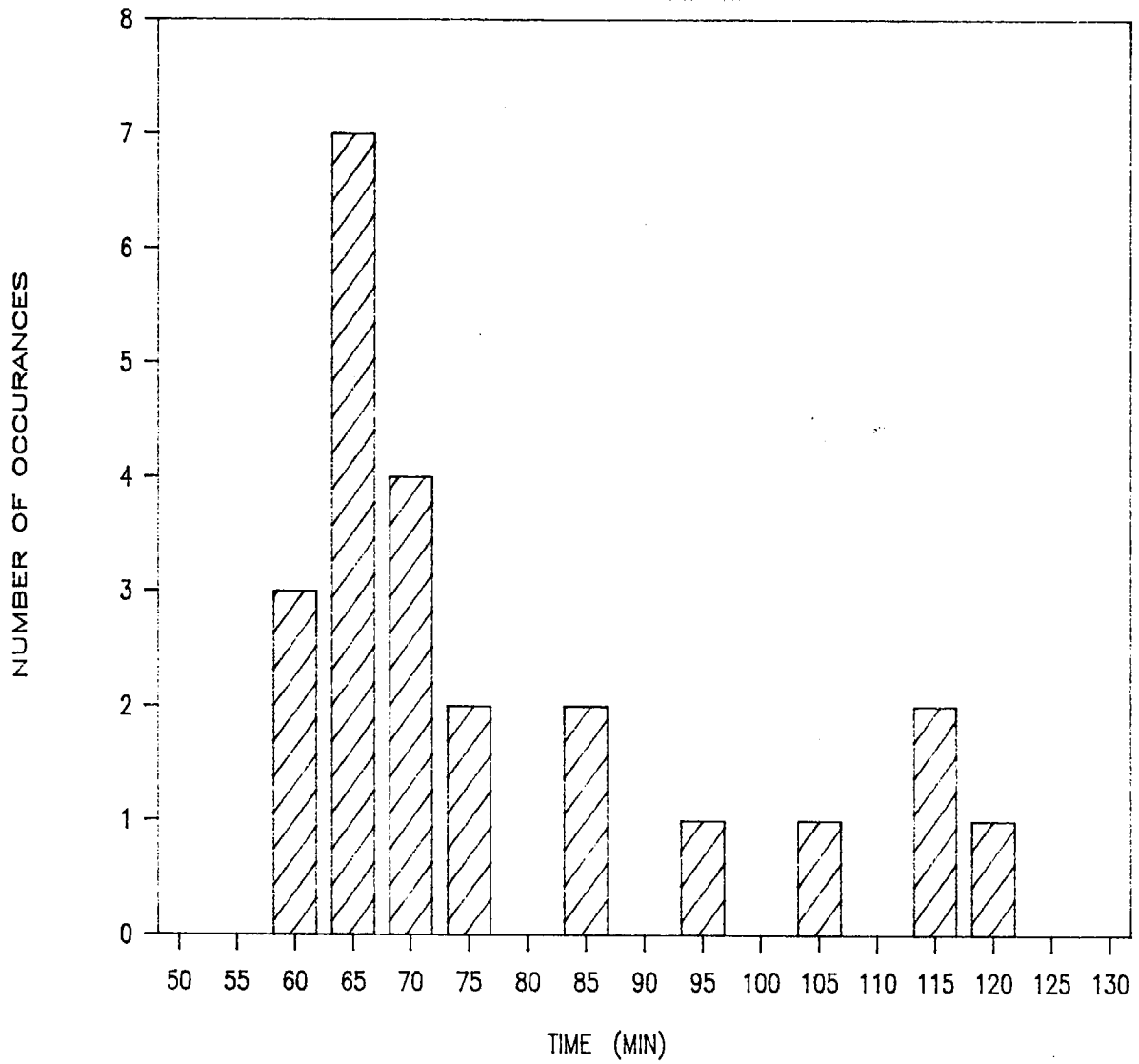
<u>Date</u>	<u>Bridge (in.)</u>	<u>Outlet (in.)</u>
2/21/87	8	8
2/22/87	8	7
3/29/87	8-9	6-7
3/29/87	7-8	6-7

Recycle Operation

<u>Date</u>	<u>Bridge (in.)</u>	<u>Outlet (in.)</u>
3/27/86	18	6
3/27/86	18	10
3/28/86	14	6
3/28/86	11	6
3/28/86	12	6
3/28/86	15	11
3/28/86	17	11
3/28/86	21	12
3/29/86	23	8
3/29/86	21	11
3/29/86	25	11
3/29/86	27	24
3/31/86	57	51

A residence time distribution was measured in March 1986. We placed 28 wooden blocks of equal size into the oil at the same time. The blocks were released from evenly spaced locations along the length of the bridge. Each block was attached to a bent wire submerged 4 inches in the oil in order to give a better indication of the bulk flow of oil and minimize surface wind effects. The time was recorded for each block as it reached the outlet. Figure 17 shows the distribution of residence times. A log-normal distribution applied to this data gives a count median residence time of 65 minutes and a GSD of 1.38.

FIGURE 17: RESIDENCE TIME DISTRIBUTION
BASED ON TRACER BLOCKS



5.0 RESULTS AND DISCUSSION

An infinite number of situations can be examined with the model; In this section I concentrate on the most reasonable situations for this problem. In particular, the residence time of oil in the sump and the ambient temperature conditions are set at realistic values.

The computer program is used to calculate a temperature profile and concentration profile through the oil layer. From the concentration profile, the flux (in $\text{gmole/m}^2 \text{ s}$) at the air/oil interface is calculated from Equation 31 and this in turn is integrated over time to calculate the total emissions at a given time (in gmole/m^2 .)

$$N_A|_L = -D_{AS} \frac{dC_A}{dz} \quad \text{at } z = L \quad (31)$$

We can divide the total emissions by the elapsed time to get the average emissions at that time (in $\text{gmole/m}^2 \text{ s}$.) As an example of these results, the program was run for a sample set of conditions. We chose a 3 hour plug-flow residence time (the time the oil resided in the sump), a day in mid-March (Julian day 75), with a mean temperature of 14 C and a temperature range of 13.3 C, with a light breeze of 0.5 m/s. Figures 18 and 19 show the temperature and concentration profiles in the oil pad (0.2 m thick) after 6 hours. Figures 20 and 21 show the flux and total emissions over time and Figure 22 shows the average emissions over time.

The effect of the heat of vaporization term in the heat-transfer problem was examined. Neglecting the term was found to change the results by less than a tenth of a percent, so the term was dropped and the iterative solution was not required.

FIGURE 18: TEMPERATURE PROFILE THROUGH OIL PAD
AFTER 6 HOURS

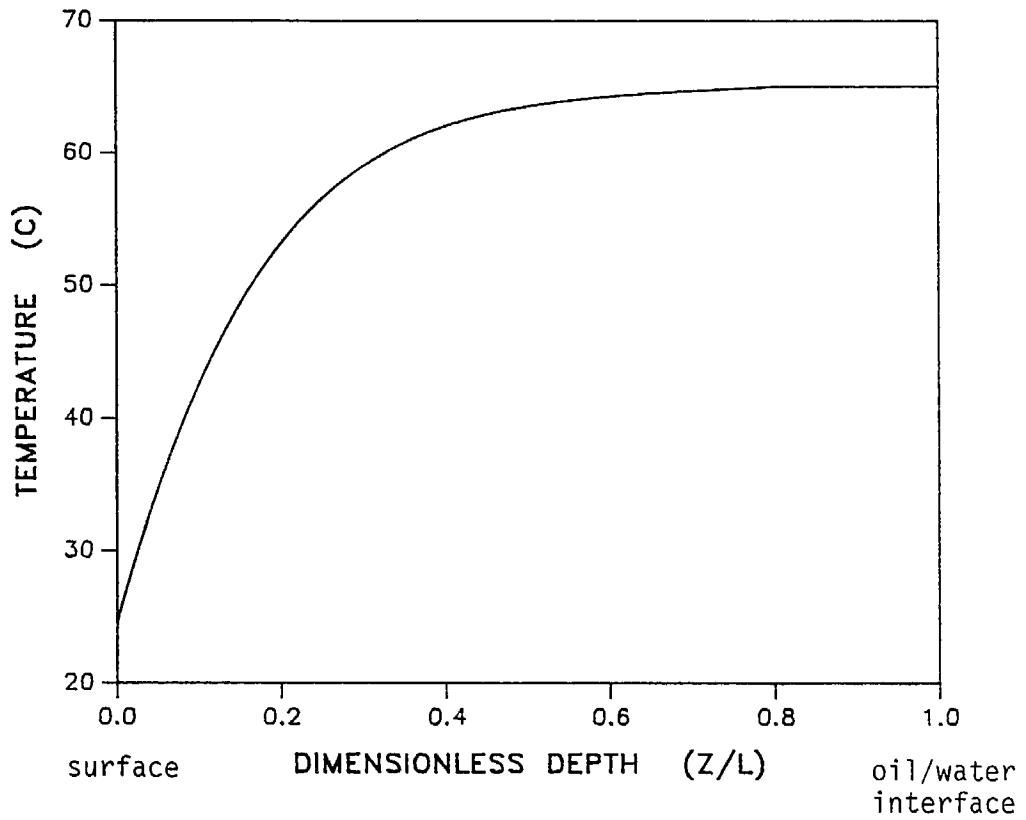


FIGURE 19: CONCENTRATION PROFILE THROUGH OIL PAD
AFTER 6 HOURS

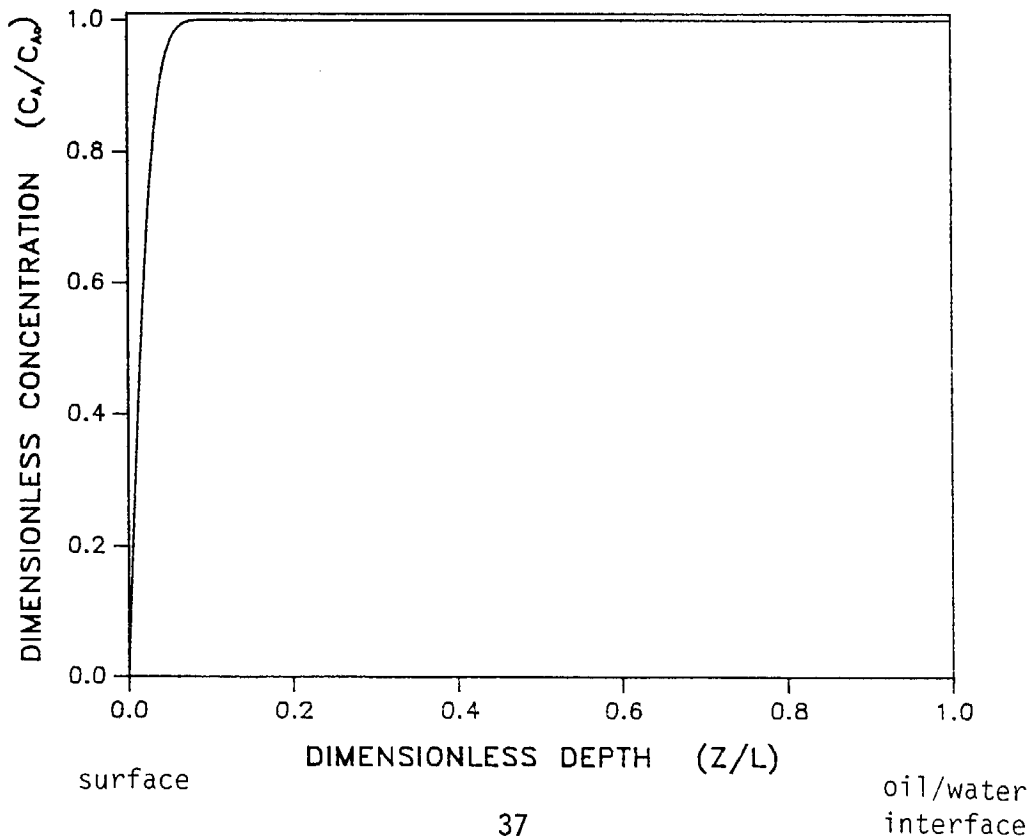


FIGURE 20: MASS FLUX OVER TIME

Initial VOC Concentration 1 gmole/m³

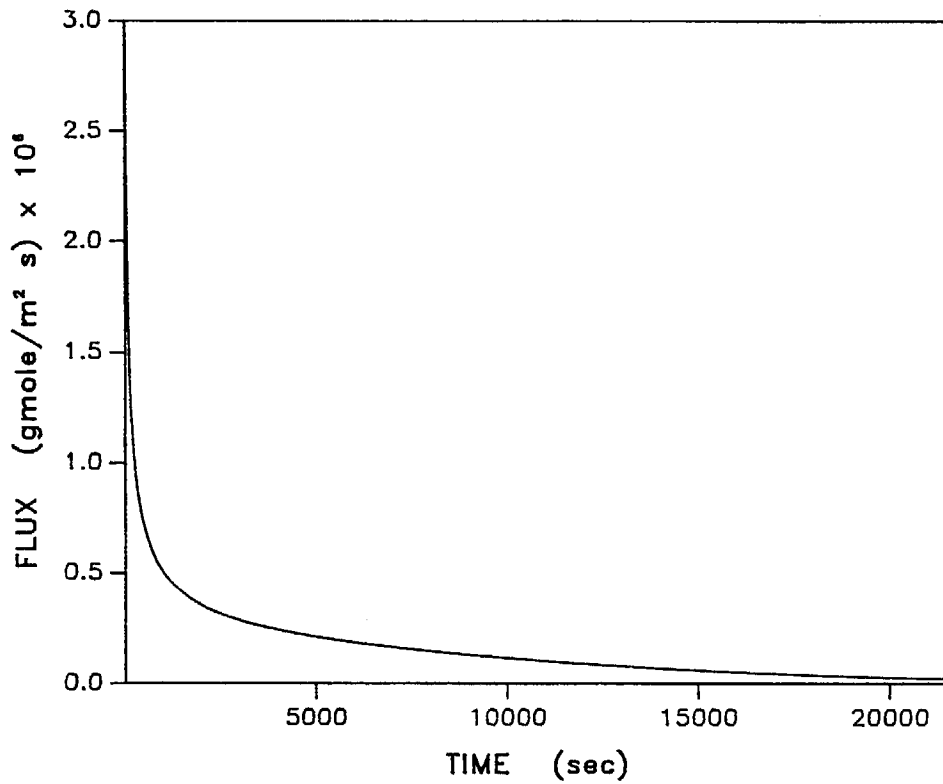


FIGURE 21: TOTAL EMISSIONS OVER TIME

Initial VOC Concentration 1 gmole/m³

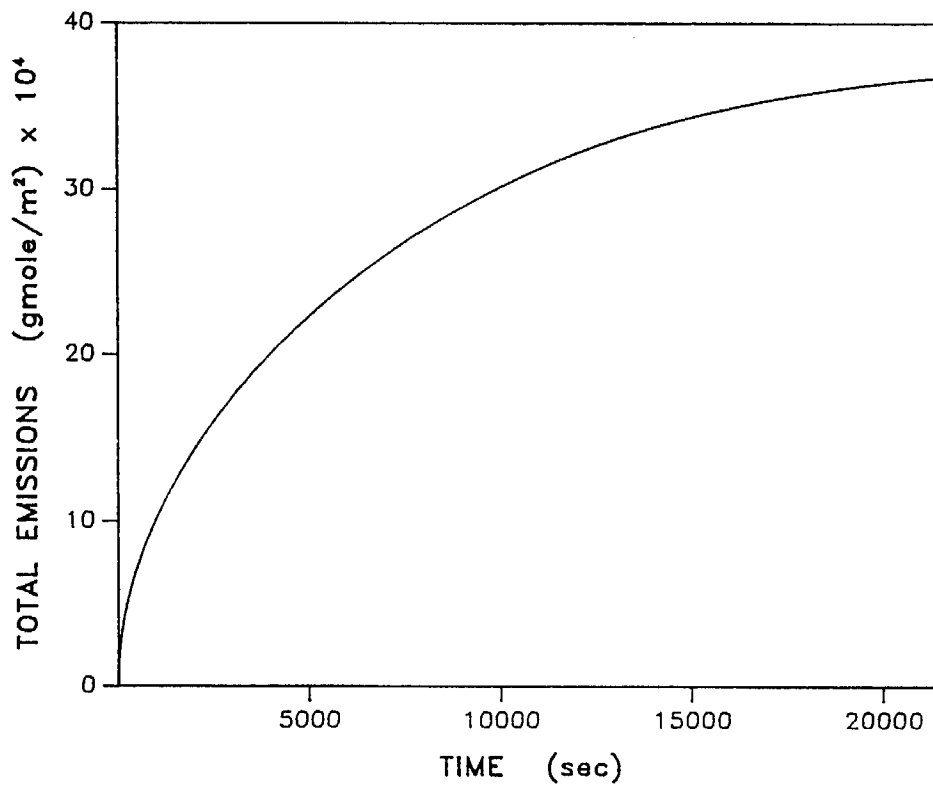
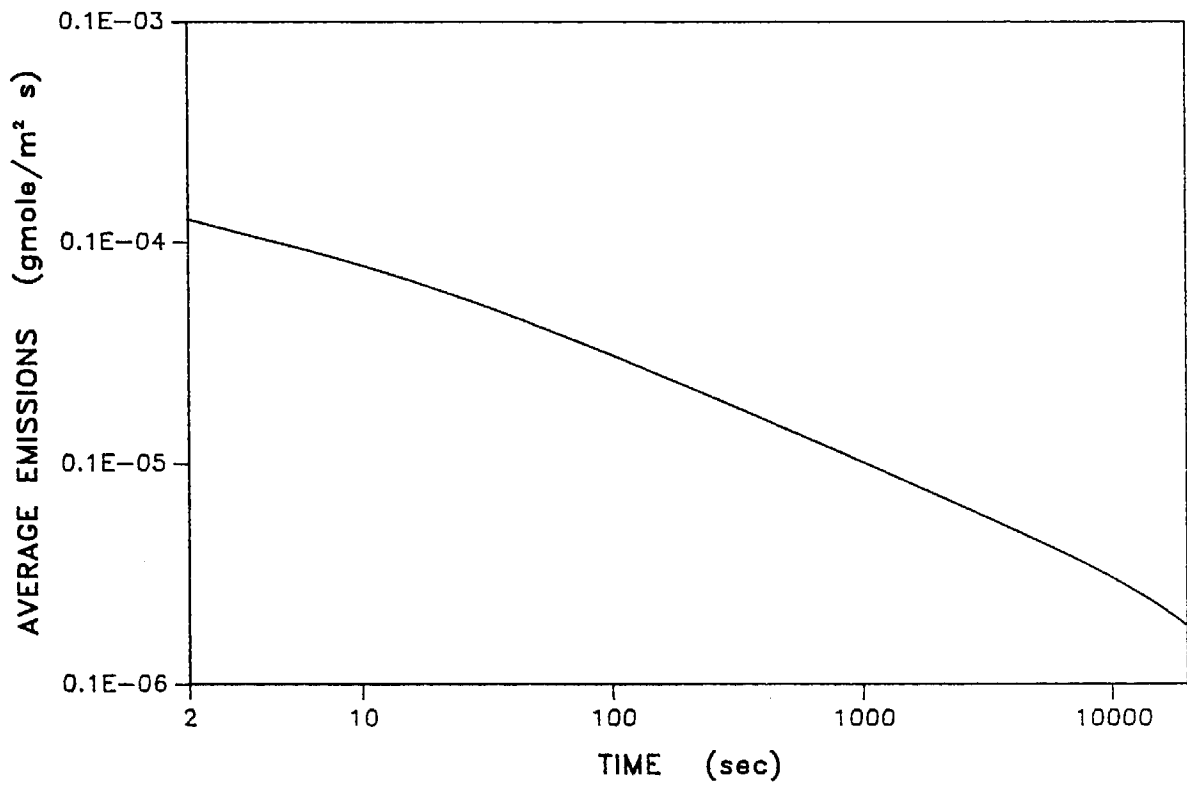


FIGURE 22: AVERAGE EMISSIONS OVER TIME

initial VOC concentration 1 gmole/m³



Average emissions were looked at for each pseudocomponent. Figure 23 shows that the results are nearly identical for trimethylcyclopentane and n-heptane and that toluene emissions are slightly higher at short times but decrease faster. The total average hydrocarbon flux is found by multiplying the emissions of each pseudocomponent by the initial concentration given in Table 5 and summing the results.

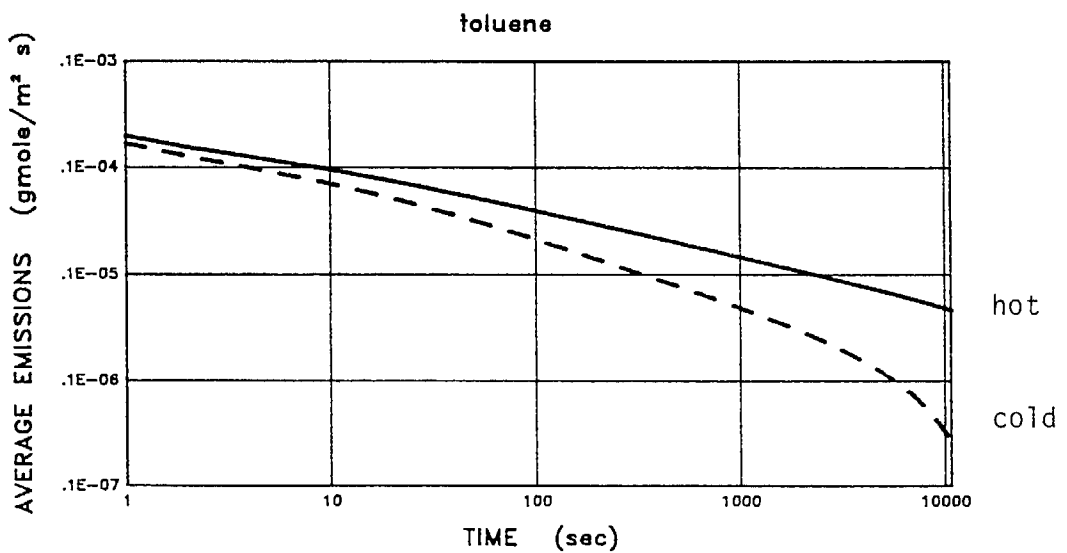
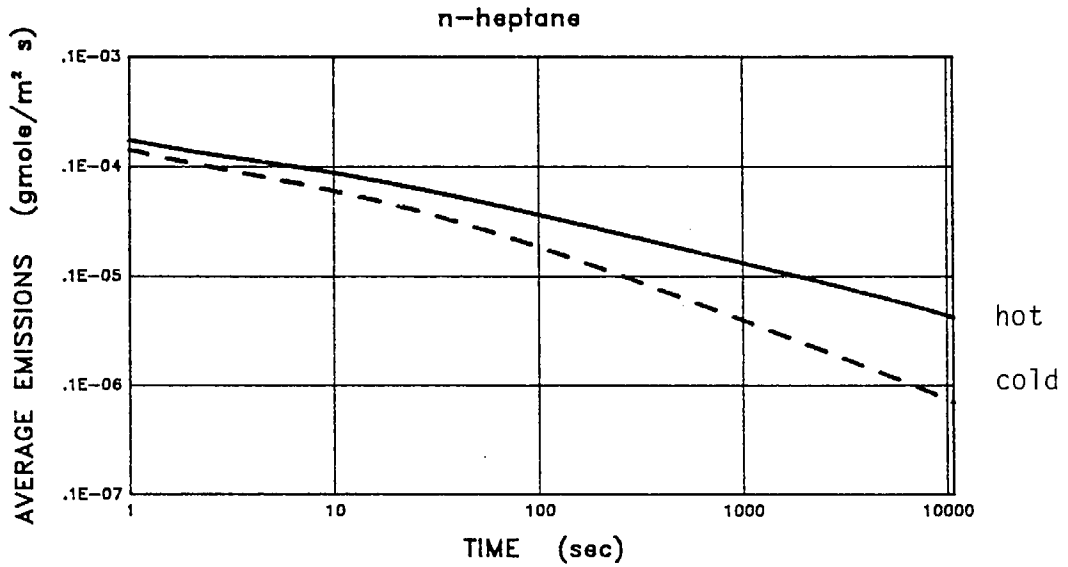
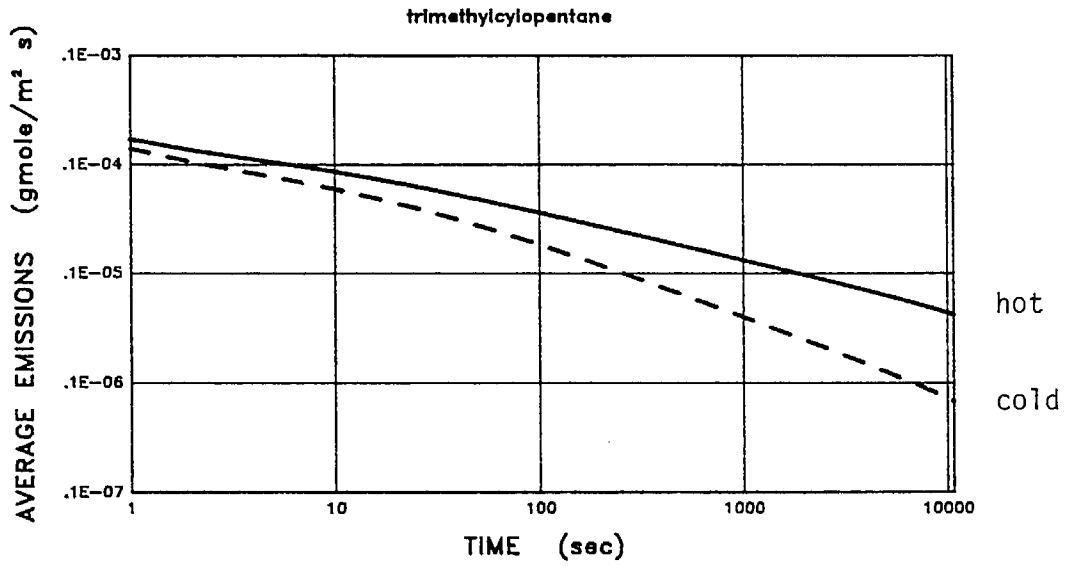
Diurnal and seasonal emission estimates are shown in Figure 24. The results are reported for a 6 hour plug-flow residence time. An initial VOC concentration of unity is used. For each month, the monthly average mean temperature and temperature range were used to calculate emissions on a day in mid-month. No correction for cloud cover was made. The maximum emissions are seen to increase by a factor of about 2.5 from winter to summer. The daily emissions in the summer increase by a factor of about 4 from early morning to mid-day.

The mid-range daily emission estimates range from approximately 1×10^{-7} to 2×10^{-7} gmole/m² s or 600 to 1200 pounds per day. These values are similar to the emission estimates made from the flux-box tests (ARB/SS-37-05, December 1986.) The emissions model can be used to predict VOC emissions from primary oil field production sumps within a good degree of accuracy.

The effect of a log-normal residence time distribution was examined with the isothermal model so that the emission estimates would not be affected by the changing ambient conditions.

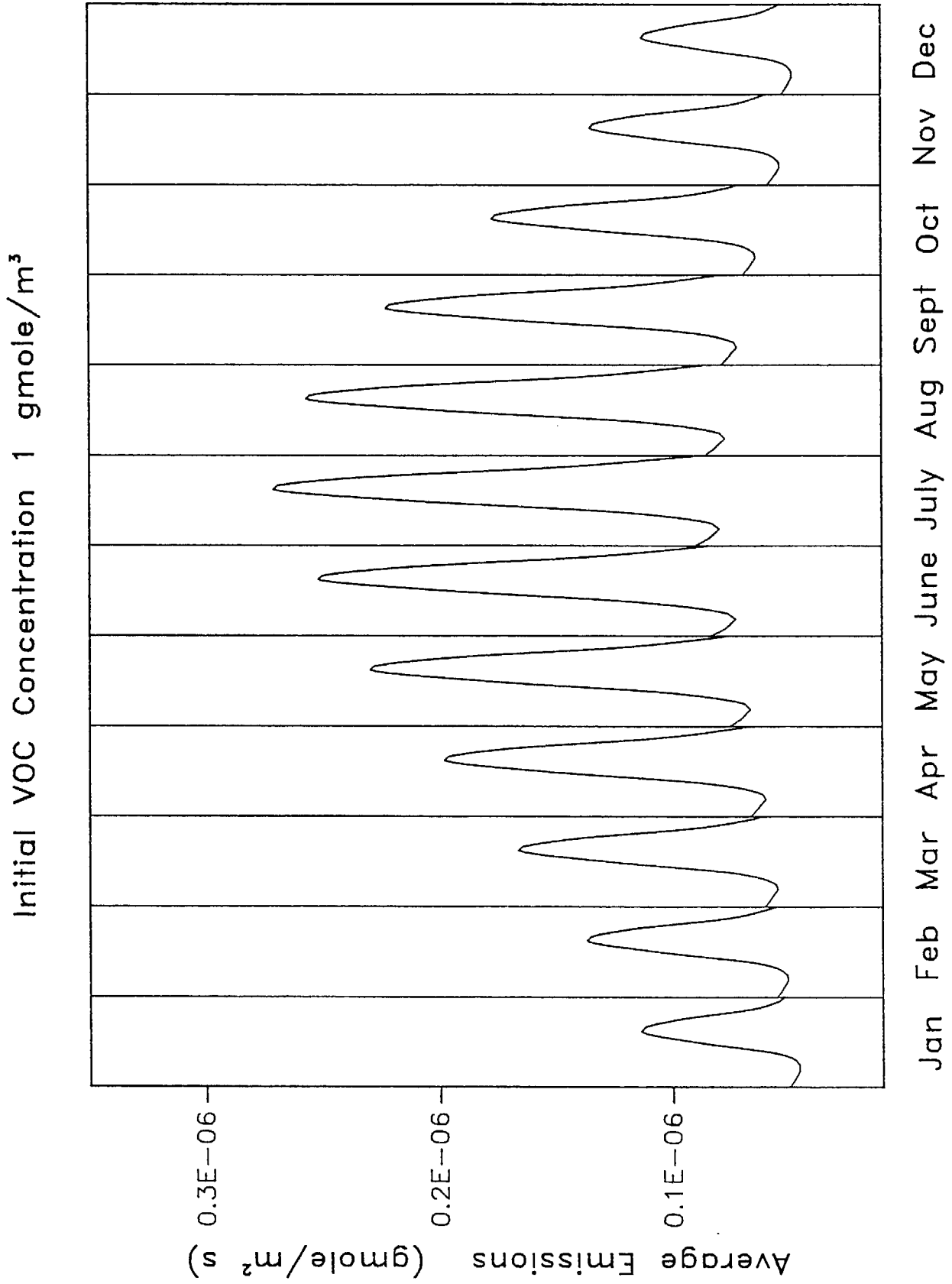
Emission estimates were calculated for a variety of count median times (CMT) and variances (σ_g). The CMT ranged from 7 minutes to 12 hours and σ_g ranged from 1.1 to 3.0. An example of the log-normal distribution function shape is

FIGURE 23:
AVERAGE EMISSIONS OVER THREE HOURS



Initial VOC Concentration 1 gmole/m³

FIGURE 24: DIURNAL AND SEASONAL EMISSIONS



shown in Figure 25. In this example the CMT is 30 minutes. For a σ_g of 1.1 all the material will have passed through the system in about 40 minutes; for a σ_g of 3.0, material resides in the system for up to 3 hours.

We found that the CMT has a pronounced effect on the emission estimates while the variance effect is much smaller. Figure 26 shows the results of this sensitivity study graphically. The emission values plotted represent the total emissions for the period of time that the fresh material (the material which entered the sump at $t = 0$) resides in the system as a function of CMT and σ_g . The maximum difference we calculated in emission values was 9% at a CMT of 12 hours and σ_g s of 1.1 and 3.0. These distributions correspond to total times in the system of approximately 17 hours to 4 1/2 days respectively. We conclude that emission estimates can be adequately predicted if a value for the average residence time is known.

FIGURE 25: LOG-NORMAL DISTRIBUTION FUNCTION

CMT = 0.5 hr or 1800 sec

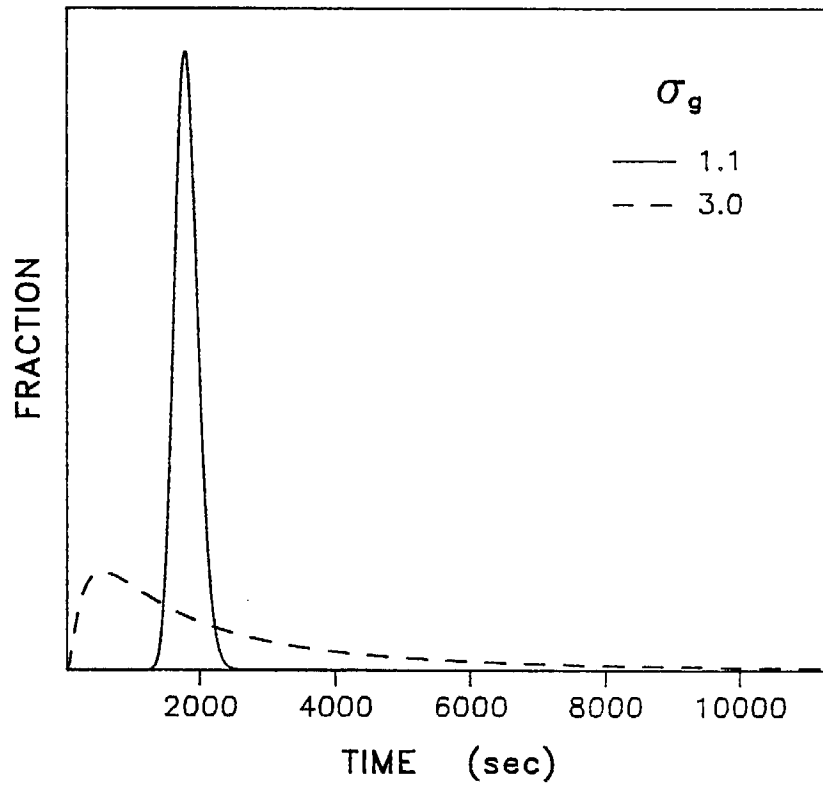
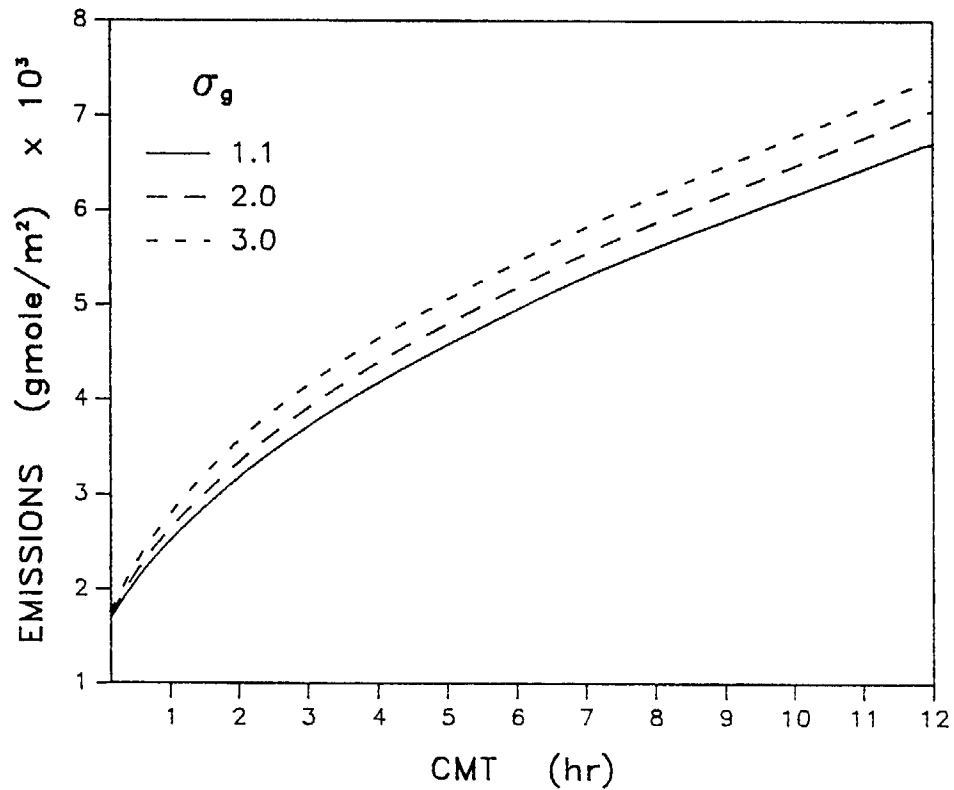


FIGURE 26: EMISSION ESTIMATES FOR VARIOUS RTD

Isothermal - T = 50°C



6.0 CONCLUSIONS

We have examined the effect of the residence time distribution on the emission estimates from a high-viscosity crude oil surface impoundment. The shape of the distribution function is found not to have a large effect on the emissions. This result concurs with the conclusion of the ARB that hydrocarbon emissions do not vary greatly from test to test over a period of years. As long as the major physical conditions are similar - ambient temperature, sump temperature, initial concentration of volatile species, etc. - the concentration profile in the oil pad will not change much once it is set up; therefore, the emission rates measured both at different points on the pad and on different days will be similar.

Theoretically predicted values of daily emissions range from 600 to 1200 pounds per day for the sump investigated. These values bracket the test data reported from the ARB flux box test method (ARB/SS-87-05, December 1986.) The two emission estimate methods, theoretical and experimental, independently predict emissions of the same order of magnitude. The mathematical model presented here represents a valid method of estimating emissions from primary crude oil sumps or other high viscosity, non-aerated liquid surface impoundments.

REFERENCES

1. Bolz, R.E., and G.L. Tuve, eds., CRC Handbook of Tables for Applied Engineering Science, 2nd Edition. CRC Press, Cleveland, Ohio (1976).
2. Ehrenfeld, J.R., et al, eds., Controlling Volatile Emissions at Hazardous Waste Sites. Noyes Publications, Park Ridge, New Jersey (1986).
3. Hiss, T.G., and E.L. Cussler, "Diffusion in High Viscosity Liquids," AICHE J., 19 (1973), 698-703.
4. Iqbal, M., An Introduction to Solar Radiation. Academic Press, Canada (1983).
5. McCutchan, M.H., "Determining the Diurnal Variation of Surface Temperature in Mountainous Terrain," J. Appl. Meteor., 18 (1979), 1224-1229.
6. Mackay, D. and R.S. Matsugu, "Evaporation Rates of Liquid Hydrocarbon Spills on Land and Water," Can. J. Chem. Eng., 51 (1973), 434-441.
7. Mitchell, J., et al, "Microclimatic Modeling of the Desert," in Heat and Mass Transfer in the Biosphere, Part 1: Transfer processes in plant environment, D.A. de Vries and N.H. Afgan, eds., Scripta Book Co., Washington, D.C. (1975), 273-286.
8. Myers, T.E., and R.M. Bricka, "Modeling Ammonia Gas Transport from Solidified Hazardous Waste," Environ. Prog., 4 (1985), 187-198.
9. Perry, R.H. and D.W. Green, eds., Perry's Chemical Engineers Handbook, 6th edition. McGraw-Hill Book Co., New York (1984).
10. Pielke, R.A., Mesoscale Meteorological Modeling. Academic Press, Orlando, Florida (1984).
11. Reid, R.C., J.M. Prausnitz, and B.E. Poling, The Properties of Liquids and Gases, 4th edition. McGraw-Hill, Inc., New York (1986).
12. Sellers, W.D., Physical Climatology. The University of Chicago Press, Chicago (1965).
13. University of California at Davis, Department of Chemical Engineering, "Research and Development on Methods for the Engineering Evaluation and Control of Toxic Airborne Effluents," Contract No. A4-159-32, Volume 2 (June 1987).
14. Vargaftik, N.B., Tables on the Thermodynamic Properties of Liquids and Gases. Hemisphere Publishing, Washington, DC (1975).
15. Wilke, C.R., and P. Chang, "Correlation of Diffusion Coefficients in Dilute Solutions," AICHE J., 1 (1955).
16. Yang, W.C., and H. Wang, "Modeling of Oil Evaporation in Aqueous Environment," Water Res., 11 (1977), 879-887.

NOMENCLATURE

A	albedo
Bi	Biot number = hL/K (dimensionless number)
C	total molar concentration (gmol/m^3)
C_A	molar concentration of species A
C_{A_0}	initial molar concentration of species A
C_{AG}^i	molar concentration of A in the air at the oil-air interface
C_{AG}^∞	molar concentration of A in the air far from the oil-air interface
C_L	total molar concentration of the liquid phase
C_G	total molar concentration of the gas phase
C_D	average drag or friction coefficient (dimensionless)
C_p	molar heat capacity or specific heat at constant pressure ($\text{kJ}/\text{kg}^\circ\text{C}$)
CMT	count median time
D_{AS}	binary diffusion coefficient (m^2/sec) sometimes written D_{AB}
H	Henry's Law Constant (dimensionless)
\tilde{H}	$H(C_G/C_L)$
h	heat transfer coefficient ($\text{W}/\text{m}^2\text{C}$)

ΔH_{vap} heat of vaporization (kgm^2/s)
 $\Delta H_{\text{vap(b.p.)}}$ heat of vaporization of a compound at its boiling point
 J_A^* molar diffusion flux of species A ($\text{gmol}/\text{m}^2 \cdot \text{s}$)
 K von Karman constant (0.4)
 K_G mass transfer coefficient in the gas phase (m/hr)
 k thermal conductivity ($\text{W}/\text{m C}$)
 \bar{k} cloud cover correction
 L thickness of the oil pad (m)
 m Julian day
 M_s molecular weight of solvent
 N_i flux of species i ($\text{gmole}/\text{m}^2 \text{s}$)
 N_i^{air} flux of species i from the bulk air
 N_i^{oil} flux of species i from the bulk oil
 n cloud cover fraction
 P total pressure (bar)
 P_c critical pressure (bar)
 p_i^{sat} pure component saturation vapor pressure
 P_r reduced pressure

Q_B	radiation heat flux from a black body
Q_{LW}	longwave radiation flux
Q_{rad}	net radiation flux
Q_s	shortwave radiation flux
R_A	homogeneous reaction rate of component A (gmol/s)
S	solar constant (1376 W/m^2)
Sc_G	Schmidt number = $\mu/\rho D$
T	temperature (C)
T_{avg}	average mean daily ambient temperature (C)
T_c	critical temperature of a compound (C)
T_F	surface temperature (F)
T_0	initial temperature of crude oil
T_∞	ambient air temperature (C)
T_r	reduced temperature (T/T_c) (dimensionless)
$T_{r(b.p.)}$	reduced temperature of a compound at its boiling point
T_s	surface temperature (C)
T_{sky}	atmospheric temperature (C)
T_Δ	daily temperature range (C)
t	time

u	wind velocity (m/ur)
u_z	wind velocity at an anemometer height of z (m/s)
V_i	molar volume of component i
x	pool diameter (m)
x_i	mole fraction of i in the liquid phase
y_i	mole fraction of i in the gas phase
z	length dimension (m)
z_a	reference height (m)
z_0	roughness height (m)
\bar{z}	zenith angle of sun to earth (rad)

GREEK

α	thermal diffusivity ($k/\rho C_p$) (m^2/s)
β	dimensionless group ($K_G \tilde{H} L/D_{AS}$)
Γ	dimensionless concentration
γ_A	activity coefficient of A (dimensionless)
δ	declination angle of the sun
ϵ	longwave emissivity
η	viscosity (kg/ms)

θ	dimensionless temperature
π	3.14159...
ρ	density (kg/m^3)
σ	Stefan-Boltzmann constant ($5.669 \times 10^{-8} \text{ W/m}^2\text{K}^4$)
σ_g	geometric standard deviation
ϕ	latitude (rad)

SUBSCRIPTS

A	organic component
a	air
b.p.	boiling point
c	critical
G	gas phase
L	liquid phase
o	initial (time zero)
r	reduced
rad	radiation
S	solvent
s	surface

vap vapor

∞ reading taken far from the oil-air interface

SUPERSCRIPTS

i reading taken at an interface

sat saturation

APPENDIX A: Transport equation for mass transfer

Note: This section is taken in part from Christine Laban's Master's Thesis (1987).

The governing differential equation describing the evaporation process is derived starting with the continuity equation describing mass transport of a single molecular species A at a point in the solvent B:

$$\frac{\partial c_A}{\partial t} = - \nabla \cdot \vec{N}_A + R_A ,$$

where c_A is the molar concentration of species A, \vec{N}_A is the flux of A at a point and R_A is the homogeneous reaction rate of A.

Assumptions:

1. There are no chemical reactions $R_A = 0$
2. The concentration gradient is in the z-direction only

The equation becomes

$$\frac{\partial c_A}{\partial t} = - \frac{\partial N_A}{\partial z}$$

The flux \vec{N}_A at a point is given by

$$\vec{N}_A = c_A \vec{v}^* + \vec{J}_A^* ,$$

Assumptions:

3. There is no convection in the liquid phase $\vec{v}^* = 0$
4. The only important transport mechanism is diffusion

$$\vec{J}_A^* = - c D_{AB} \frac{\partial x_A}{\partial z}$$

where c is the total molar concentration, D_{AB} is the binary diffusion coefficient and x_A is the mole fraction. Substituting equations (2) and (3) into (1) yields:

$$\frac{\partial c_A}{\partial t} = - \frac{\partial}{\partial z} \left[c D_{AB} \frac{\partial x_A}{\partial z} \right]$$

5. The solution is dilute and c is constant

$$J_A^* = D_{AB} \frac{\partial c_A}{\partial z}$$

Therefore the governing differential equation is

$$\frac{\partial c_A}{\partial t} = - \frac{\partial}{\partial z} \left(D_{AB} \frac{\partial c_A}{\partial z} \right)$$

The initial and boundary conditions are:

Initial Condition: When the oil enters the sump, the concentrations of the evaporating components are uniform throughout the oil pad

$$c_A = c_{A0} \quad \text{at } t = 0.$$

Boundary Condition (1): There is no flux of volatile components at the oil/water interface.

$$N_A = -D_{AB} \frac{\partial c_A}{\partial z} = 0$$

$$\text{or } \frac{\partial c_A}{\partial z} = 0 \quad \text{at } z = 0.$$

The second boundary condition requires continuity of flux at the air/oil interface, therefore the flux from the bulk oil to the interface equals the flux from the interface to the bulk air. The flux from the bulk oil is

$$N_A^{oil} = -D_{AB} \frac{\partial c_A}{\partial z} \quad \text{at } z = L$$

and the flux from the bulk air is

$$N_A^{\text{air}} = K_G(c_{A_G}^i - c_{A_G}^\infty)$$

$c_{A_G}^i$ is the molar concentration of A in the air at the interface and $c_{A_G}^\infty$ is the bulk concentration of A in the air and is taken to be zero. Therefore,

$$N_A^{\text{air}} = K_G c_{A_G}^i$$

In order to express the interfacial gas phase concentration in terms of the liquid phase concentration, interfacial equilibrium is assumed. This equilibrium can be stated in terms of Henry's law:

$$y_A/x_A = H,$$

where y_A and x_A are the mole fractions of A in the gas and liquid.

Assuming that the liquid and gas phases are ideal, Raoult's law applies and H is given by p_A/p where p_A = pure component saturation vapor pressure and p is the total pressure. The above equation can be rearranged in terms of concentrations:

$$y_A = \frac{c_{A_G}^i}{c_G} = \frac{H c_{A_L}^i}{c_L} = H x_A$$

where c_L and c_G are the total molar concentrations of the liquid and gas phases respectively. Therefore,

$$c_{A_G}^i = \left(H \frac{c_G}{c_L} \right) c_{A_L}^i.$$

Substituting into equation (11):

$$N_A^{\text{air}} = \left(K_G H \frac{c_G}{c_L} \right) c_{A_L}^i = K_G H c_{A_L}^i$$

where $\tilde{H} = \frac{Hc_G}{c_L}$ and the L subscript is dropped on $c_{A_L}^i$.

Boundary Condition (2) then becomes:

$$-D_{AB} \frac{\partial c_A}{\partial z} = K_G \tilde{H} c_A \quad \text{at } z = L.$$

Initial VOC concentration is defined as c_{A0}

$$\text{IC: } c_A = c_{A0} \quad \text{at } t = 0$$

Chemical equilibrium exists at the oil/water interface ($z=0$), hence there is no net mass flux

$$\text{BC 1} \quad \tilde{N}_A = 0 \quad \text{at } z = 0$$

$$\frac{\partial c_A}{\partial z} = 0 \quad \text{at } z = 0$$

Mass flux is continuous at the oil/air interface ($z=L$)

$$\text{BC 2} \quad N_A^{\text{oil}} = -D_{AB} \frac{\partial c_A}{\partial z}$$

$$N_A^{\text{air}} = K_G (c_{Ag}^i - c_{Ag}^\infty)$$

Assumptions:

6. The concentration of species A in the bulk air is small compared to the concentration at the interface

$$c_{gA}^i - c_{gA}^\infty \cong c_{gA}^i$$

7. The gas and liquid phases behave ideally, so Henry's Law can be used to calculate the vapor phase composition. Henry's Law states

$$y_A = Hx_A$$

and

$$y_A = \frac{C_{Ag}^i}{C_g}$$

$$x_A = \frac{C_{AL}^i}{C_L}$$

$$\frac{C_{Ag}^i}{C_g} = H \frac{C_{AL}^i}{C_L}$$

$$C_{Ag}^i = H \left(\frac{C_g}{C_L} \right) C_{AL}^i$$

$$C_{Ag}^i = \tilde{H} C_{AL}^i \quad \text{where } \tilde{H} = H \left(\frac{C_g}{C_L} \right)$$

so

$$N_A^{air} = K_G \tilde{H} C_{AL}^i$$

Equating the fluxes we get

$$-D_{AB} \frac{\partial c_A}{\partial z} = K_G \tilde{H} C_{AL}^i \quad \text{at } z = L$$

APPENDIX B: Numerical Solution to the Mass Transfer Problem

The governing differential equation for mass transfer and the corresponding initial and boundary conditions are

$$\begin{aligned}\frac{\partial c_A}{\partial t} &= \frac{\partial}{\partial z} \left(D_{AB} \frac{\partial c_A}{\partial z} \right) \\ c_A &= c_{A0} \quad \text{at } t = 0 \\ \frac{\partial c_A}{\partial z} &= 0 \quad \text{at } z = 0 \\ -D_{AB} \frac{\partial c_A}{\partial z} &= K_G \tilde{H} c_A \quad \text{at } z = L\end{aligned}$$

Let $D_{AB} = D_{AB}^{\circ} F(z, t)$, where D_{AB}° is a constant and $F(x, t)$ incorporates the variance of the diffusion coefficient with time and position.

We non-dimensionalize the problem as shown

$$\begin{aligned}\Gamma &= \frac{c_A}{c_{A0}} \\ x &= \frac{z}{L} \\ t^* &= \frac{D_{AB}^{\circ} t}{L^2}\end{aligned}$$

The GDE and boundary conditions become

$$\begin{aligned}\frac{\partial \Gamma}{\partial t^*} &= \frac{\partial}{\partial x} \left(F(x, t) \frac{\partial \Gamma}{\partial x} \right) \\ \Gamma &= 1 \quad \text{at } t^* = 0 \\ \frac{\partial \Gamma}{\partial x} &= 0 \quad \text{at } x = 0\end{aligned}$$

$$-\frac{\partial \Gamma}{\partial x} = \beta \Gamma \text{ at } x = 1$$

where

$$\beta = \frac{K_G^{\sim} HL}{D_{AB} F(L, t)}$$

An implicit numerical solution to the governing differential equation is given by Mitchell (REF 1). The solution is of the tridiagonal matrix form

$$-AU_{m-1} + BU_m - CU_{m+1} = D$$

where

$$U_m = \Gamma(m)$$

The following conventions are used

<u>axis</u>	<u>grid spacing</u>	<u>integer</u>	<u>first value*</u>	<u>last value*</u>
x	h	m	1	ME
t	k	n	-	-

*For FORTRAN code

$$\text{and } A = \frac{h^2}{2} a_m^{n+1}$$

$$B = \frac{h^2}{k} + \frac{h^2}{2} a_m^{n+1} + \frac{h^2}{2} a_{m+1}^{n+1}$$

$$C = \frac{h^2}{2} a_{m+1}^{n+1}$$

$$D = \frac{h^2}{2} a_m^n U_{m-1} + \left[\frac{h^2}{k} - \frac{h^2}{2} a_m^n - \frac{h^2}{2} a_{m+1}^n \right] U_m + \frac{h^2}{2} a_{m+1}^n U_{m+1}$$

where

$$a_m = \frac{1}{h} \left[\int_{(m-1)h}^{mh} \frac{dx}{F(x)} \right]^{-1}$$

$$F(x) = \left[\frac{n(T_{ref})}{n(T)} \right]^{2/3} \frac{T}{T_{ref}}$$

The equation is solved by the Thomas algorithm method. Both Mitchell and Carnhan (Ref. 2) provide techniques to solve a tri-diagonal matrix by Thomas algorithm.

Consider the boundary conditions in the matrix:

BC 1:
$$\frac{\partial \Gamma}{\partial x} = 0 \text{ at } x_1 = 0$$

$$\frac{\Gamma(2) - \Gamma(1)}{\Delta x} = 0$$

$$\Gamma(2) = \Gamma(1)$$

Substituting this into the solution, we get

$$[A(2) + B(2)]\Gamma(2) + C(2)\Gamma(3) = D(2)$$

BC 2:
$$-\frac{\partial \Gamma}{\partial x} = \beta \Gamma \text{ at } x = 1$$

$$-\frac{[\Gamma(ME) - \Gamma(M)]}{\Delta x} = \beta \Gamma(ME)$$

where

$$M = ME - 1$$

$$\Gamma(ME) = \left[\frac{1}{1 + \beta \Delta x} \right] \Gamma(M)$$

Substituting this into the solution, we get

$$A(M)\Gamma(M-1) + \left[B(M) + \frac{C(M)}{1 + \beta \Delta x} \right] \Gamma(M) = D(M)$$

Appendix C

Derivation of the Governing Differential Equation Describing Heat Transfer

Starting with the thermal energy equation in terms of the internal energy U:

$$1) \quad \rho \frac{D\hat{U}}{Dt} = -(\nabla \cdot \mathbf{q}) - (\underline{\underline{\pi}} : \nabla \underline{\underline{v}}) + \sum_{i=1}^n (\underline{\underline{j}}_i \cdot \underline{\underline{g}}_i)$$

It can be shown that:

$$2) \quad \underline{\underline{\pi}} = \underline{\underline{\tau}} + \underline{\underline{\xi}}_p$$

$$3) \quad \rho \frac{D\hat{U}}{Dt} = \rho \frac{D\hat{H}}{Dt} - \rho \frac{Dp\hat{V}}{Dt} = \rho \frac{D\hat{H}}{Dt} - \rho \frac{D\hat{V}}{Dt} - \rho \hat{V} \frac{Dp}{Dt}$$

$$4) \quad \rho \hat{V} \frac{D\hat{V}}{Dt} = \rho \nabla \cdot \underline{\underline{v}}$$

$$5) \quad \underline{\underline{\xi}}_p : \nabla \underline{\underline{v}} = \rho \nabla \cdot \underline{\underline{v}}$$

where "^" means per unit mass.

Substituting 2), 3), 4) and 5) into 1) and rearranging:

$$6) \quad \rho \frac{D\hat{H}}{Dt} = -(\nabla \cdot \mathbf{q}) - (\underline{\underline{\tau}} : \nabla \underline{\underline{v}}) + \frac{Dp}{Dt} + \sum_{i=1}^n (\underline{\underline{j}}_i \cdot \underline{\underline{g}}_i)$$

Note that $H = H(T, \hat{p}, \eta_i)$ may be expressed as the total differential ($\eta_i = \text{mol}/1000 \text{ g}$):

$$7) \quad \rho \frac{D\hat{H}}{Dt} = \rho \frac{\partial \hat{H}}{\partial T} \frac{DT}{Dt} + \rho \frac{\partial \hat{H}}{\partial \hat{p}} \frac{D\hat{p}}{Dt} + \rho \sum_{i=1}^n \frac{\partial \hat{H}}{\partial \eta_i} \frac{D\eta_i}{Dt}$$

It can be shown that:

$$8) \quad \rho \frac{\partial \hat{H}}{\partial T} \rho, \eta_i = \rho \hat{c}_p \frac{DT}{Dt}$$

$$9) \quad \rho \frac{\partial \hat{H}}{\partial p} \rho, \eta_i \frac{Dp}{Dt} = \rho \left[-T \frac{\partial \hat{V}}{\partial T} \rho, \eta_i + \hat{V} \right] \frac{Dp}{Dt} =$$

$$\left[\rho \hat{V} - \frac{\partial \ln \hat{V}}{\partial \ln T} \rho, \eta_i + 1 \right] \frac{Dp}{Dt}$$

Letting $\frac{\partial \hat{H}}{\partial \eta_i} \rho, T, \eta_j = \bar{H}_i$

where "—" means partial molal, then:

$$10) \quad \rho \frac{DH}{Dt} = \rho \hat{c}_p \frac{DT}{Dt} - \frac{\partial \ln \hat{V}}{\partial \ln T} \rho, \eta_i \frac{Dp}{Dt} + \frac{Dp}{Dt}$$

$$+ \rho \sum_{i=1}^n \bar{H}_i \frac{D\eta_i}{Dt}$$

Substituting this expression for $\rho \frac{DH}{Dt}$ into the previous expression 6) and rearranging yields:

$$11) \quad \rho \hat{c}_p \frac{DT}{Dt} = -(\nabla \cdot \mathbf{q}) - (\underline{\tau} : \nabla \underline{v}) + \frac{\partial \ln \hat{V}}{\partial \ln T} \rho, \eta_i \frac{Dp}{Dt} + \sum_{i=1}^n \underline{j}_i \cdot \underline{g}_i$$

$$- \rho \sum_{i=1}^n \bar{H}_i \frac{D\eta_i}{Dt}$$

Consider $\rho \frac{D\eta_i}{Dt}$:

$$12) \quad \rho \frac{D\eta_i}{Dt} = \rho \frac{\partial \eta_i}{\partial t} + \rho \underline{v} \cdot \nabla \eta_i = \frac{\partial \rho \eta_i}{\partial t} - \eta_i \frac{\partial \rho}{\partial t}$$

$$+ (\nabla \cdot \rho \eta_i \underline{v} - \eta_i \nabla \cdot \rho \underline{v})$$

$$13) \quad \rho \frac{D\eta_i}{Dt} = \frac{\partial \rho \eta_i}{\partial t} + \nabla \cdot \rho \eta_i \underline{v} - \eta_i \left[\frac{\partial \rho}{\partial t} + \nabla \cdot \rho \underline{v} \right]$$

Noting that since $\rho [=] \text{g/m}^3$ and $\eta_i [=] \text{mol/1000 g}$,

$$14) \quad \rho \eta_i [=] \text{mol/m}^3 [=] c_i.$$

From the continuity equation:

$$15) \quad \frac{\partial \rho \eta_i}{\partial t} = \frac{\partial c_i}{\partial t} = - \nabla \cdot \underline{N}_i + R_i = - \nabla \cdot c_i \underline{v}_i + R_i$$

$$16) \quad \nabla \cdot \rho \eta_i \underline{v} = \nabla \cdot c_i \underline{v}$$

Substituting 15) and 16) into 13):

$$17) \quad \rho \frac{D\eta_i}{Dt} = R_i - [\nabla \cdot c_i \underline{v} - \nabla \cdot c_i \underline{v}_i] \\ = R_i - \nabla \cdot c_i (\underline{v} - \underline{v}_i)$$

$$18) \quad \rho \frac{D\eta_i}{Dt} = R_i - \nabla \cdot \underline{J}_i$$

Therefore,

$$19) \quad \rho \sum_{i=1}^n \bar{H} \frac{D\eta_i}{Dt} = \sum_{i=1}^n \bar{H}_i [R_i - (\nabla \cdot \underline{J}_i)]$$

Finally,

$$20) \quad \rho \hat{c}_p \frac{DT}{Dt} = - (\nabla \cdot \underline{q}) - (\underline{\tau} : \nabla \underline{v}) + \frac{\partial \ln \hat{V}}{\partial \ln T} p, \eta_i \frac{Dp}{Dt} + \sum_{i=1}^n \underline{j}_i \cdot \underline{g}_i \\ + \sum_{i=1}^n \bar{H}_i [(\nabla \cdot \underline{J}_i) - R_i]$$

Assumptions:

0

$$(1) \quad \text{Zero velocity, } \frac{DT}{Dt} = \frac{\partial T}{\partial t} + \underline{v} \cdot \nabla T$$

- (2) Constant thermal conductivity, $-\nabla \cdot \underline{q} = \nabla \cdot (k \nabla T) = k \nabla^2 T$
- (3) No viscous dissipation, $\underline{\tau} : \nabla \underline{v} = 0$
- (4) No gravitational forces, $\sum_{i=1}^n \underline{j}_i \cdot \underline{g}_i = 0$
- (5) The term $\frac{\partial \rho}{\partial T}$ is small for a liquid over a short temperature range; $\frac{D\rho}{Dt} \approx 0$ since all pressures are hydrostatic pressures.

$$\frac{\partial \ln \hat{V}}{\partial \ln T} \rho, \eta_i \frac{D\rho}{Dt} = \frac{-T}{\rho} \frac{\partial \rho}{\partial T} \rho, \eta_i \frac{D\rho}{Dt} = 0$$

- (6) No reactions, $R_i = 0$
- (7) One dimensional, $\nabla^2 T = \frac{\partial^2 T}{\partial z^2}$
- (8) Molecular weight of VOC's = molecular weight of non-volatile compounds,

$$\underline{j}_i = \frac{M_B}{M} \underline{j}_i^* \approx -D_{ij} \nabla c_i$$

- (9) For an ideal solution, the partial molar enthalpy equals the pure molar enthalpy.

$$\bar{H}_i = H_i = c_{pi} (T - T_0)$$

- (10) The diffusion term is negligible compared to the conduction term,

$$\sum_{i=1}^n c_{pi} (T - T_0) D_{ij} \frac{\partial^2 c}{\partial z^2} \ll k \frac{\partial^2 T}{\partial z^2}$$

Therefore, the governing differential equation is:

$$21) \quad \rho \hat{c}_p \frac{\partial T}{\partial t} = k \frac{\partial^2 T}{\partial z^2}$$

or

$$\frac{\partial T}{\partial t} = \alpha \frac{\partial^2 T}{\partial z^2}$$

where

$$\alpha = \frac{k}{\rho c_p}$$

The oil pad is at a uniform temperature to when it enters the sump

$$\text{IC: } T = T_0 \text{ at } t = 0$$

We assume that the temperature is constant at the water/oil interface

$$\text{BC1: } T = T_0 \text{ at } z = 0$$

The second boundary condition at the air/oil surface requires continuity of energy flux:

$$-k \frac{\partial T}{\partial z} \Big|_{\text{liq}} + \sum_{i=1}^n N_i H_i \Big|_{\text{liq}} = -k \frac{\partial T}{\partial z} \Big|_{\text{vap}} + \sum_{i=1}^n N_i H_i \Big|_{\text{vap}} - Q_{\text{rad}}$$

where

$$-k \frac{\partial T}{\partial z} \Big|_{\text{vap}} = \text{convective heat flux} = h(T - T_\infty)$$

Q_{rad} = net flux of long and short wave radiation toward interface

T_∞ = Temperature of the air

Therefore,

$$-k \frac{\partial T}{\partial z} \Big|_{\text{liq}} = h(T - T_\infty) + \sum_{i=1}^n N_i (H_i \Big|_{\text{vap}} - H_i \Big|_{\text{liq}}) - Q_{\text{rad}}$$

Boundary Condition (2) at air/oil interface:

$$-k \frac{\partial T}{\partial z} = h(T - T_\infty) + \sum_{i=1}^n N_i \Delta H_{\text{vap}} - Q_{\text{rad}} \text{ at } z = L$$

APPENDIX D: Numerical Solution to the Heat Transfer Problem

The governing differential equation for heat transfer and the corresponding initial and boundary conditions are

$$\frac{\partial T}{\partial t} = \alpha \frac{\partial^2 T}{\partial z^2}$$

where

$$\alpha = \frac{k}{\rho c_p}$$

$$T = T_0 \quad \text{at } t = 0$$

$$T = T_0 \quad \text{at } z = 0$$

$$-k \frac{\partial T}{\partial z} = h(T - T_\infty) \quad \text{at } z = L$$

We non-dimensionalize the problem using the relations

$$\theta = \frac{T - T_\infty}{T_0 - T_\infty}$$

$$X = \frac{z}{L}$$

$$t' = \frac{\alpha t}{L^2}$$

The GDE and boundary conditions become

$$\frac{\partial \theta}{\partial t'} = \frac{\partial^2 \theta}{\partial X^2}$$

$$\theta = 1$$

$$\theta = 1$$

$$-\frac{\partial \theta}{\partial X} = B_i \theta - \Phi$$

where the Biot number, Bi , is $\frac{hL}{k}$, and $\Phi = \frac{Q_{rad} L}{k(T_0 - T_\infty)}$

We discretize the GDE in the following manner; the procedure begins with

$$\left(\frac{\partial \theta}{\partial t'}\right)_{x, t'} + \frac{\Delta t'}{2} = \left(\frac{\partial^2 \theta}{\partial x^2}\right)_{x, t'} + \frac{\Delta t'}{2}$$

$$\frac{\theta_{m,n+1} - \theta_{m,n}}{\Delta t'} = \frac{1}{2} \left[\frac{\theta_{m+1,n+1} - 2\theta_{m,n+1} + \theta_{m-1,n+1}}{\Delta x^2} + \frac{\theta_{m+1,n} - 2\theta_{m,n} + \theta_{m-1,n}}{\Delta x^2} \right]$$

where m is the spatial node and n is the temporal node. The equation is of the form

$$-A\theta_{m-1}^{n+1} + B\theta_m^{n+1} - C\theta_{m+1}^{n+1} = D_m$$

where $A = 1$

$$B = 2 \left(1 + \frac{\Delta x^2}{\Delta t'}\right)$$

$C = 1$

$$D = \theta_{m+1}^n - 2 \left(1 - \frac{\Delta x^2}{\Delta t'}\right) \theta_m^n + \theta_{m-1}^n$$

This forms a tridiagonal matrix which is solved with a Thomas algorithm.

Consider the boundary conditions in this problem:

BC 1: $\theta = 1$ at $x = 0$

$$\theta(1) = 1$$

Substituting this into the solution. We get

$$-1 + B\theta(2) - \theta(3) = D(2)$$

BC 2:

$$-\frac{\partial \theta}{\partial x} = Bi\theta - \Phi \quad \text{at } x = 1$$

$$\frac{-\theta(ME) + \theta(M)}{\Delta x} = Bi\theta(ME) - \Phi$$

Solving for $\theta(ME)$, we get

$$\theta(ME) = \frac{\theta(M) + \Phi \Delta x}{1 + Bi \Delta x}$$

Substituting this into the solution, we get

$$\theta(M-1) + B\theta(M) - \theta(ME) = D(M)$$

$$\theta(M-1) + \left[B + \frac{1}{1 + Bi \Delta x} \right] \theta(M) = D(M) - \frac{\Phi \Delta x}{1 + Bi \Delta x}$$

Appendix E
Emissions Model Computer Program

```

*****
*
*   PROGRAM: VOC FLUX FOR
*   AN IMPLICIT FINITE-DIFFERENCE SOLUTION TO THE COUPLED MASS- AND
*   HEAT-TRANSFER PROBLEM
*
*****
*
*   NOMENCLATURE
*
*****
*
*   VARIABLE      DESCRIPTION
*   -----
*   A              Coefficient in Thomas Algorithm (mass transfer)
*   ALPHA          Thermal diffusivity (m2/s)
*   ANGLE          Hour angle of the sun; noon = 0
*   AT            Coefficient in Thomas Algorithm (heat transfer)
*   AVE           Average emissions (gmole/m2.s)
*   B             Coefficient in Thomas Algorithm (mass transfer)
*   BETA          hl/k
*   BETAT        Coefficient in Thomas Algorithm (heat transfer)
*   BT           Wagner equation term
*   CA           Coefficient in Thomas Algorithm (mass transfer)
*   C            Wagner equation term
*   CANOT       Initial concentration of solute species A
*   CB          Wagner equation term
*   CC          Wagner equation term
*   CD          Wagner equation term
*   CONSTANT1   CONSTANT IN COSZ
*   CONSTANT2   CONSTANT IN COSZ
*   COSZ        Radiation term
*   CT          Coefficient in Thomas Algorithm (heat transfer)
*   D           Solution matrix for Thomas Algorithm -
*              first perturbation
*   DAB         Diffusion coefficient at reference temperature
*   DAY        Julian day
*   DELT       Time increment (s)
*   DELTA     Declination of the sun (rad)
*   DEPTH     Penetration of the oil pad
*   DNOT      Longitudinal angle of sun position
*   DP        Second perturbation of D
*   DPP       Third perturbation of D
*   DT        Coefficient in Thomas Algorithm (heat transfer)
*   DTAU      Dimensionless temporal increment
*   DX        Spatial step size
*   DX1       Spatial step size
*   DX2       Spatial step size
*   ELAPSED   Dimensionless time (day)
*   F         Flux of species A
*   FLUX      Integrated flux or emissions
*   FLUX1     Diffusion coefficient multiplier at previous time
*   FOLD      Function of F
*   GAMMA    First perturbation of dimensionless concentration
*   GAMMAP   Second perturbation of dimensionless concentration
*   GAMMAPP  Third perturbation of dimensionless concentration
*   GAMMAPPP Dimensionless concentration
*   GOLD     Function of F at previous time step
*   GP       Function of F
*   GPOLD    Function of F at previous time step
*   H        Heat transfer coefficient
*
*****
*
*   HOUR          Time of day to start calculation
*   ICOUNT       Counter for printout
*   M             Counter
*   MCOUNT       Number of spatial steps
*   ME           Number of temporal steps
*   NCOUNT      Data printout interval
*   NPRINT       Saturation vapor pressure
*   PASAT        Critical pressure (bar)
*   PC          Flux for printout
*   PFLUX       Emissions for printout
*   PFLUX1      Latitudnal angle of site
*   PHI         3.14159...
*   PI          Impoundment diameter (m)
*   POOLD       Total radiation, longwave plus shortwave
*   Q           dx2/dtau
*   RATIO        Residence time of oil in the system
*   RESTIME     Solar constant
*   S           Schmidt number
*   SCG         Boltzmann constant
*   SIGMA       Solar radiation contribution
*   SOLAR       Temperature at node i (C)
*   T           Elapsed dimensionless time into calculation
*   TAU         Average mean daily temperature
*   TAVG        Critical temperature (C)
*   TC         Critical temperature of oil (F)
*   TDEGF       Daily temperature range
*   TDELT       Parameter used in surface temperature iteration
*   TDIFF       Dimensionless temperature
*   THETA       Length of calculation (s)
*   TIME        Elapsed time of calculation (s)
*   TINFK       Ambient temperature (C)
*   TINFK       Ambient temperature (F)
*   TLOW        Parameter for Simpson's rule
*   TMAX        Dimensionless length of calculation (s)
*   TNOT        Initial temperature of oil (K)
*   TOL         Initial temperature of oil (C)
*   TOL         Parameter used in surface temperature iteration
*   TSURF       Estimated value of surface temperature (C)
*   TSURFK      Estimated value of surface temperature (K)
*   UTEN        Wind velocity at ten meters
*   VISC        Viscosity
*   VISCREP     Viscosity of oil at reference temperature
*   X           Term in PASAT calculation
*   XK         Thermal conductivity
*   XL         Dimensionless distance
*   XQ         Dimensionless radiation term
*
*****
*
*   MAIN PROGRAM
*
*****
*
*   IMPLICIT REAL(A-H,O-Z)
*   INTEGER(I-N)
*   DIMENSION DT(10001), THETA(10001), FLUXTEM(10001)
*   DIMENSION AT(10001), BT(10001), CT(10001)
*   COMMON XL, ME, DELT, TIME, TEMP(10001), F(10001)
*   COMMON TMAX, FLUX(10001), NCOUNT, TINET, CANOT, UTEN
*   COMMON CA, CB, CC, CD, TC, PC, DAB

```

```

*****
* READ VARIABLE VALUES AND PHYSICAL PROPERTIES OF THE VOC
*****
OPEN(UNIT=99, FILE='FLUX.DAT', STATUS='OLD')
READ(99, *, RESTIME, DAY, HOUR, TAVG, TDELTA, UTEN, CANOT,
$CA, CB, CC, CD, FC, PC, DRB
CLOSE(UNIT=99)
*****
* SET THE OTHER VARIABLES
*****
XL = 0.2
ALPHA = 9.E-8
H = 10.0
PI = 3.14159265
IFREQ = 1
*****
* SET TIME-RELATED VARIABLES AND INITIAL VALUES OF TIME
*****
TIME = RESTIME*3600
DELTA = 05
TLOW = DELT
CINCS = TIME/DELTA
N = INT(CINCS)
NE = N + 1
ELAPSED = HOUR/2400
ANGLE = (360*ELAPSED - 180.)*2*PI/360.
*****
* SET THE SPATIAL STEP SIZE
*****
ME = 1621
M = ME - 1
DX1 = 1./100.
DX2 = 1./2000.
DX12 = 1./((100. + 2000.)/2.)
*****
* ENTER ENVIRONMENT TEMPERATURES AND SOLAR RADIATION PARAMETERS
*****
TNOT = 65.
TDEGF = 1.8*TNOT + 32.
TNOTK = TNOT + 273.
TINF = -0.32815 + 0.96592*TAVG - 0.43503*TDELTA*COS(2*PI*ELAPSED)
$ - 0.14453*TDELTA*SIN(2*PI*ELAPSED)
$ + 0.09995*TDELTA*COS(4*PI*ELAPSED)
$ + 0.02450*TAVG*SIN(4*PI*ELAPSED)
TINFK = TINF + 273.
SIGMA = 5.669E-8
C = .8
TSURF = 40.
*****
* OPEN FILES FOR OUTPUT DATA
*****
OPEN(UNIT=2, FILE='TEMP.OUT', STATUS='NEW')
OPEN(UNIT=4, FILE='FLUX.OUT', STATUS='NEW')
OPEN(UNIT=3, FILE='AVG.OUT', STATUS='NEW')
OPEN(UNIT=8, FILE='FLUXI.OUT', STATUS='NEW')
*****
* INITIALIZE TEMPERATURE SOLUTION MATRIX
*****
DTAU = DELTA*ALPHA/XL**2
DO 7 I=2, M
IF(I.LT.20) DX = DX1
IF(I.GT.20) DX = DX2
IF(I.EQ.20) DX = DX12
AT(I) = 1.0
BT(I) = 2.*(1+DX**2/DTAU)
CT(I) = 1.0
*****

```

```

*****
* AT(2) = 0.
* TMAX = TIME*DTAU/DELTA
* HCOUNT = 0
*****
* CALCULATE THE DECLINATION OF THE SUN
*****
S = 1116.
PHI = 0.611
DNOT = 2*PI*DAY/365
DELTA = 0.006918 - 0.399912*COS(DNOT) + 0.070257*SIN(DNOT)
$ - 0.006758*COS(2*DNOT) + 0.000907*SIN(2*DNOT)
$ - 0.002697*COS(3*DNOT) + 0.001480*SIN(3*DNOT)
CONSTANT1 = -SIN(PHI)*SIN(DELTA)
CONSTANT2 = COS(PHI)*COS(DELTA)
*****
* INITIALIZE DIMENSIONLESS TEMPERATURES AND COUNTERS
*****
DO 3 I = 1, ME
FLOATI = I
THETA(I) = 1.0
TAU = 0.0
NCOUNT = 0
NPRINT = 0
ICOUNT = 0
MCOUNT = 0
*****
* DETERMINE TEMPORAL STEP SIZE
*****
40 IF(TIMET.GE.2140.) DELT = 10.
IF(TIMET.LT.2140.) DELT = 5.
IF(TIMET.LT.1140.) DELT = 2.
IF(TIMET.LT.540.) DELT = 1.
IF(TIMET.LT.240.) DELT = .5
IF(TIMET.LT.90.) DELT = .2
IF(TIMET.LT.30.) DELT = .1
DTAU = DELTA*ALPHA/XL**2
*****
* INCREMENT TIME STEP AND COUNTERS
*****
TAU = TAU + DTAU
TIMET = TIMET + DELT
ICOUNT = ICOUNT + 1
NCOUNT = NCOUNT + 1
NPRINT = NPRINT + 1
FLOATI = ICOUNT
*****
* CALCULATE AMBIENT TEMPERATURE AND RADIATION
*****
ELAPSED = ELAPSED + DELT/86400.
TINF = -0.32815 + 0.96592*TAVG - 0.43503*TDELTA*COS(2*PI*ELAPSED)
$ - 0.14453*TDELTA*SIN(2*PI*ELAPSED)
$ + 0.09995*TDELTA*COS(4*PI*ELAPSED)
$ + 0.02450*TAVG*SIN(4*PI*ELAPSED)
TINFK = TINF + 273.
ANGLE = ANGLE + 7.272052E-5*DELTA
COSZ = COS(ANGLE) + CONSTANT1 + CONSTANT2*COS(ANGLE)
SOLAR = 7.5*COSZ
IF(SOLAR.LT.0) SOLAR = 0.
TSURFK = TSURF + 273.
XK = 0.0698*(1 - 0.0003*(TDEGF - 32))*.17307
BETAT = XL*H/XK
Q = (SOLAR + SIGMA*((0.0552*TINFK**1.5)**4 - TSURFK**4))
XQ = Q*XL/(XK*(TNOT-TINF))
*****

```



```

6  VISC(I) = EXP(8105./(T(I) + 273.) - 22.76)
*
*  CALCULATE DIFFUSION COEFFICIENT FUNCTION
*
DO 290 I = 1, ME
290  F(I) = (VISCREF/VISC(I))*((2./3.)*(T(I) + 273.)/TREF)
*
*  SET INITIAL ARRAYS A, B, AND C
*
DO 1 I = 2, M
  IF(I.LT.20) DX = DX1
  IF(I.EQ.20) DX = DX2
  IF(I.GT.20) DX = DX2
  RATIO = DX*DX/DTAU
  GP(I) = 1./(1./F(I+1) + 1./F(I))
  G(I) = 1./(1./F(I) + 1./F(I-1))
  GOLD(I) = 1./(1./FOLD(I+1) + 1./FOLD(I-1))
  A(I) = G(I)
  B(I) = RATIO + GP(I) + G(I)
  C(I) = GP(I)
*
*  COMPUTE RIGHT-HAND SIDE VECTOR D
*
DO 5 I = 2, M
  IF(I.LT.20) DX = DX1
  IF(I.EQ.20) DX = DX2
  IF(I.GT.20) DX = DX2
  RATIO = DX*DX/DTAU
  D(I) = GOLD(I)*GAMMA(I+1)
  $ + (RATIO - GOLD(I) - GOLD(I-1))*GAMMA(I)
  DP(I) = GOLD(I)*GAMMA(I-1)
  $ + (RATIO - GPOLD(I) - GOLD(I-1))*GAMMAP(I)
  $ + GOLD(I)*GAMMAP(I-1)
  DPP(I) = GOLD(I)*GAMMAP(I+1)
  $ + (RATIO - GPOLD(I) - GOLD(I-1))*GAMMAP(I)
  $ + GOLD(I)*GAMMAP(I-1)
*
*  COMPUTE NEW DIMENSIONLESS CONCENTRATIONS
*
CALL TRIDIAG (ME, A, B, C, D, GAMMA, BETA, DX2)
B(2) = DX1*DX1/DTAU + GP(2) + G(2)
B(M) = DX2*DX2/DTAU + GP(M) + G(M)
CALL TRIDIAG (ME, A, B, C, DP, GAMMAP, BETA, DX2)
B(2) = DX1*DX1/DTAU + GP(2) + G(2)
B(M) = DX2*DX2/DTAU + GP(M) + G(M)
CALL TRIDIAG (ME, A, B, C, DPP, GAMMAP, BETA, DX2)
B(2) = DX1*DX1/DTAU + GP(2) + G(2)
B(M) = DX2*DX2/DTAU + GP(M) + G(M)
*
*  SET BOUNDARY VALUES
*
GAMMA(1) = GAMMA(2)
GAMMA(ME) = 0.0
GAMMAP(1) = GAMMAP(2)
GAMMAP(ME) = (GAMMA(H) - GAMMA(ME))/DX2
GAMMAP(1) = GAMMAP(2)
GAMMAP(ME) = (GAMMAP(M) - GAMMAP(ME))/DX2
*
*  SOLVE FOR GAMMA WITH PERTURBATION SOLUTION
*
DO 10 I=1, ME
FOLD(I) = F(I)
30  GAMMAP(I) = GAMMA(I) + GAMMAP(I)/BETA + GAMMAP(I)/BETA**2

```

```

FLUX (NCOUNT) = -DAB*F(ME)*CANOT*(3)*GAMMAT(ME) - 4)*GAMMAT(H)
S-GAMMAT(M-1))/(2.*XL*DX2)
IF (TIMET.LT.TIME) GO TO 55
*
*  PRINT DIMENSIONLESS CONCENTRATIONS WHEN APPROPRIATE
*
OPEN (UNIT=1, FILE='CONC.OUT', STATUS='NEW')
DEPTH = 1.
DO 27 I=1, ME
  DX = DX1
  IF(I.GT.20) DX = DX2
  WRITE(1,*) DEPTH, GAMMAT(I)
27  DEPTH = DEPTH - DX
55  CLOSE(UNIT=1)
  RETURN
END
*
*
*  SUBROUTINE TRIDIAG
*
*
*  SUBROUTINE TRIDIAG (ME, A, B, C, D, V, BETA, DX)
  DIMENSION V(ME), W(10001), G(10001), P(10001)
  DIMENSION A(ME), B(ME), C(ME), D(ME)
*
*  COMPUTE INTERMEDIATE ARRAYS
*
  H = ME - 1
  B(2) = B(2) - A(2)
  B(M) = B(M) - C(H)/(1.0+DX*BETA)
  W(2) = C(2)/B(2)
  G(2) = D(2)/B(2)
  DO 10 I = 3, M
    W(I) = C(I)/B(I) - A(I)*W(I-1)
    G(I) = (D(I) + A(I)*G(I-1))/B(I) - A(I)*W(I-1)
*
*  COMPUTE FINAL SOLUTION VECTOR V
*
  V(M) = G(M)
  DO 20 I = 2, M-1
    V(ME-I) = G(ME-I) + W(ME-I)*V(ME+1-I)
  RETURN
END
*
*
*  FUNCTION SIMPS ( A, B, N, F )
*
*
*  INITIALIZE PARAMETERS
*
  DIMENSION F(N)
  SUMEND = 0.0
  SUMRID = 0.0
*
*  EVALUATE SUMEND AND SUPRID

```

```

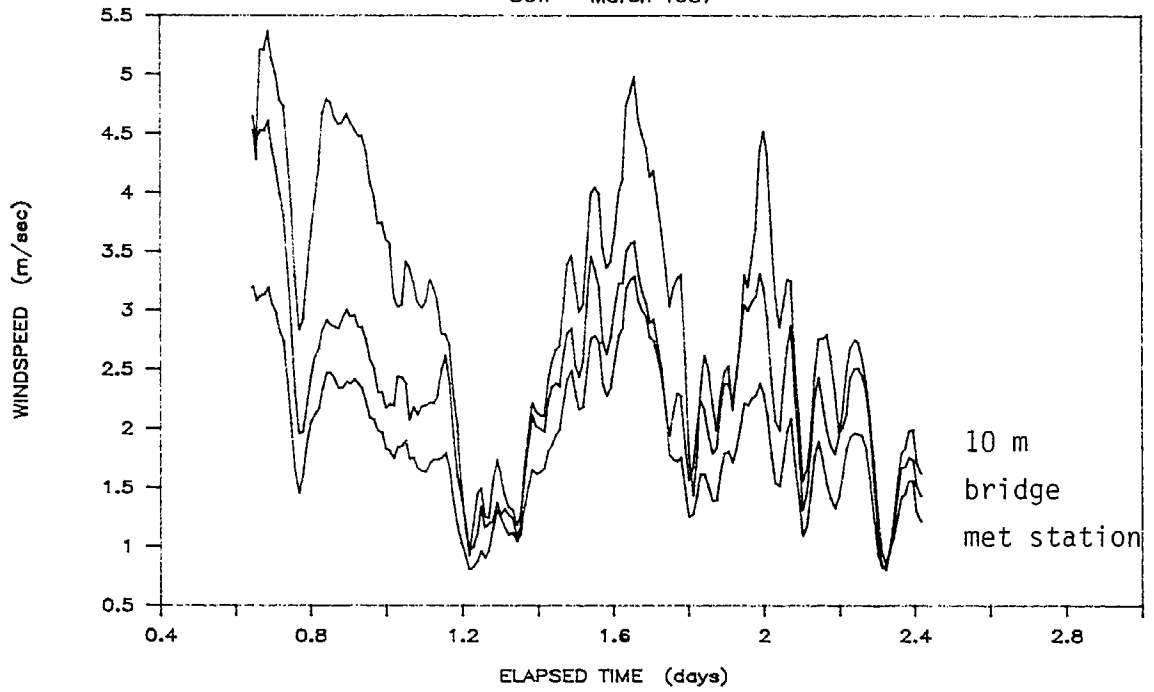
*
DO 1 K=2,N-2,2
IF(K.GE.1800) DELT = 10.
IF(K.LT.1800) DELT = 5.
IF(K.LT.1600) DELT = 2.
IF(K.LT.1300) DELT = 1.
IF(K.LT.1000) DELT = .5
IF(K.LT.700) DELT = .2
IF(K.LT.400) DELT = .1
IF(K.LT.200) DELT = .05
SUMEND = SUMEND + F(K+1)*DELT
IF(K.GT.1800) DELT = 10.
IF(K.LE.1800) DELT = 5.
IF(K.LE.1600) DELT = 2.
IF(K.LE.1300) DELT = 1.
IF(K.LE.1000) DELT = .5
IF(K.LE.700) DELT = .2
IF(K.LE.400) DELT = .1
IF(K.LE.200) DELT = .05
SUMMID = SUMMID + F(K)*DELT
1
*
*
*
RETURNS ESTIMATED VALUE OF THE INTEGRAL
SIMPS = (F(1)*0.05 + F(N)*10. + 4.*SUMEND + 2.*SUMMID)/3.
RETURN
END

```

Appendix F

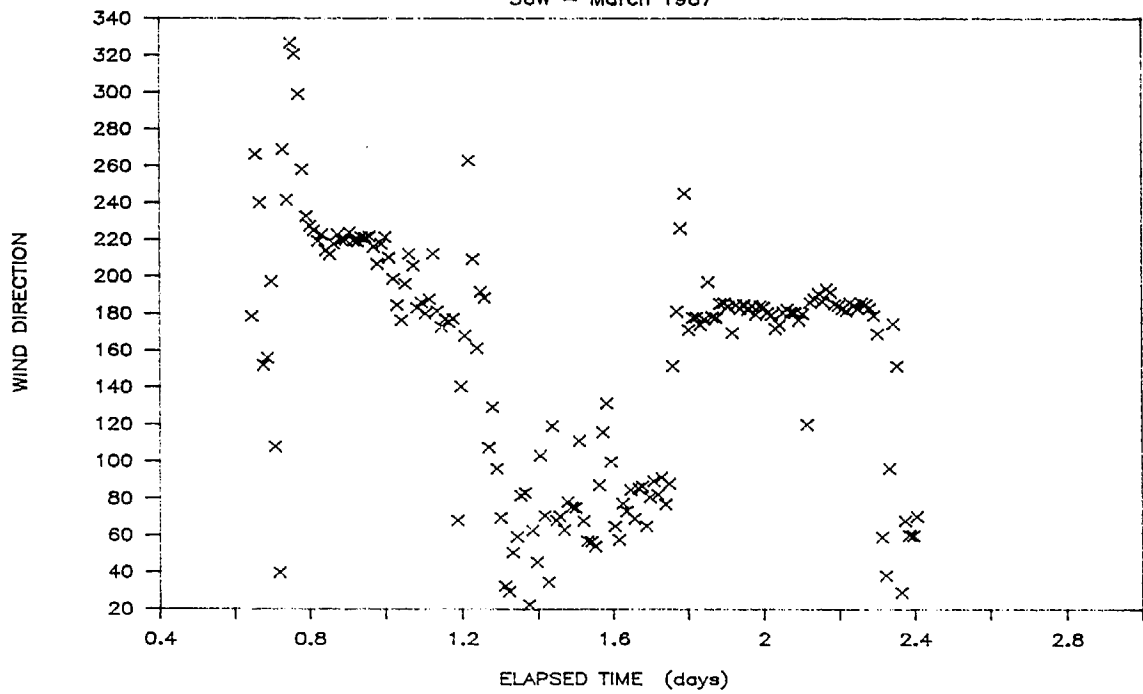
WINDSPEED

36W - March 1987



WIND DIRECTION

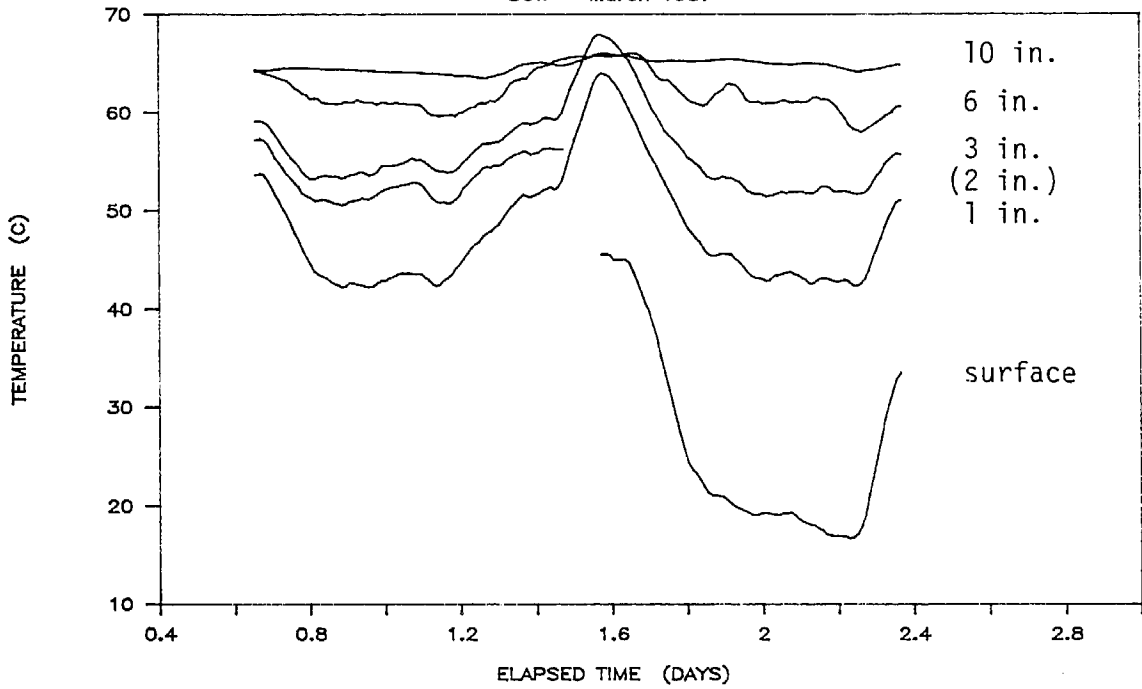
36W - March 1987



Appendix G - Temperature Data

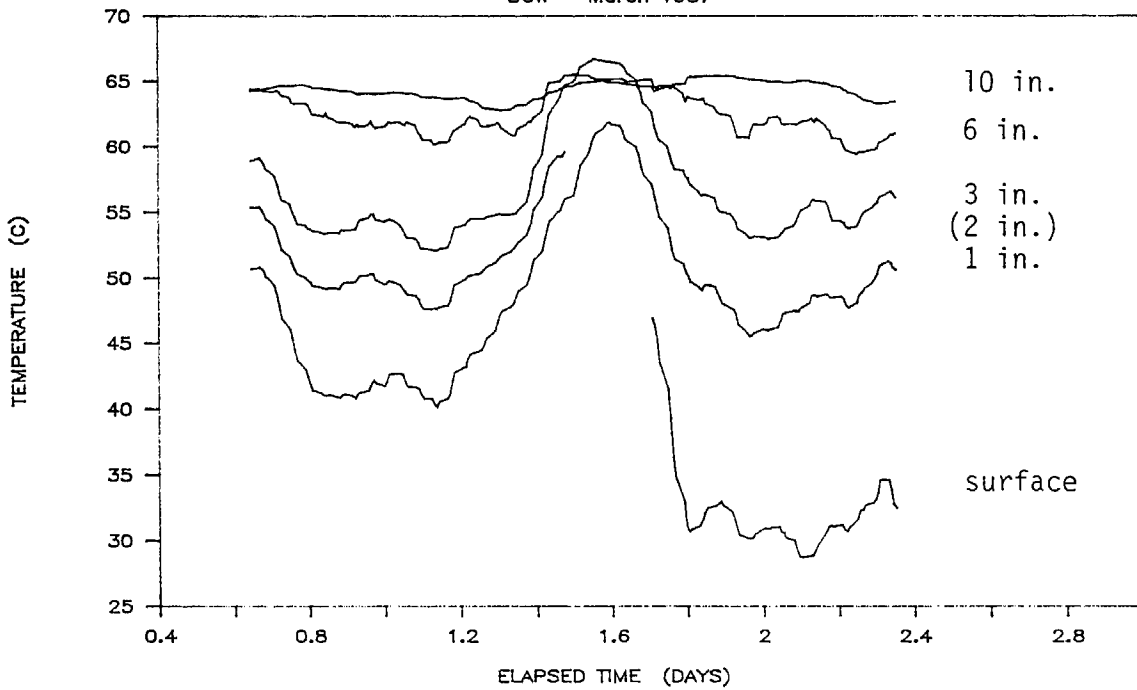
FLOAT A

36W - March 1987



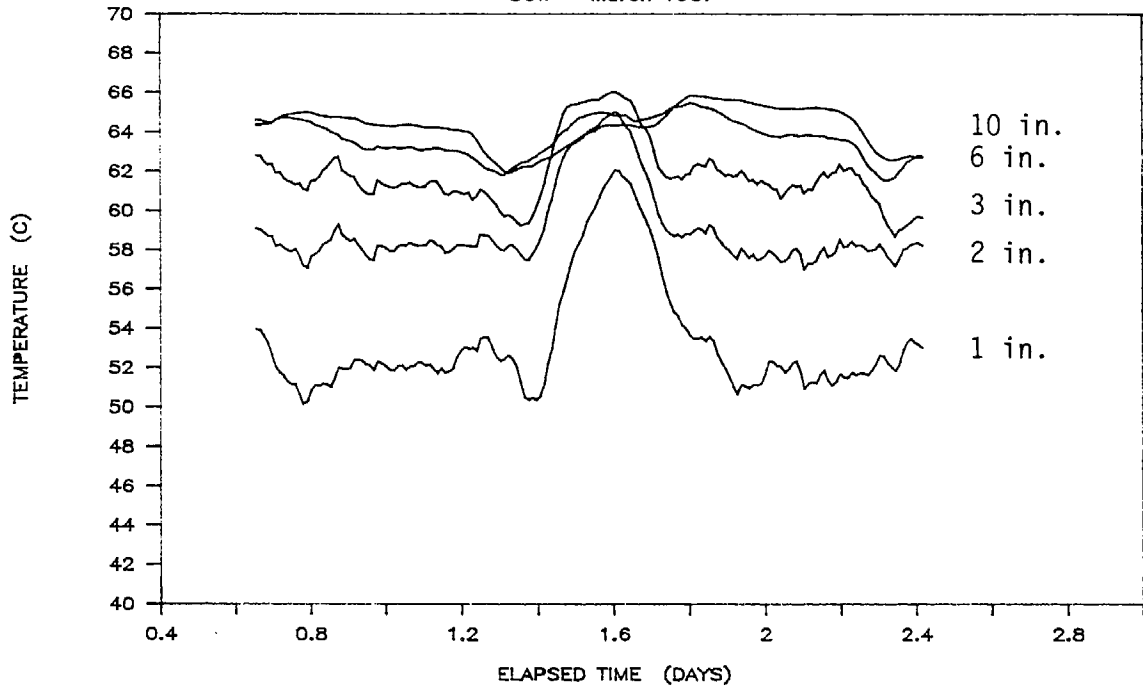
FLOAT B

36W - March 1987



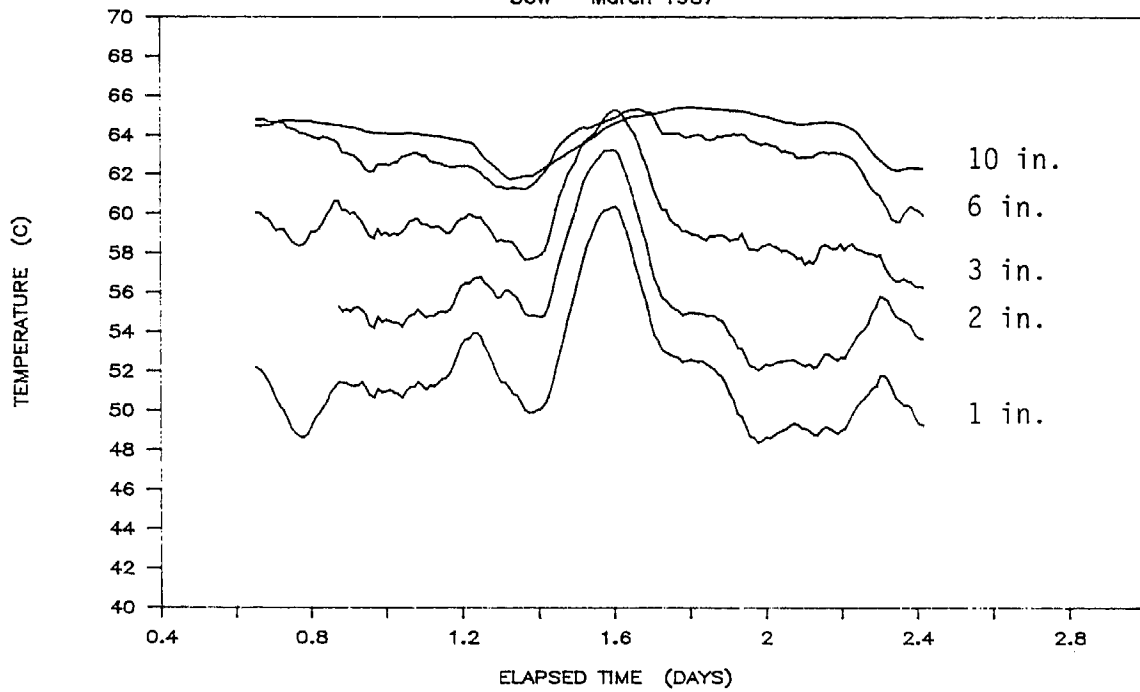
FLOAT C

36W - March 1987



FLOAT D

36W - March 1987



Appendix H
Residence Time Model Computer Program


```

SUBROUTINE NEWC
IMPLICIT REAL(A-H,O-Z)
IMPLICIT INTEGER(I-N)
COMMON XL, ME, DELT, TIME, T(10001), NCOUNT, F(100001)
COMMON THAX, FLUX(100001), NCOUNT, TIMET, CANOT, UTEN
COMMON CA, CB, CC, CD, TC, PC, DAB
DIMENSION A(10001), B(10001), C(10001), D(10001)
DIMENSION VISC(10001), FOLD(10001)
DIMENSION GAMMA(10001), GAMMAT(10001)
DIMENSION DE(10001), DPP(10001), GAMMAPP(10001)
DIMENSION G(10001), GP(10001), GOLD(10001), GPOLD(10001)
*****
* SET SPATIAL STEP SIZE
*****
M = ME - 1
FLOATH = M
DX1 = 1./100.
DX2 = 1./2000.
DTAU = 1./((100. + 2000.)/2.)
IF(TIMET.GT.DELT) GO TO 52
*****
* CALCULATE THE MASS-TRANSFER COEFFICIENT
*****
SCG = 2.35
POOLD = 300.
XK = (0.0292/3600.)*(UTEN**0.78)*(POOLD**0.11)*(SCG**0.67)
*****
* INITIALIZE DIMENSIONLESS CONCENTRATION
*****
DO 3 I = 1, ME
FOLD(I) = 1.0
FLOATH = I
GAMMA(I) = 1.0
GAMMAT(I) = 0.0
GAMMAPP(I) = 0.0
F(ME) = 1.
*****
* CALCULATE HENRY'S LAW CONSTANT
*****
*****
***** NOTE T FOR ISOTHERMAL CASE *****
52 T(ME) = 50.
X = 1 - (T(ME)+273.)/TC
PASAT = PC*EXP(1./((1.-X)))*(CA*X + CB*X**1.5 + CC*X**3 + CD*X**6)
H = 0.01*PASAT/I.
BETA = XL*X*N/H/(DAB*F(ME))
*****
* CALCULATE VISCOSITY
*****
TREF = 330.
VISCREF = EXP(8105./TREF - 22.76)
DO 6 I=1,ME
*****
***** NOTE T FOR ISOTHERMAL CASE *****
T(I) = 50.
6 VISC(I) = EXP(8105./T(I) + 273.) - 22.76)
*****
* CALCULATE DIFFUSION COEFFICIENT FUNCTION
*****
DO 290 I = 1, ME
290 F(I) = (VISCREF/VISC(I))**2./3.)*((T(I) + 273.)/TREF)
*****
* SET INITIAL ARRAYS A, B, AND C
*****

```

```

OPEN(UNIT=4, FILE='PROBIT.OUT', STATUS='NEW')
*****
* INITIALIZE DIMENSIONLESS TEMPERATURES AND COUNTERS
*****
MOUNT = 0
NCOUNT = 0
NPRINT = 0
4 ICOUNT = 0
*****
* DETERMINE TEMPORAL STEP SIZE
*****
40 IF(TIMET.GE.2140.) DELT = 10.
IF(TIMET.LT.2140.) DELT = 5.
IF(TIMET.LT.1140.) DELT = 2.
IF(TIMET.LT.540.) DELT = 1.
IF(TIMET.LT.240.) DELT = .5
IF(TIMET.LT.90.) DELT = .2
IF(TIMET.LT.30.) DELT = .1
IF(TIMET.LT.10.) DELT = .05
*****
* INCREMENT TIME STEP AND COUNTERS
*****
TIMET = TIMET + DELT
ICOUNT = ICOUNT + 1
NCOUNT = NCOUNT + 1
NPRINT = NPRINT + 1
FLOATH = ICOUNT
*****
* SET ISOTHERMAL TEMPERATURE
*****
DO 85 I=1,ME
FLOATH = I
85 TEMP(I) = 50.
*****
* CALL SUBROUTINE TO SOLVE MASS-TRANSFER PROBLEM
*****
* CALCULATE LOG-NORMAL DISTRIBUTION AND EMISSIONS
*****
14 CALL NEWC
PFLUX = FLUX(NCOUNT)*1.E6
IF(NCOUNT.LT.2) GO TO 16
ARGU = -(LOG(TIMET) - LOG(CMT))**2/(2*(LOG(SIGMAG))**2)
XLOGNORM = EXP(ARGU)/(2.*PI)**0.5*TIMET*LOG(SIGMAG)
XLOSS = SIMPS(TLOW, TIMET, NCOUNT, FLUX)
PROBFLUX(NCOUNT) = XLOGNORM*XLOSS
EMISSION = SIMPS(TLOW, TIMET, NCOUNT, PROBFLUX)
IF(NPRINT.NE.20) GO TO 16
WRITE(4,*) TIMET, EMISSION
NPRINT = 0
16 IF(IFREQ.NE.ICOUNT) GO TO 40
IF(TIMET.LE.TIME) GO TO 4
27 CLOSE(UNIT=4)
END
*****
*****
SUBROUTINE NEWC.FOR
*****
AN IMPLICIT FINITE-DIFFERENCE SOLUTION TO THE MASS-TRANSFER
PROBLEM WITH A PERTURBATION TECHNIQUE
USE THIS PROGRAM FOR LARGE BETA
*****
*****

```

```

DO 1 I = 2, M
  IF(I.LT.80) DX = DX1
  IF(I.EQ.80) DX = DX2
  IF(I.GT.80) DX = DX12
  RATIO = DX*DX/DTAU
  GP(I) = 1./(1./F(I+1) + 1./F(I))
  G(I) = 1./(1./F(I) + 1./F(I-1))
  GOLD(I) = 1./(1./FOLD(I+1) + 1./FOLD(I))
  A(I) = G(I)
  B(I) = RATIO + GP(I) + G(I)
  C(I) = GP(I)
1
*****
* COMPUTE RIGHT-HAND SIDE VECTOR D
*****
DO 5 I = 2, M
  IF(I.LT.80) DX = DX1
  IF(I.EQ.80) DX = DX2
  IF(I.GT.80) DX = DX12
  RATIO = DX*DX/DTAU
  D(I) = GPOLD(I)*GAMMA(I+1)
  $ + (RATIO - GPOLD(I) - GOLD(I))*GAMMA(I)
  $ + GOLD(I)*GAMMA(I+1)
  DP(I) = GPOLD(I)*GAMMAP(I+1)
  $ + (RATIO - GPOLD(I) - GOLD(I))*GAMMAP(I)
  $ + GOLD(I)*GAMMAP(I+1)
  DPP(I) = GPOLD(I)*GAMMAP(I+1)
  $ + (RATIO - GPOLD(I) - GOLD(I))*GAMMAP(I)
  $ + GOLD(I)*GAMMAP(I+1)
5
CONTINUE
*****
* COMPUTE NEW DIMENSIONLESS CONCENTRATIONS
*****
CALL TRIDIAG (ME,A,B,C,D,GAMMA,BETA,DX2)
B(2) = DX1*DX1/DTAU + GP(2) + G(2)
B(M) = DX2*DX2/DTAU + GP(M) + G(M)
CALL TRIDIAG (ME,A,B,C,DP,GAMMAP,BETA,DX2)
B(2) = DX1*DX1/DTAU + GP(2) + G(2)
B(M) = DX2*DX2/DTAU + GP(M) + G(M)
CALL TRIDIAG (ME,A,B,C,DPP,GAMMAP,BETA,DX2)
B(2) = DX1*DX1/DTAU + GP(2) + G(2)
B(M) = DX2*DX2/DTAU + GP(M) + G(M)
*****
* SET BOUNDARY VALUES
*****
GAMMA(1) = GAMMA(2)
GAMMA(M) = 0.0
GAMMAP(1) = GAMMAP(2)
GAMMAP(M) = (GAMMA(M) - GAMMA(ME))/DX2
GAMMAP(1) = GAMMAP(2)
GAMMAP(M) = (GAMMAP(M) - GAMMAP(ME))/DX2
*****
* SOLVE FOR GAMMA WITH PERTURBATION SOLUTION
*****
DO 30 I=1, ME
  FOLD(I) = F(I)
  GAMMAT(1) = GAMMA(I) + GAMMAP(I)/BETA + GAMMAP(I)/BETA**2
  FLUX(INCOUNT) = -DAB*F(ME)*CANOT*(3*GAMMAT(ME) - 4*GAMMAT(M)
  $ + GAMMAT(M-1))/(2.*XL*DX2)
  IF('TIMET.LT.TIME) GO TO 55
  RETURN
END
*****
*
*
*
*****

```

```

*****
* SUBROUTINE TRIDIAG
*****
SUBROUTINE TRIDIAG (ME,A,B,C,D,V,BETA,DX)
  DIMENSION V(ME), W(10001), G(10001), P(10001)
  DIMENSION A(ME), B(ME), C(ME), D(ME)
  *****
  * COMPUTE INTERMEDIATE ARRAYS
  *****
  M = ME - 1
  B(2) = B(2) - A(2)
  B(M) = B(M) - C(M)/(1.0+DX*BETA)
  W(2) = C(2)/B(2)
  G(2) = D(2)/B(2)
  DO 10 I = 3, M
    W(I) = C(I)/B(I) - A(I)*W(I-1)
    G(I) = (B(I) + A(I)*G(I-1))/B(I) - A(I)*W(I-1)
  *****
  * COMPUTE FINAL SOLUTION VECTOR V
  *****
  V(M) = G(M)
  DO 20 I = 2, M-1
    V(ME-I) = G(ME-I) + W(ME-I)*V(ME+1-I)
  RETURN
END
*****
*
*
*
*****
* FUNCTION SIMPS ( A, B, N, F )
*****
*****
* INITIALIZE PARAMETERS
*****
DIMENSION F(N)
SUMEND = 0.0
SUMHD = 0.0
*****
* EVALUATE SUMEND AND SUMHD
*****
DO 1 K=2,N-2,2
  IF(K.GE.1800) DELT = 10.
  IF(K.LT.1800) DELT = 5.
  IF(K.LT.1600) DELT = 2.
  IF(K.LT.1300) DELT = 1.
  IF(K.LT.1000) DELT = .5
  IF(K.LT.700) DELT = .2
  IF(K.LT.400) DELT = .1
  IF(K.LT.200) DELT = .05
  SUMEND = SUMEND + F(K+1)*DELT
  IF(K.GT.1800) DELT = 10.
  IF(K.LE.1800) DELT = 5.
  IF(K.LE.1600) DELT = 2.
  IF(K.LE.1300) DELT = 1.
  IF(K.LE.1000) DELT = .5
  IF(K.LE.700) DELT = .2
  IF(K.LE.400) DELT = .1
  IF(K.LE.200) DELT = .05
  SUMHD = SUMHD + F(K)*DELT
1
*****

```

```
* * *  
RETURNS ESTIMATED VALUE OF THE INTEGRAL  
SIMPS = (F(1)*0.05 + F(N)*10. + 4.*SUMEND + 2.*SUMHID)/3.  
RETURN  
END
```

II. VOLATILE ORGANIC EMISSIONS FROM SOIL

1.0 INTRODUCTION

The environmental impacts from leaky underground storage tanks, including those containing gasoline, are quite severe in California and are getting worse as more occurrences are reported. Up until September 30, 1986, 1790 cases of tank leakage had been reported with 458 cases adversely affecting the local groundwater (1). The remedial actions for these cases include excavation of the faulty units and replacement with approved storage vessels. The contaminated soil requires treatment or disposal at a Class I facility since this soil is viewed as hazardous waste. However, in California all Class I hazardous waste sites are scheduled for closure by 1990. Consequently, alternatives to disposal must be explored and include burning the soil to remove contaminants, landtreatment using biological activity, steam stripping, and soil aeration.

Soil aeration is the treatment option which is the least costly and therefore the most desirable for tank owners. However, the environmental impacts, in terms of air pollution, need to be carefully studied. This aspect of soil aeration is the objective of this research. The factors controlling the emission rates of contaminants into the atmosphere are numerous and involve vapor and aqueous phase diffusion, adsorption onto soil solids, biodegradation, and convection in the aqueous phase due to surface evaporation of water. It is the purpose of these initial experiments to serve as a basis for future theoretical and laboratory studies.

Study of volatilization from soil of anthropogenic contaminants, primarily pesticides, has a long history, particularly in the soil and environmental science disciplines. Those factors controlling volatilization of pesticides can be used as a basis for the study of gasoline and other hazardous waste problems due to the similar physical characteristics of the molecules. For example,

adsorption of the contaminants onto soil particles has been shown to be highly dependent upon soil conditions such as contaminant loading, soil moisture contents, and temperature. In several studies (5,8,21,23,24), emissions of pesticide from the soil was shown to be highly dependent upon soil moisture content and decreased to nearly zero for sufficiently low values of soil moisture. Temperature in the soil was shown to be very important in determining the vapor concentration in the soil and therefore the driving force for diffusion (5,21,23). Adsorption of pesticides was shown to obey a linear equilibrium partitioning between the vapor, aqueous, and solid phases for small soil pesticide concentrations (5,21). Transport mechanisms for soil contaminants have also been studied. Volatilization rates from the soil were shown to be dependent upon aqueous and vapor phase diffusion and upon convection of soluble contaminant in the aqueous phase (15, 22-24).

Though it is clear that transport of organic contaminants through and away from soils involves a complicated set of mechanisms, this paper does not attempt to address each separately. Instead, the objective is to present experimentally measured emission fluxes of gasoline from soil under controlled laboratory conditions. The following sections will describe the experimental method and describe the transport processes by correlating the emissions data with a simple model. The effect of a diurnal soil temperature cycle on VOC emissions from dry soil will be analyzed. In addition, a simple multicomponent emission rate model will be proposed and the effect of soil moisture on the diffusivity of a VOC in soil will be accounted for.

2.0 LABORATORY SIMULATOR DESIGN & PERFORMANCE

Description of Experimental Apparatus

The experimental apparatus used to obtain emission rates of VOC's from gasoline contaminated soils was of the headspace analysis type and is shown in Figures 1 - 3. The VOC's were allowed to move into the headspace above the soil surface by diffusion in vapor phase. Once in the headspace, the VOC's were carried to the detector by a pure airstream. Concentrations in the airstream were recorded on a total hydrocarbon basis using a FID detector and data acquisition system. The sections comprising the apparatus are discussed in more detail in the following paragraphs.

The air pretreatment section, shown in Figure 1, was designed to control the temperature, relative humidity (RH), and volumetric flow rate of the air sweeping the diffusion cell. Compressed air was passed through a column of "drierite" and activated carbon in order to adjust the air stream to near zero RH and hydrocarbon concentration. From this stream two precision metering valves controlled the volumetric flow rates of both dehydrated and completely saturated (100 RH) air streams. The dehydrated air stream flowed through a heat exchanger in order to adjust the temperature to the desired value. A water column maintained at the desired temperature of the experiment was used in order to adjust the temperature and RH of the saturated air stream. A constant temperature bath maintained the water column and the heat exchanger at the desired temperature. The two air streams were then allowed to merge and the resulting RH and temperature were recorded using a humidity/temperature probe and a Campbell Scientific 21X microdata logger. The volumetric flow rate of the air from the pretreatment section was controlled using a Matheson Model 603 flow meter.

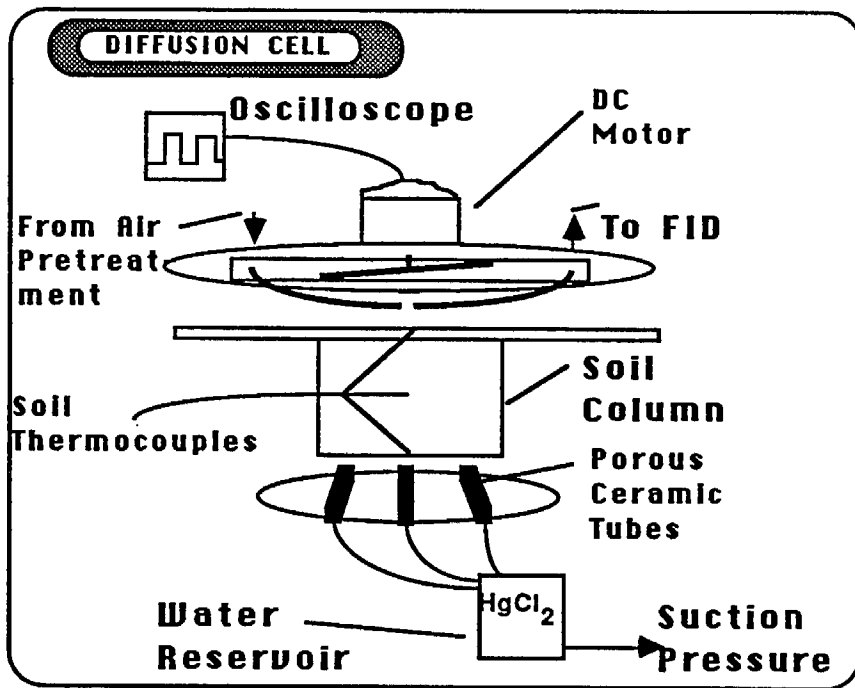


Figure 2. Experimental apparatus: diffusion cell.

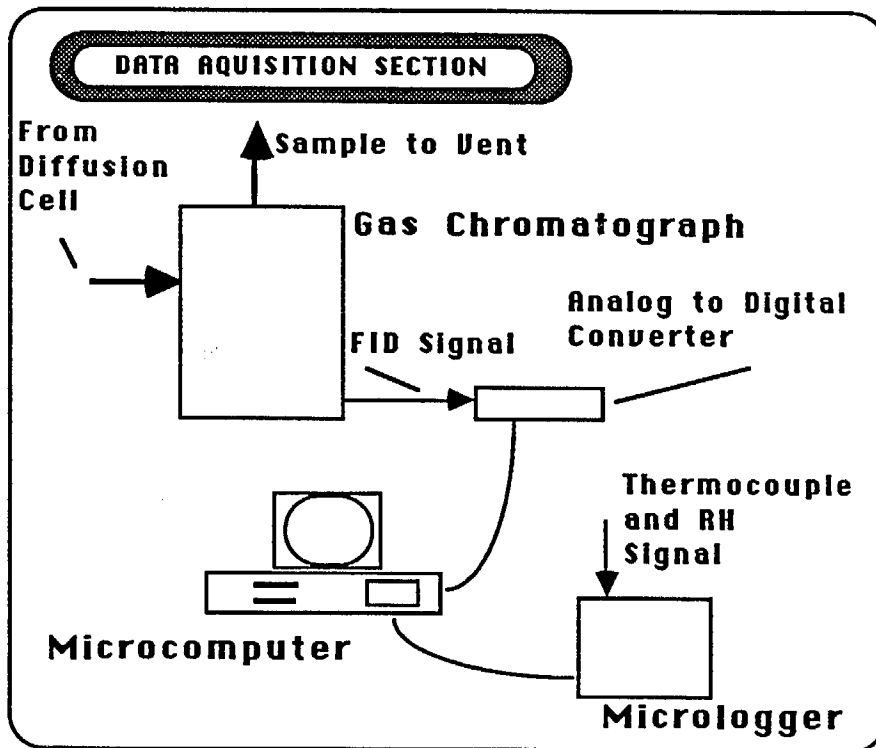


Figure 3. Experimental apparatus: data acquisition section.

2.1 Description Of Experimental Procedure

For each experiment contaminated soil was obtained by adding 500 mg of unleaded gasoline to 500 g of dry soil in order to have a 1000 ppm mixture. The soil was allowed to mix for 24 hours in a rotary tumbler to uniformly mix the gasoline and soil. Dry contaminated soil was transferred to the empty diffusion cell and lightly tamped such that approximately 150 g filled the soil column. In order to reduce gasoline vapor loss during the transfer operations the soil column was covered with a film of aluminum foil. Soil moisture was admitted to the base of the soil column in several experiments. While the soil was being wetted up to the surface, vapor loss was again reduced by covering the soil column. Due to this initial vapor loss, it was estimated that the uncertainty in the initial concentration of the soil was on the order of 10%.

Before an experimental measurement the soil moisture and temperature were allowed to attain equilibrium values. The same holds true for the sweep air RH and temperature. The reported soil temperature, air relative humidity, and air temperature were average values obtained from data taken over the entire duration of each experiment. A calibration of the FID using several concentrations of propane yielded a linear response and a response factor was obtained for each trial by measuring a known concentration of propane before and after each run. It was assumed that the response factor obtained through a calibration with propane was also valid for gasoline emissions. Since the molecules in gasoline are chemically similar to propane, in that they are all hydrocarbons, we believe that this is a good assumption. Concentration measurements for gasoline vapors were converted to ppm of propane through the calibration and then to mass concentration of gasoline.

After reaching equilibrium for all relevant environmental parameters for each run, the experiment was started. Emission data were taken at 1 minute intervals for the first 10 minutes and at 5 minute intervals thereafter for the 12 hour duration of each experiment. Environmental conditions of soil temperature, air relative humidity, and air temperature were recorded at 5 minute intervals throughout. The level of water in the reservoir was checked periodically in order to estimate the rate of evaporation and evaluate any disruptions that might occur in soil moisture content. Since biodegradation is not considered in this study, the reservoir was filled with a .1% HgCl_2 in order to suppress any soil microbial activity.

Methods for improving the accuracy of gasoline emission measurements have been evaluated based upon experiences gathered in this study. One such improvement is the control of soil moisture. The porous ceramic tubes situated at the bottom of the soil column did not perform adequately in all experiments in which soil moisture control was important. Often at the beginning of an experiment, a small convective flow of soil moisture from the top of the soil column to the bottom occurred. This was a result of admitting the sweep air to the diffusion cell and the slight over pressure which resulted drove some moisture out. In addition, the porous ceramic tubes were defective in that air from the diffusion cell was convected through the soil column from top to bottom during some experiments. This occurrence was only a small effect, however, one that is not desirable for this study.

One set of experimental trials was conducted on 3 dry soils from the same batch. A reduction in total emissions occurred between the 1st and 3rd sample due to the handling of the soil. This observation, reported in the results section for dry soils at 40 C, demonstrated the necessity of preparing

single batch soil samples by adding the proper mass of gasoline to 150 grams of dry soil instead of 500 grams. This improvement will reduce the uncertainty in future experiments on gasoline contaminated soils.

2.2 Diffusion Cell Mixing

The degree of mixing in the diffusion cell is important in these studies because of the necessity of comparing predictions of gasoline emissions with experimental results. Our mathematical model assumes uniform conditions at the air/soil interface. Also, in order to accurately evaluate the air mass transfer resistance, through a determination of k_g , a perfectly mixed diffusion cell was assumed. The validity of a perfectly mixed headspace above the soil surface in the diffusion cell will be presented next.

A variable speed impeller was the source of mixing in the headspace and was controlled by a variable power supply and monitored by an optical transducer and oscilloscope. In order to evaluate the degree of mixing, a step input of 20.3 ppm propane was introduced into the empty diffusion cell and the response recorded. Impeller speed was varied from 0 to 4000 RPM in steps of 1000 RPM and in this way, 5 traces were obtained. The response to ideal mixing is given by

$$C = C_0 (1 - \exp(-t/\tau)) \quad (1)$$

where $\tau = V/Q$. In these trials, $V = 32 \text{ cm}^3$ and $Q = 750 \text{ cc/min}$ yielding $\tau = 2.56$ sec. This value represents the characteristic time constant for the diffusion cell and is interpreted as the mean residence time for a molecule in the headspace. Figure 5 shows the response of the cell at an impeller speed of 4000 RPM and a comparison with eqn (1) using $\tau = 3.6$ sec shows good agreement. Responses at 1000, 2000, and 3000 RPMs were identical to this response indicating well-mixed

SOIL MOISTURE CONTENT vs. SUCTION

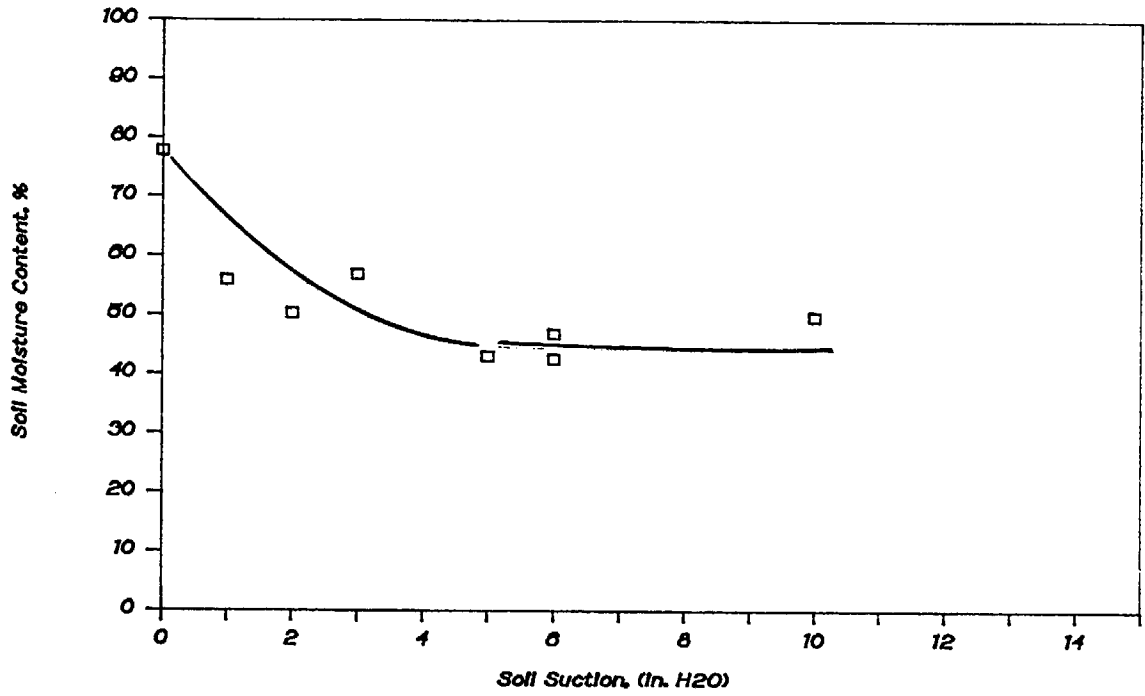


Figure 4. Soil moisture vs. suction pressure for soil sample. (Yolo Loam)

Response to a Step Input vs. RPM

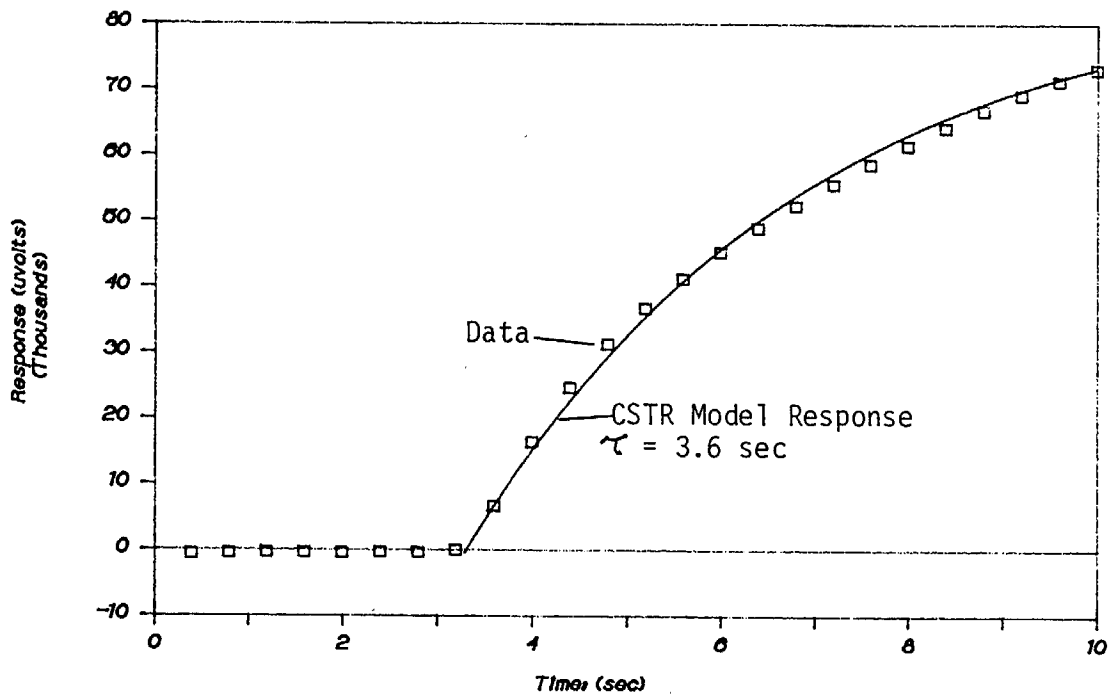


Figure 5. Evaluation of mixing in the headspace above the soil column.

conditions over the entire range of impeller speeds. The difference between the measured time constant (3.6 sec) and the expected value (2.56 sec) can be attributed to adsorption of the tracer (C_3H_{10}) onto metallic surfaces inside the diffusion cell. If adsorption is assumed to be in equilibrium at all times, a longer time constant can be theoretically derived. While this explanation is only a postulation, we believe enough evidence has been presented to assume ideal mixing in the diffusion cell headspace.

By having a well mixed headspace, the mass transfer resistance in the gas phase is uniform and the resistance to mass transfer in the gas phase can be determined experimentally. Figures 6 and 7 are the results of experimental measurements of mass transfer rates from solid naphthalene to the headspace. Concentrations of naphthalene in the headspace were measured as a function of RPM of the impeller. The mass transfer coefficient, k_g , in the gas phase can be calculated from a measure of the emission rate, N , and headspace concentration, C , by

$$k_g = N / (C^* - C) \quad (2)$$

where C^* = the vapor concentration of Naphthalene in equilibrium with solid Naphthalene at the temperature of the experiment. Figures 6 and 7 demonstrate that k_g varies linearly with RPM of the impeller over the 1000 to 4000 RPM. It will be shown in a later section that the magnitude of the gas phase mass transfer resistance will be negligible compared to the soil phase resistance, thereby justifying the use of the soil surface boundary condition in the Penetration model, which will be derived in a later section. Two plots of k_g vs RPM are presented because both dry soil and moist soil experiments were conducted. With dry soil experiments, the impeller causes entrainment of soil particles. A fine metal screen with openings on the order of 100 micrometers was used to eliminate entrainment. The reduction in k_g caused by the presence of this screen was measured and is shown in Fig 7. The presence of the screen reduces k_g by a small degree.

Diffusion Cell Mass Transfer Coeff.

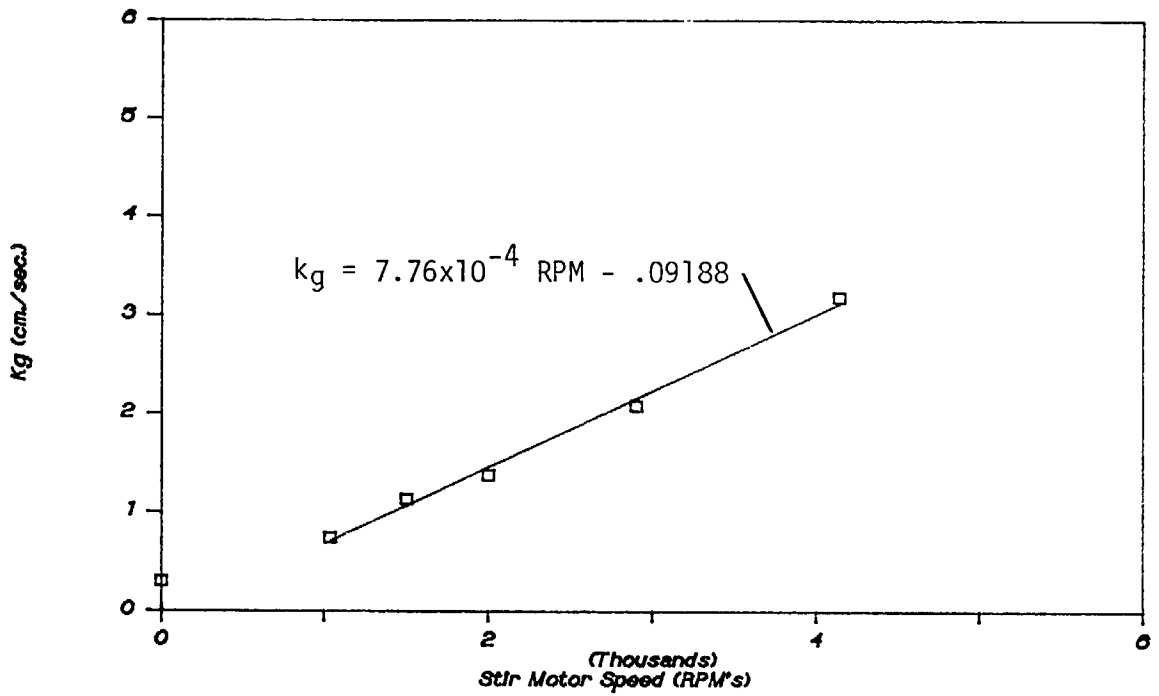


Figure 6. Gas phase mass transfer coefficient, k_g , above moist soil.

Diffusion Cell Mass Transfer Coeff.

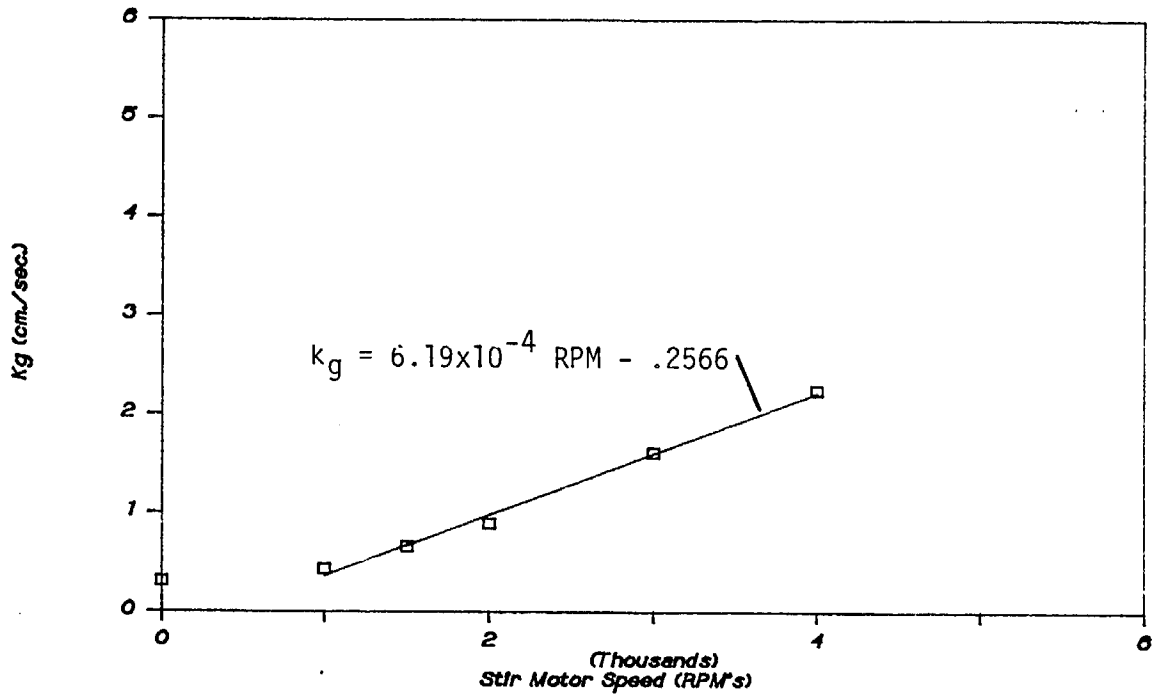


Figure 7. Gas phase mass transfer coefficient, k_g , above dry soil.

3.0 EXPERIMENTAL OBJECTIVES

The primary objective of this research is to experimentally measure VOC emission rates from gasoline contaminated soils under a variety of realistic environmental conditions. A possible strategy for these experiments is shown in Figure 8 where attention is placed at the corner of the cube, which represents three important parameters and their ranges. However, due to the complexity of the VOC emission process and the difficulties in controlling these three parameters during experiments, a simpler approach was taken. One series of experiments, in which the gasoline emission rates from moist soil were measured, was conducted at a soil temperature of $\sim 25^{\circ}\text{C}$. Another series of experiments was conducted using dry soil at both 40°C and 25°C . These measurements demonstrate the impact that soil moisture has on the emission rates of gasoline. Also, they provide a data set for comparison of theoretical models. In summary therefore, the primary objective was to provide data sets for the evaluation of theoretical emission rate models.

A second objective is to develop techniques for the measurement of soil transport parameters. The primary parameter of interest in gasoline contaminated soils is the "apparent" diffusivity of a gasoline component in the soil, D_{app} . The use of this transport parameter assumes that diffusion of the component is the dominant mechanism and includes the effects of adsorption to solid surfaces and into soil organic matter and also the meandering path through the soil. It will be shown that D_{app} can be approximately determined by fitting a simple model to experimental data.

The final objective is the study of the component make-up of unleaded gasoline by a gas chromatography - mass spectroscopy (GCMS) analysis. By doing so, we intend to identify the prevalence of toxic compounds and evaluate their

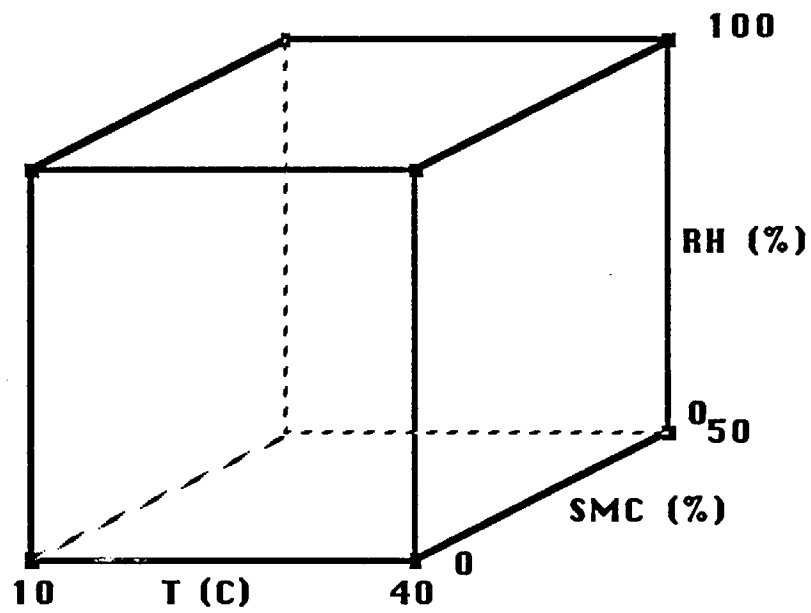


Figure 8. Ranges of soil temperature, SMC, and sweep air RH considered in experiments on emissions from gasoline contaminated soils.

potential for volatilization by observing the location of each on the GCMS spectrum. In addition, components in the highest concentrations can be identified and used in further studies for the determination of D_{app} for each. And finally, regions in the GC spectrum can be represented by surrogate compounds in order to more accurately predict emission rates in multicomponent models.

4.0 RESULTS OF INITIAL EXPERIMENTS

4.1 VOC Emission Rates From Gasoline Contaminated Soils

Gasoline emission measurements obtained thus far represent an initial attempt to characterize VOC fluxes from contaminated soils. Measurements were obtained for three cases; moist soil at 25°C and 35% SMC, dry soil at 25°C and at 40°C. Figures 9 and 10 represent typical emission rate measurements obtained in this case for dry soil at 41°C. Emission rates decrease quickly from relatively high rates to comparatively constant low rates at long times. The conditions in the diffusion cell were relatively constant over the entire period of the experiment as shown in Figure 10.

The trend in the emission rate data suggested comparison with the penetration model as shown in Figures 11 and 12.* A plot of emission rate data vs. $1/\sqrt{t}$ should result in a linear relationship if agreement with the penetration model exists. However, due to as yet unexplained complexities in the adsorption and diffusion process, the emission rates were greater at the beginning of the experiment and lower at long times when compared to a penetration model. This situation illustrates the difficulty in comparing multicomponent data with a single component model. Future efforts will focus on obtaining results for soils contaminated with single components in order to evaluate models and obtain transport parameters such as D_{app} .

*The penetration model is derived in section 5.1-1 and an analytical solution is obtained in Section 5.1-3.

Gasoline Emission Rate

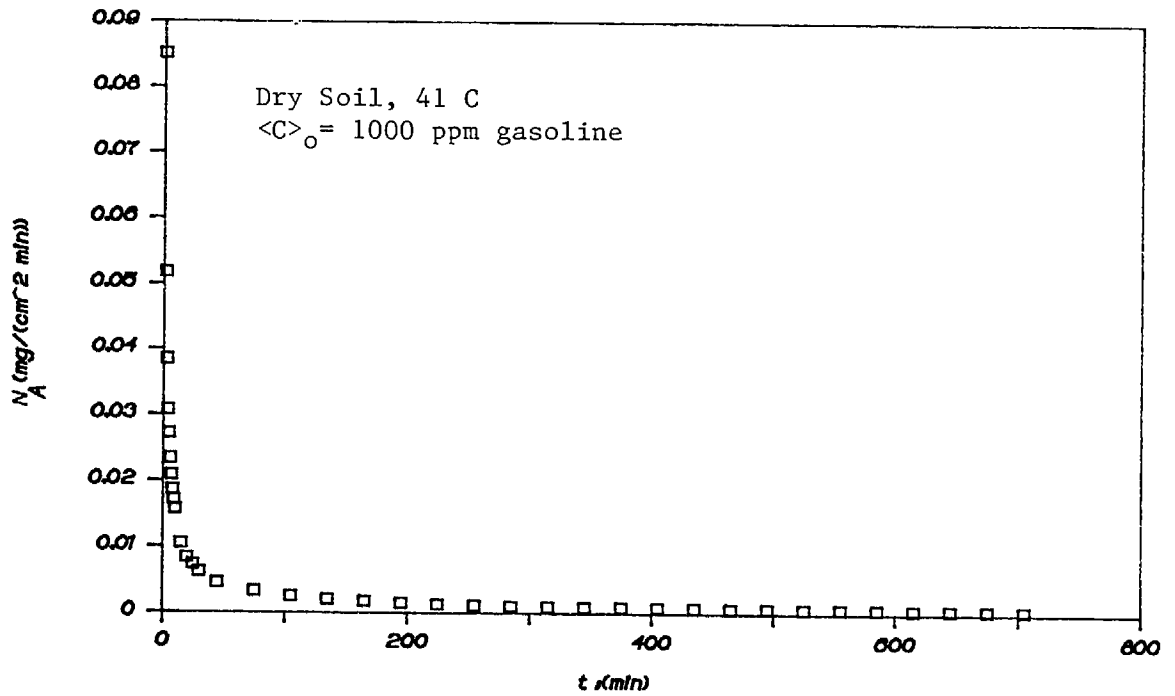


Figure 9. Emission rates of VOC from gasoline contaminated soil.

Experimental Results: Environ. Cond.

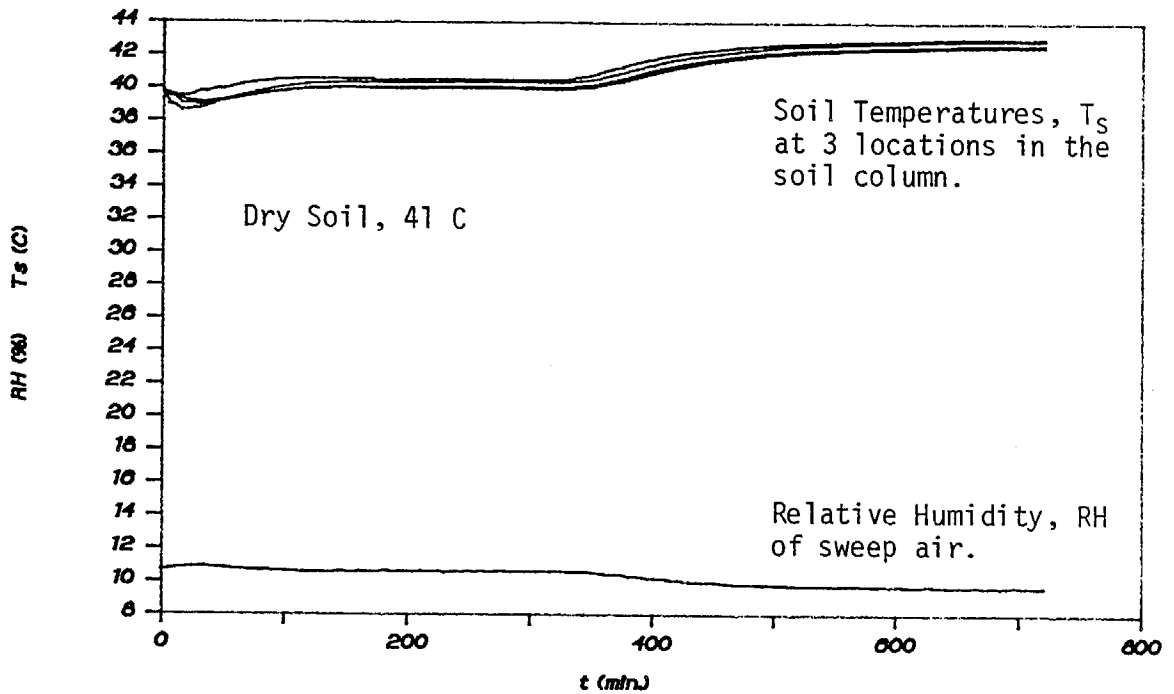


Figure 10. Environmental Conditions in the diffusion cell.

Penetration Model

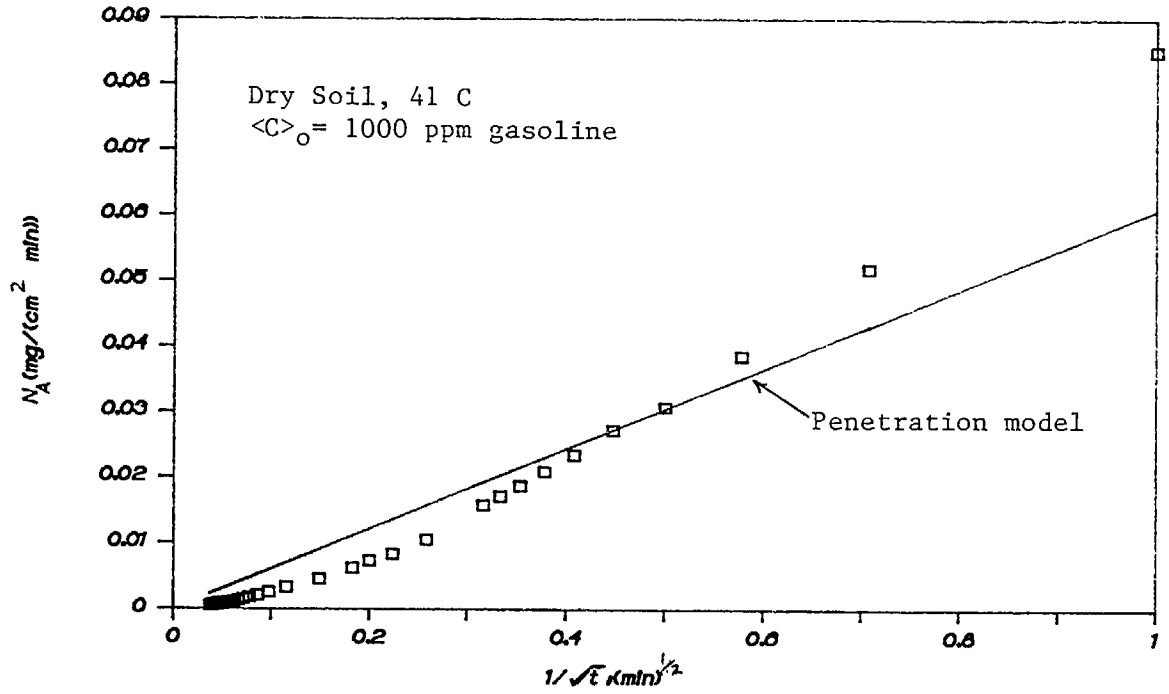


Figure 11. Best fit of the penetration model to the data.

Penetration Model

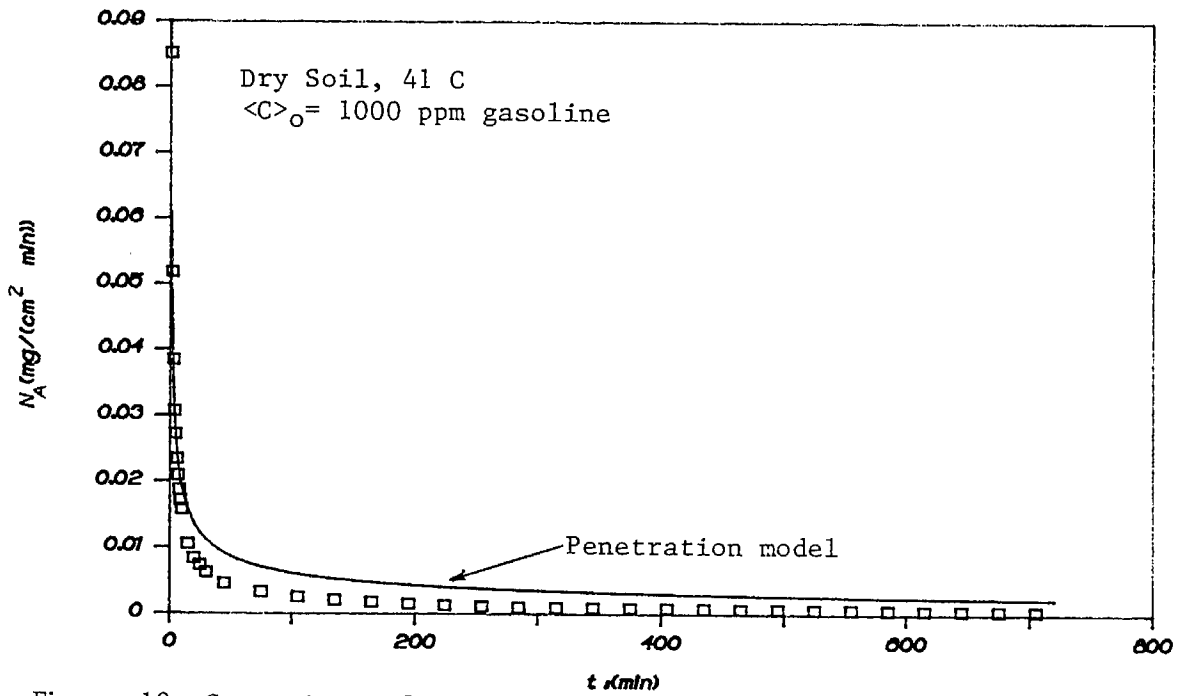


Figure 12. Comparison of penetration model with data.

4.2 Soil Transport Parameter, D_{app}

A summary of initial experimental results on VOC emissions from gasoline contaminated soils is included in Table 1. The environmental conditions under which the measurements were made and the date of measurement are listed. Also, the emission rate data were analyzed and several results are included. These are the total emission for a 12 hour period, M , the "apparent" diffusivity, D_{app} , and the percentage loss of the gasoline over a 12 hour period. It is apparent that soil moisture has a significant effect on the emission rate of gasoline from soils by comparing the value of M for dry & moist soils at 25°C. M values for moist soils are seen to be approximately 6 times the dry soil result. This is due to the competitive adsorption between water and gasoline and the preferential adsorption of water. The effect of soil temperature on the emissions of gasoline can be seen by comparison of dry soil results for 40°C and 25°C. Emissions of gasoline increase by a factor of 3-4 when temperature is increased from 25°C to 40°C which is consistent with the notion of increasing volatility with temperature.

The apparent diffusivity of gasoline in soil D_{app} , is difficult to interpret by itself. However, when compared to the diffusivity of a typical molecule in a non-adsorbing solid/gas media, D_{eff} , these experimental measurements of D_{app} are much lower. D_{eff} can be estimated theoretically or from tabulated results (3,20).

Table 1. A Summary of Initial Experimental Measurements of VOC Emissions from Gasoline Contaminated Soils; Initial Soil Concentration, 1000 ppm.

Date	$\langle T_s \rangle$ (°C)	θ (%)	RH (%)	M(12 hrs.) (mg/cm ²)	D_{app} (cm ² /sec)	Cumulative Loss(12 hrs.) (%)
3/6/87	24.7	35.2	51.1	2.175		30.7
3/7/87	25.4	35.6	57.9	2.016	1.36×10^{-5}	27.4
3/7/87	26.3	31.7	53.8	2.305		38.3
6/12/87	41.0	0	0	1.132	8.09×10^{-6}	15.72
7/9/87	42.0	0	0	1.028	1.17×10^{-5}	14.73
7/12/87	39.2	0	0	1.710	4.22×10^{-5}	24.16
7/13/87	41.0	0	0	1.430	2.80×10^{-5}	19.19
7/14/87	40.5	0	0	1.106	1.82×10^{-5}	15.36
6/16/87	25.0	0	0	0.3794	1.32×10^{-6}	5.21

Values for D_{app} measured from these experiments are at least two orders of magnitude smaller than D_{eff} . The dramatic decrease in apparent diffusivity of a gasoline component is due to the adsorption process between vapor and solid surfaces. Adsorption processes in the soil are therefore very important in understanding emission rates from soils.

4.3 Toxic Component Identification

A component analysis was performed on the unleaded gasoline used in these studies by the UC Davis Facility for Advanced Instrumentation. This characterization was obtained in order to evaluate the prevalence of toxic components in the gasoline. Also, we intend to represent the numerous components in gasoline by only a few representative species in future modeling studies. Table 2

lists the prevalence of benzene and other components having the benzene ring structure. Over 18% of the gasoline on a molar basis is composed of these molecules. In addition, these compounds are situated in the more volatile region of the GC spectrum and therefore are expected to be emitted at higher rates than most of the other gasoline components.

Figures 13 through 16 are the results of a GCMS analysis of unleaded gasoline. Component separation was performed by gas chromatography and the identification and quantitation by mass spectroscopy. Figure 13 is the gc spectrum of unleaded gasoline and shows the dominant component peaks as identified by scan number. Over 107 distinct components were detected by the analysis but only 5 were identified. Figures 14 through 16 are the mass spectra of a xylene isomer, of toluene, and benzene respectively. Figure 13 can be conveniently divided into 5 distinct regions of volatility and represented by one dominant compound in each region. Table 3 lists these representative compounds and their prevalence in the surrogate mixture representing gasoline. Region 1 on Figure 13 is represented by Toluene and accounts for the presence of $C_5 - C_7$ compounds. Xylene represents the $C_6 - C_8$ compounds, trimethylcyclohexane and n-nonane the C_9 compounds, and n-decane, the C_{10} compounds. These results can be used in future computational studies for VOC emissions from gasoline contaminated soils.

TABLE 2. Prevalence of Benzene, Toluene, and Xylene Isomers in Unleaded Gasoline.

<u>Components</u>	<u>Formula</u>	<u>%(Molar)</u>
Benzene	C_6H_6	1.35
Toluene	C_7H_8	5.30
Xylene Isomers	C_8H_{10}	11.71

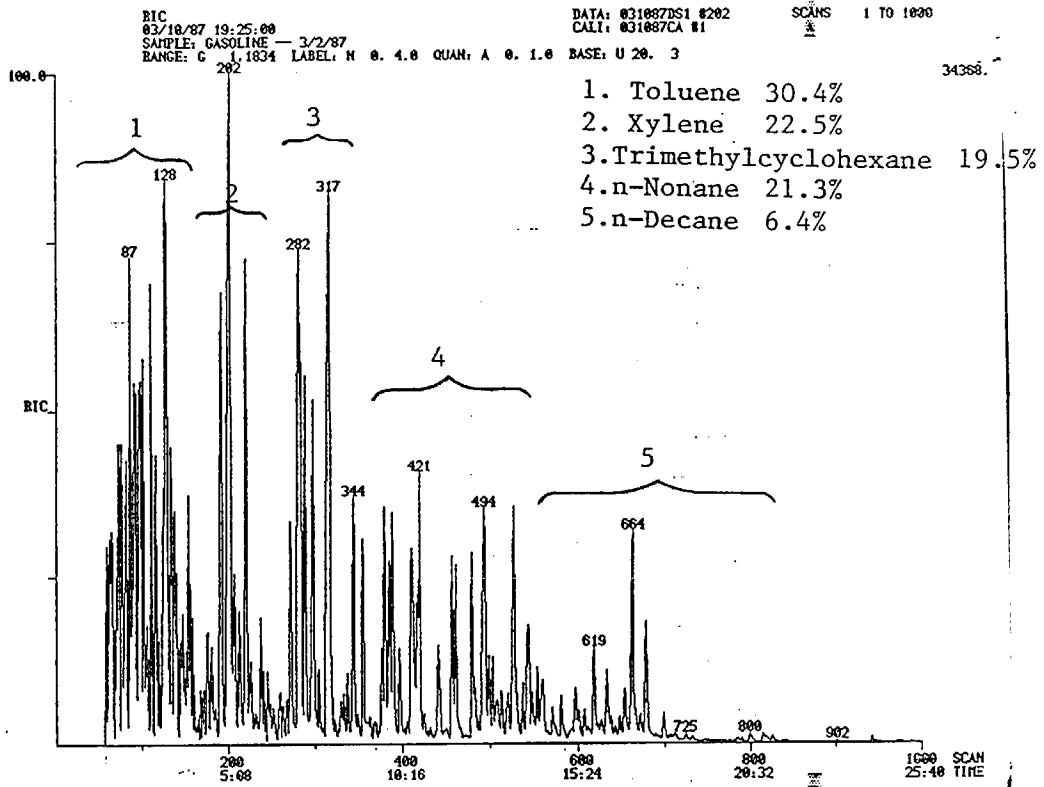


Figure 13. Gas chromatography - mass spectroscopy analysis of unleaded gasoline. 1 - 5 are representative components in the unleaded gasoline sample.

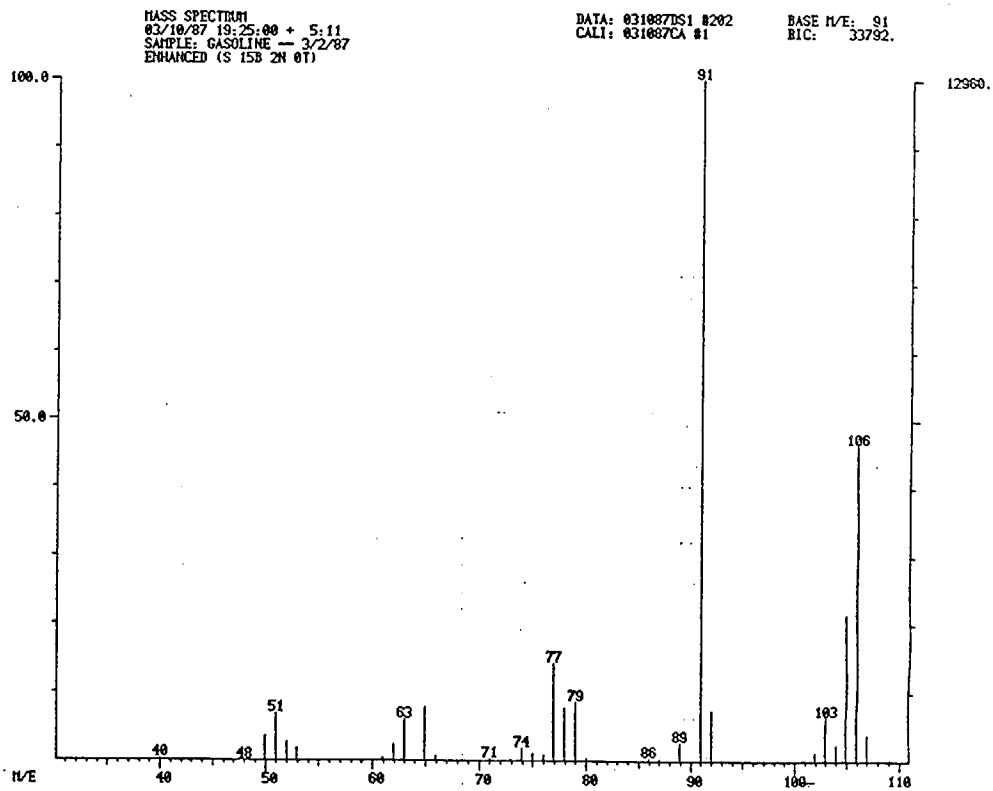


Figure 14. Mass spectrum of Xylene, MW = 106

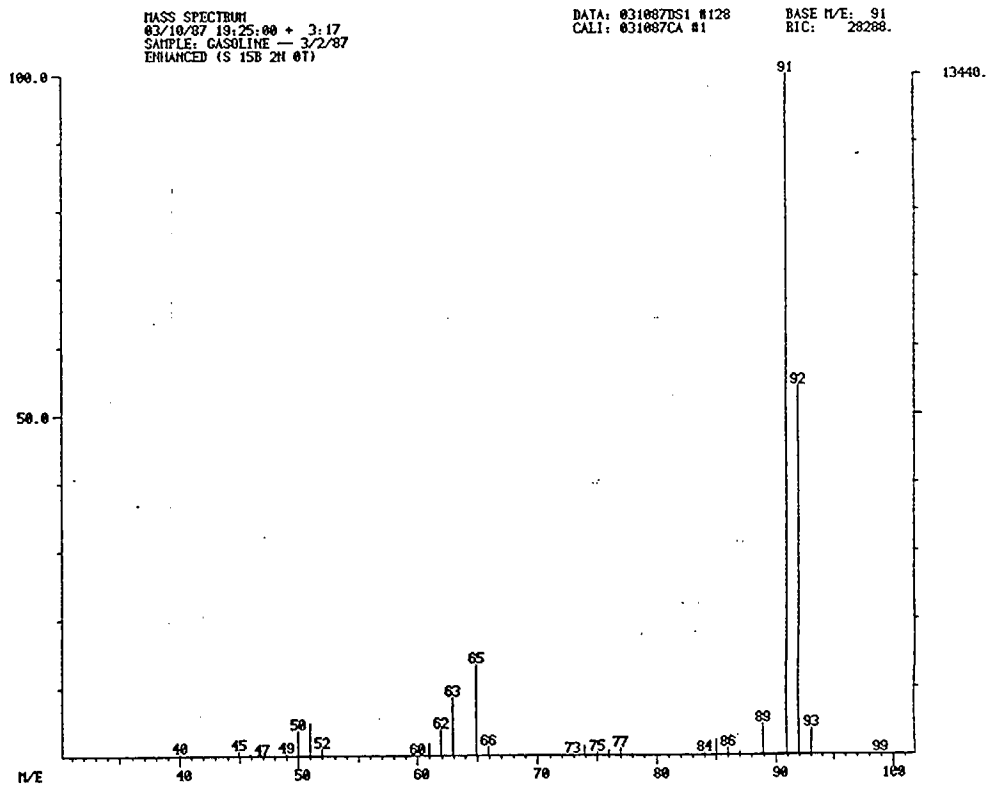


Figure 15. Mass spectrum of Toluene, MW = 92.

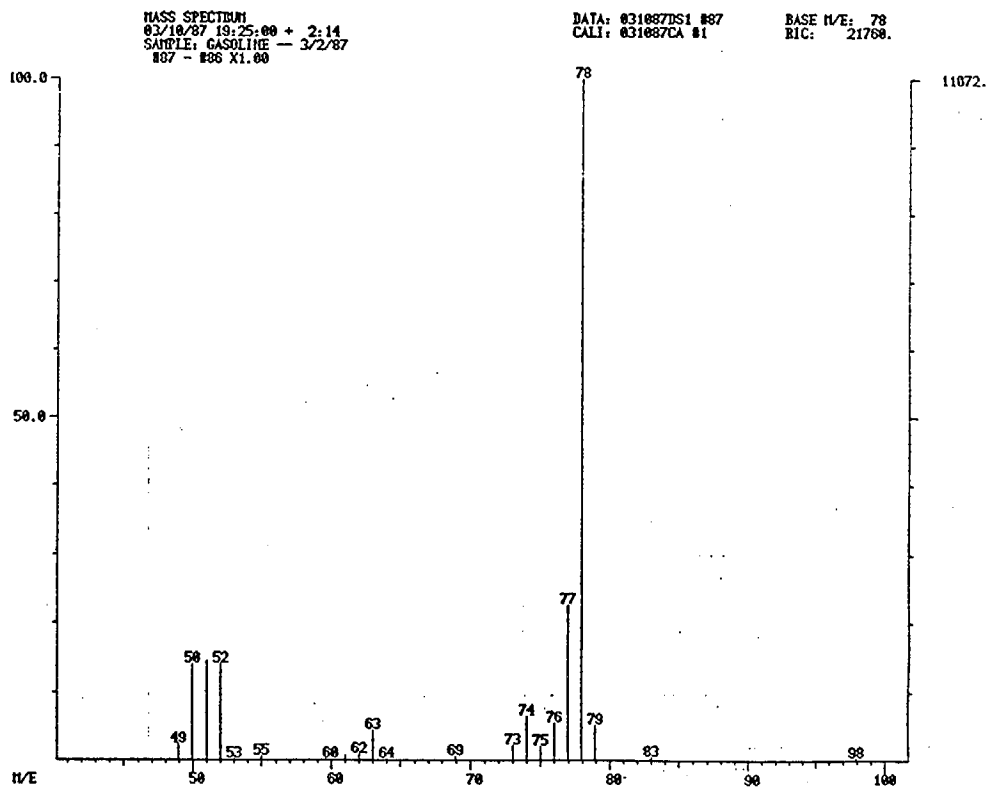


Figure 16. Mass spectrum of Benzene, MW = 78.

TABLE 3. Representative Compounds in Unleaded Gasoline

<u>Component</u>	<u>Range</u>	<u>MW</u>	<u>D_{AB}</u>	<u>%(Molar)</u>
Toluene	C ₅ -C ₇	92.15	.076	30.365
Xylene	C ₇ -C ₈	106.17	.0699	22.486
Trimethyl Cyclohexane	C ₉	126.24	.0630	19.451
n-Nonane	C ₉	128.26	.0623	21.348
n-Decane	C ₁₀	142.29	.0589	6.350

4.4 Soil Moisture Content Effect on Emission Rates

A study was conducted recently to determine the effects of soil bulk density, soil moisture, and air-filled porosity on the steady-state diffusion of benzene in soil (13). As a result of experiments, the authors evaluated the correctness of the Millington and Quirk (16) relation

$$D_{\text{eff}} = D_{\text{AB}} (P_a^{10/3} / P_T^2)$$

The effective diffusivity, D_{eff} , is influenced by the presence of soil particles and is decreased by a reduction in the soil cross-sectional area available for diffusion by the contaminant and also by the meandering path required for diffusion through the soil. The presence of soil moisture reduces D_{eff} by closing off a fraction of the pores and also reducing the cross-sectional area in other pores.

The soil moisture content is incorporated into this relation through the air-filled porosity. When the soil moisture is measured as cm^3 water/ cm^3 soil, then air-filled porosity can be calculated from P_T and the soil moisture content, P_w

$$P_a = P_T - P_w$$

The bulk density influences the effective diffusivity through the total porosity. Through an independent measurement of the bulk density of a dried soil sample, ρ_B , and its particle density, ρ_p , the total porosity can be calculated

$$P_T = 1 - \frac{\rho_B}{\rho_p}$$

In the experiments, the authors (13) measured the diffusion rates of benzene through soils of varying soil moisture. This fact leaves open the question of what fraction of the measured emissions occurred through the water phase. It was pointed out that when the solubility of benzene in water is small enough, the diffusion through the water phase is negligible. Chemicals with partition coefficients between the soil water and soil air much smaller than 10^4 will diffuse mainly in the vapor phase. Those chemicals having a partition coefficient much greater than 10^4 diffuse mainly through the aqueous phase (6, 7, 13, 14).

This expression for the effective diffusivity was shown to be valid by comparison with experimental measurements (13). This expression should be used only for VOC's having the appropriate partition coefficient between soil/water and soil/air.

5.0 MATHEMATICAL PREDICTIONS OF VOC EMISSION RATES FROM GASOLINE CONTAMINATED SOILS.

Any mathematical descriptions of VOC emission rates from contaminated soils should be as rigorous and detailed as possible. In the formulation of the model the transport mechanisms of importance should be incorporated in order to describe the physics of contaminant transport to the greatest possible degree. However, it soon becomes practical to limit the description to only the most dominant transport mechanisms. Such is the case for gasoline emissions from soils where vapor phase diffusion, adsorption to the solid soil particles, and absorption into soil organic matter are of major concern.

A reasonably complete summary of transport processes relevant to contaminant movement through and out of soils is included in Table 4. Also, included are the model parameters corresponding to that particular process. For gasoline contaminated soils, vapor phase diffusion is most important because of the high vapor pressures typical of gasoline components, the low solubilities of these components in water, and the low rate of biodegradation compared to the rate of volatilization. The work of Jury et. al. (9-12) have demonstrated how soil pesticides can be separated into 3 categories of compounds based upon, primarily, volatility considerations.

In the process of evaluating experimental data acquired during laboratory measurements of gasoline volatilization from soils, the Penetration model correctly predicts the trend in experimental emission rate data. The processes described by this type of model are vapor phase diffusion, adsorption to soil particle surfaces, and absorption into soil organic matter. In its derivation, the penetration model incorporates a linear adsorption constant relating vapor phase and surface concentrations. In addition, the model assumes constant physical and chemical properties of the component under consideration. These properties are listed in Table 5. These assumptions are good for the set of experiments obtained thus far because temperature (which affects both diffusivity and adsorption constant) in the soil was maintained at a nearly constant value. As a final consideration, the penetration model requires that the concentration of contaminant at the soil

TABLE 4. Transport Processes For Contaminant Chemicals Through Soils.

TRANSPORT PROCESS	MODEL PARAMETERS
Vapor Phase Diffusion	$\epsilon_V, D_V, a_V, \theta, K_H,$
Liquid Phase Diffusion	$\epsilon_V, K_D, a_V, \theta, D_L$
Vapor Phase Convection	$K_H, \Delta P$
Liquid Phase Convection	$\theta, V_E, K_D,$
Biodegradation	μ

TABLE 5. Physical & Chemical Properties Of Importance In The Penetration Model

D_{eff}	The effective diffusivity of species i through a soil of known water content & void space. (cm^2/sec).
K_H	Henry's Law Constant for Adsorption (cm^{-1}).
a_V	Surface Area per unit Volume of Soil (cm^{-1}).
ϵ_V	Void fraction of vapor in the soil.

surface be zero. This approximation is an excellent one due to the much greater mass transfer resistance inside the soil compared to that in the air phase above the soil; $\frac{1}{k_s} \gg \frac{1}{k_g}$. The Penetration model is explained further in a later section of this report.

5.1 Mathematical Model of Diffusion/Adsorption of Gasoline Components in a Soil Under a Diurnal Temperature Cycle.

In order to analyze the effects of a time varying temperature cycle on the emissions from soils, a simple diffusion model will be derived for a dry soil. The temperature fluctuations will affect the adsorption of contaminant onto the soil surface and into soil organic matter. An increase in temperature will cause less adsorption; thereby increasing the vapor phase concentration of the species. Larger emissions occur out of the soil surface under this condition due to the increased diffusion driving force inside the soil column. The underlying question to be addressed is by how much the emissions are increased or decreased by the influence of a diurnal temperature cycle in the soil. For comparison purposes, an isothermal soil column at the mean temperature, \bar{T} , will be considered.

5.1-1 Model Formulation

The physical situation to be analyzed is diffusion and adsorption of a gasoline component in a dry soil. The soil is assumed to be contaminated uniformly to a finite depth and the compound of interest is adsorbed to the soil surfaces. The soil is assumed to be uniform with constant bulk density and void fraction. The governing partial differential equation describing this physical situation is derived in Appendix I and is given by

$$\epsilon_Y \left(1 + \frac{a_V}{K_H \epsilon_Y}\right) \frac{\partial \langle C_A \rangle^Y}{\partial t} = \frac{\partial}{\partial z} \left(\epsilon_Y D_{\text{eff}} \frac{\partial \langle C_A \rangle^Y}{\partial z} \right) \quad (1)$$

$$@ t = 0 \quad @ z < \infty \quad \langle C_A \rangle^Y = \langle C_A \rangle_0^Y \quad (2)$$

$$@ z = 0 \quad t > 0 \quad \langle C_A \rangle^Y = 0 \quad (3)$$

$$@ z = \infty \quad t > 0 \quad \langle C_A \rangle^Y = \langle C_A \rangle_0^Y \quad (4)$$

where

$\langle C_A \rangle^Y$ = the intrinsic phase average concentration of species A in a small volume of soil ($\frac{\text{moles}}{\text{cc}}$)

$$\langle C_A \rangle^Y = \frac{1}{V_Y} \int_{V_Y} C_A dv$$

$\langle C_A \rangle_0^Y$ = the initial intrinsic phase average soil concentration of species A ($\frac{\text{moles}}{\text{cc}}$)

This equation describes the rate of change of the average concentration of species A in a small volume of the vapor phase due to the diffusion of A and the adsorption of A. The boundary conditions as stated by equation 4 implies that the soil is contaminated to an infinite depth. This description, while not strictly realistic, closely approximates the conditions in the soil at short times. A completely equivalent form of eqns 1 - 4 using the total soil concentration, $\langle C_A \rangle = \epsilon_Y \langle C_A \rangle^Y + a_V K_H^{-1} \langle C_A \rangle^Y$ is given by

$$\frac{\partial \langle C_A \rangle}{\partial t} = \frac{1}{(\epsilon_Y + a_V/K_H)} \frac{\partial}{\partial z} \left(\epsilon_Y D_{\text{eff}} \frac{\partial \langle C_A \rangle}{\partial z} \right) \quad (5)$$

finite depth and the compound of interest is adsorbed to the soil surfaces. The soil is assumed to be uniform with constant bulk density and void fraction.

The governing partial differential equation describing this physical situation is derived in Appendix I and is given by

$$\left(1 + \frac{a_V}{K_H \epsilon_Y}\right) \frac{\partial \langle C_A \rangle^Y}{\partial t} = \frac{\partial}{\partial z} \left(D_{\text{eff}} \frac{\partial \langle C_A \rangle^Y}{\partial z} \right) \quad (1)$$

$$\text{@ } t = 0 \quad 0 < z < \infty \quad \langle C_A \rangle^Y = \langle C_A \rangle_0^Y \quad (2)$$

$$\text{@ } z = 0 \quad t > 0 \quad \langle C_A \rangle^Y = 0 \quad (3)$$

$$\text{@ } z = \infty \quad t > 0 \quad \langle C_A \rangle^Y = \langle C_A \rangle^Y \quad (4)$$

where

$\langle C_A \rangle^Y$ = the intrinsic phase average concentration of species A in a small volume of soil ($\frac{mg}{cc}$)

$$\langle C_A \rangle^Y = \frac{1}{V_Y} \int_{V_Y} C_A dv$$

$\langle C_A \rangle_0^Y$ = the initial intrinsic phase average soil concentration of species A ($\frac{mg}{cc}$)

This equation describes the rate of change of the average concentration of species A in a small volume of the vapor phase due to the diffusion of A and the adsorption of A. The boundary conditions as stated by equation 4 implies that the soil is contaminated to an infinite depth. This description, while not strictly realistic, closely approximates the conditions in the soil at short times. Equation 1, the conservation equation for species A in soil, can be solved for the average concentration of A in the vapor phase as a function of time t, and depth, z. This will be solved for both isothermal soil conditions and for a diurnal fluctuation in soil temperature. The flux of species A out of the soil surface at $z = 0$ can be evaluated as a function of time and a comparison of the two cases made (isothermal & non-isothermal). It is possible that the emission flux of A at $z = 0$ can be described adequately using the isothermal case evaluated at the mean temperature of the soil.

Temperature fluctuations in the soil result from the diurnal heating and cooling of the soil by solar heating during the day and by convective/radiation cooling at night. The classic solution to the soil temperature profile can be obtained from many sources (2,4,17,20) and is given by

$$\langle T_s \rangle (z,t) = \bar{T} + \Delta T e^{-z(\frac{\omega}{2k})^{1/2}} \sin(\omega t + z(\frac{\omega}{2k})^{1/2}) \quad (5)$$

In addition, the temperature dependence of the linear adsorption coefficient and the vapor phase diffusivity of species A are given by (19)

$$K_H = RT K_{Ho} \exp \left[- \frac{\Delta H_a}{RT} \right] \quad (6)$$

$$\Delta H_a \sim 5 \text{ kcal/mol}$$

$$R = 1.987 \times 10^{-3} \text{ kcal/(mol K)}$$

$$K_{Ho} = \text{pre exponential constant} = 1.6434 \times 10^6 \text{ cm}^{-1}$$

$$D_{AB} = D_{AB}(300) \left(\frac{T}{300} \right)^{1.75} \quad (7)$$

$$D_{AB}(300) \sim .08 \text{ cm}^2/\text{sec} \quad (\text{C}_6\text{H}_{12} \text{ in Air})$$

$$A = \text{C}_6\text{H}_{12}$$

$$B = \text{Air}$$

For the purpose of this analysis, the value of K_H was obtained from experimental data by a method outlined in Appendix II. As a result, the value of the pre exponential factor K_{Ho} was obtained. The value of the diffusivity of the gasoline component cyclohexane, C_6H_{12} , in Air was obtained by using a correlation in the literature(18). Cyclohexane was chosen to represent a typical gasoline component however other components present in gasoline could just as easily have been substituted with similar results.

5.1-2 Model Predictions

Equations 1 - 4 were solved using eqn 5 to describe the soil temperature variation and using eqns 10 and 11 to describe the temperature dependence of the Henry's Law adsorption coefficient and the diffusivity. The initial concentration of cyclohexane in dry soil used in this analysis was 1000 ppm or 1 mg of C_6H_{12} per gram of dry soil. This initial loading corresponds to 1.257 mg of cyclohexane per cc of soil when a value for the bulk density of dry soil is used; $\rho_B = 1.257$ gm/cc. Values for other soil properties relevant to this problem are $\epsilon_V = .50$, $\kappa = 4 \times 10^{-3}$ cm²/sec and $a_V = 10^4$ cm²/cc soil. The soil temperature was allowed to fluctuate around a mean value of $\bar{T} = 300$ K and amplitude of $\Delta T = 5$ and 15 K; typical of summer conditions in California.

5.1-3 Analytical Solution: Isothermal Case

Analytical solutions to equations 1-4 are available for isothermal soil conditions and assuming constant coefficients. The resulting solution is termed the penetration model, is restricted to suitably short times, and predicts the average soil concentration of A as a function of z and t by

$$\langle C_A \rangle = \langle C_A \rangle_0^Y \operatorname{erf} \left(\frac{z}{\sqrt{4D_{app}t}} \right) \quad (8)$$

The rate of emission of A away from the surface of the soil is given as

$$N_A = \langle C_A \rangle_0^Y D_{eff} \sqrt{1/(D_{app}\pi t)} \quad (9)$$

where $D_{app} = \epsilon_V D_{eff} / (\epsilon_V + a_V/K_H)$ is the "apparent" diffusivity of A through dry soil. The total emissions of A over a specified interval of time can be obtained by integrating equation 9.

$$M_A = 2 \langle C_A \rangle_0^Y D_{eff} \sqrt{t/(D_{app}\pi)} \quad (10)$$

It is through the use of equation 9 and experimental data on gasoline emission rates from dry soils that D_{app} can be estimated for gasoline components. This procedure is outlined in Appendix II.

5.1-4 Numerical Solution: Nonisothermal Case

Numerical solutions to equations 1-4 were obtained for both isothermal and non isothermal soil conditions. Finite differences approximations to equation 1 were solved numerically using an explicit method with multiple time and space intervals. The numerical method was evaluated under isothermal soil conditions by comparing results with equations 13 and 14. The agreement for $\langle C_A \rangle^Y$ was excellent for all times except at short times near the soil surface. Relative errors in M_A were as high as 2.55% and for N_A as high as .8% for times approaching zero. This situation arises due to the presence of very large gradients in $\langle C_A \rangle^Y$ initially near the soil surface. At later times, for example at $t = 12$ hours, the agreement was much better with the relative error in M_A less than .5% and for N_A less than .04%.

Before evaluating the effect of diurnal soil temperature fluctuations on gasoline emission rates from dry soils, a comparison of numerical results with experimental data will be made. Figures 17 and 18 are comparisons of N_A and M_A versus time for experimental data taken at $\bar{T} = 298$ K and for numerical results obtained under identical isothermal conditions. Even though the numerical results shown here were based upon parameters obtained from this data set, the agreement is not good over the entire time period, of which only the first hour is shown. The numerical results underpredict N_A and M_A initially and overpredict at later times. The poor agreement between the Penetration model and our emission rate data sets has prompted a search for a more sophisticated description of gasoline diffusion and adsorption in soils. Specifically, we will be measuring emission rates of a single component of gasoline instead of the entire complex mixture. This will be

Gasoline Emissions from Dry Soil vs. Time

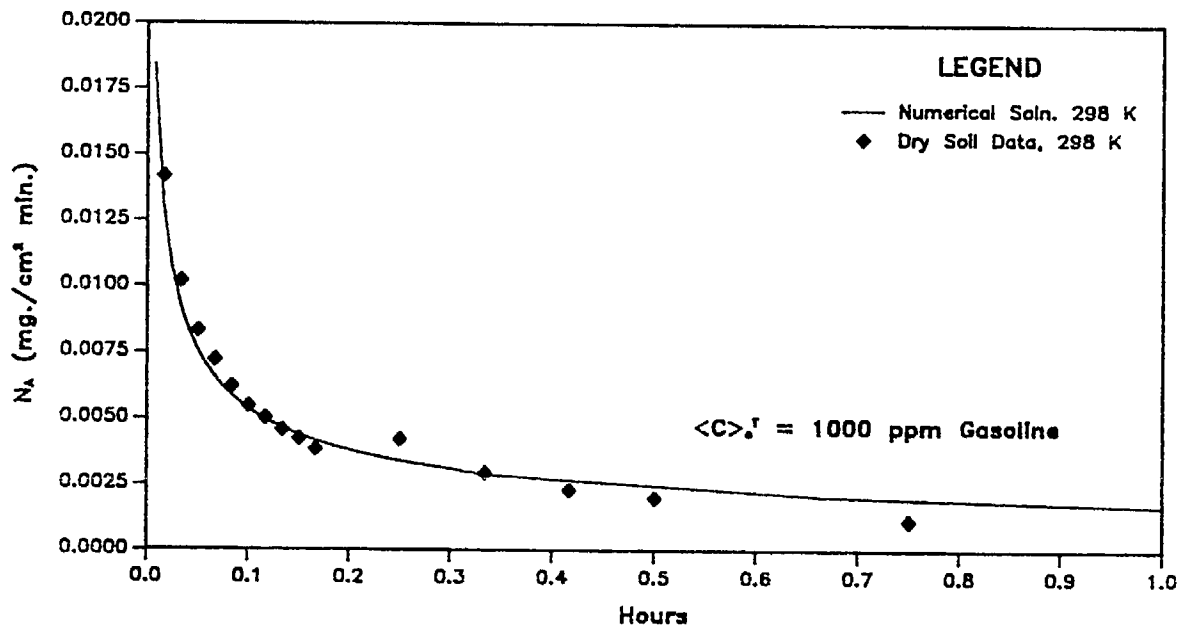


Figure 17. Comparison of the penetration model with data for N_A vs. time. Isothermal soil column.

Total Gasoline Emissions from Dry Soil

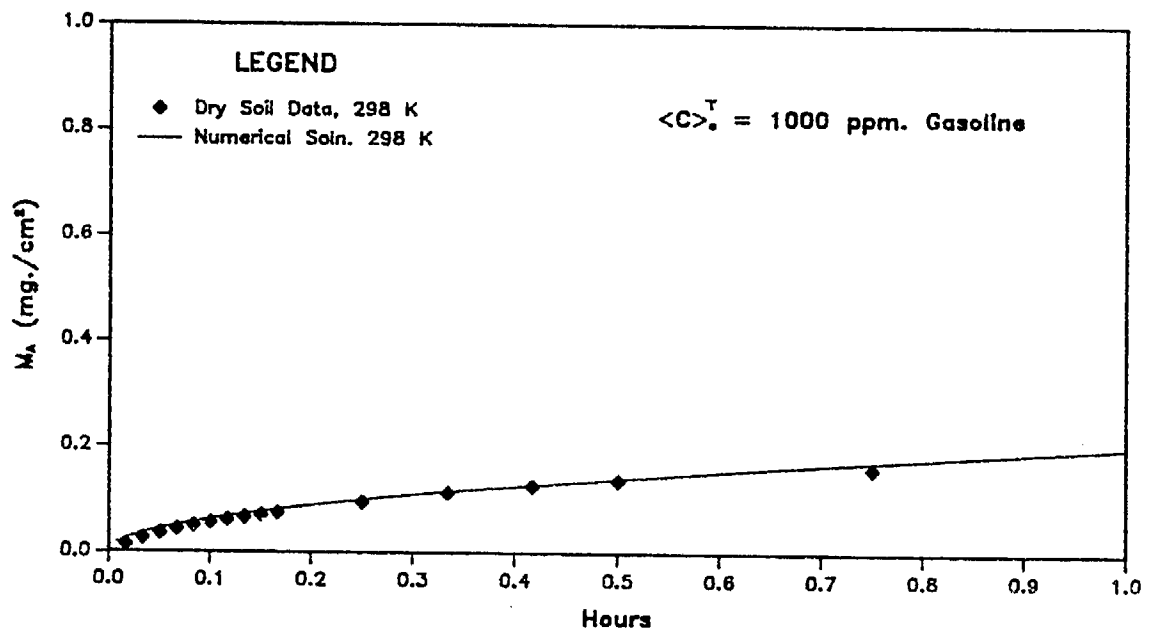


Figure 18. Comparison of the penetration model with data for M_A vs. time. Isothermal soil column.

accomplished by uniformly contaminating a soil column with a single gasoline component. In order to improve the agreement between the emission rate model and the data sets, we intend to investigate the effects of non-linear adsorption and micro-pore diffusional resistance. It is expected that agreement between numerical results and experiments will be much better in that case.

The effect of increased soil temperatures on the emission rates and total soil emissions of A from an isothermal soil column are shown in Figures 19 and 20. These numerical solutions demonstrate the dramatic increases in emission rates caused by small increases in soil temperatures. As temperatures in the soil increase, desorption of A occurs from surfaces thereby increasing the vapor phase concentration of A. The diffusivity of A also increases with increasing temperature, though relatively minor in magnitude when compared to the adsorption phenomenon. For this analysis, emission rates increased by a factor of approximately $\sqrt{2}$ for an increase of 15°C in soil temperature. This can be predicted a priori from equation 9 and the results tabulated in Appendix II for K_H vs. temperature. This occurs because K_H is the dominant term in D_{app} which has a square root dependence in equation 9.

5.1-5 Effect of Diurnal Soil Temperature Cycle on VOC Losses

In reality, diurnal temperature fluctuations do occur in the soil and it's effect on N_A and M_A are shown in Figures 21 and 22. In these cases, the numerical simulations were initiated at sunrise, thereby subjecting the soil to a heating cycle at the start. It is shown that N_A fluctuates about the curve for which $\Delta T = 0 \text{ K}$ (isothermal soil column) with a period of 1 day and that the fluctuations in N_A have a higher amplitude above this curve than below it. This last conclusion is obtained from Figure 22 because the M_A curves are above that for which $\Delta T = 0 \text{ K}$. Mass transfer is enhanced due to the presence of a diurnal

Gasoline Emissions from Dry Soil vs. Time

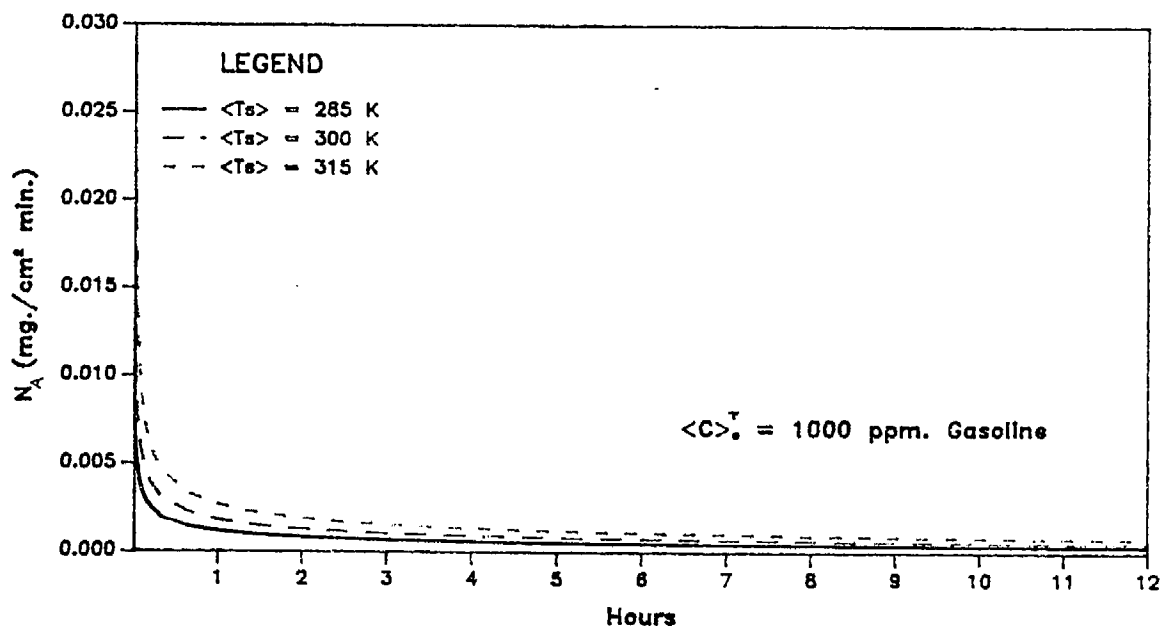


Figure 19. Effect of soil temperature on N_A predictions using the penetration model. Isothermal soil column.

Total Gasoline Emissions from Dry Soil

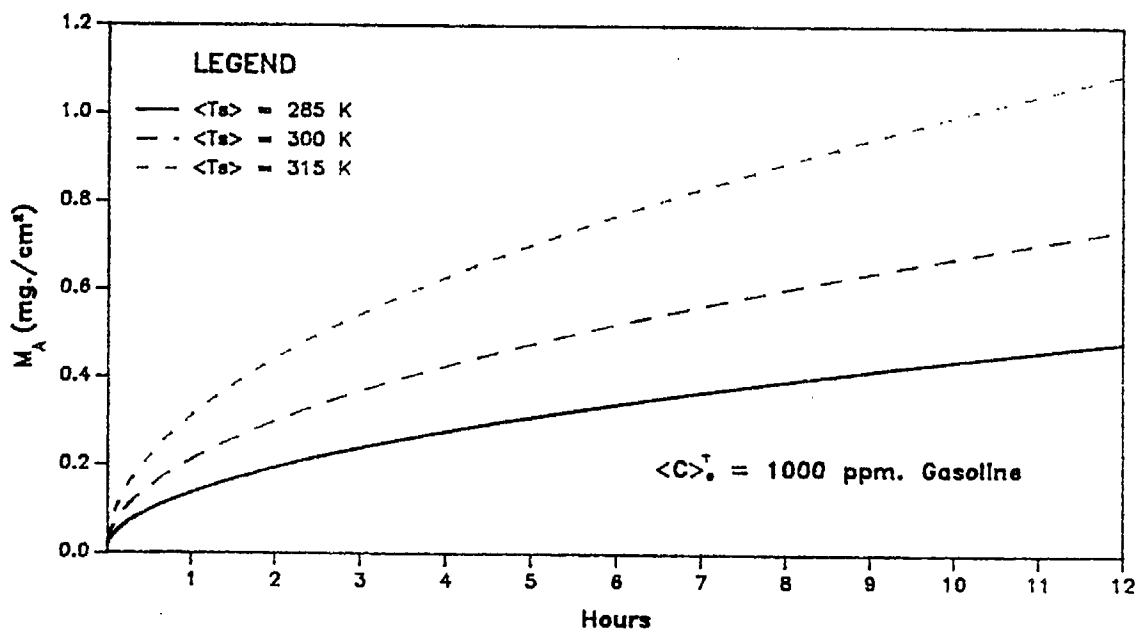


Figure 20. Effect of soil temperature on M_A predictions using the penetration model. Isothermal soil column.

Gasoline Emissions from Dry Soil vs. Time

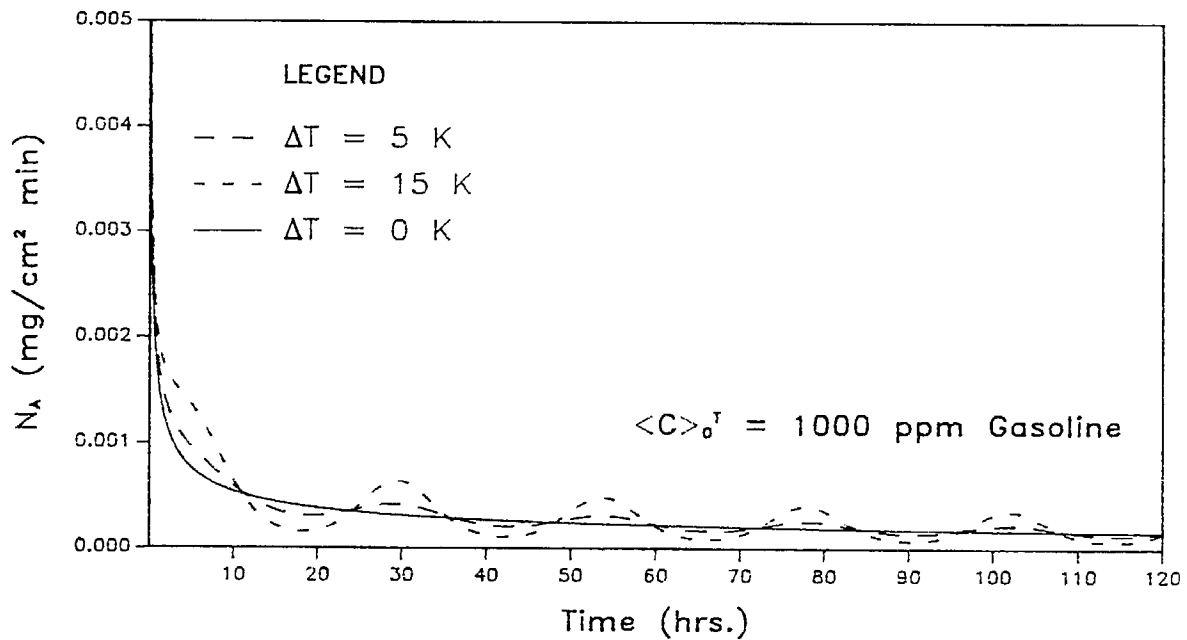


Figure 21. Effect of a diurnal soil temperature cycle on N_A using a penetration model starting at sunrise. $\bar{T} = 298^{\circ}\text{K}$.

Total Gasoline Emissions from Dry Soil

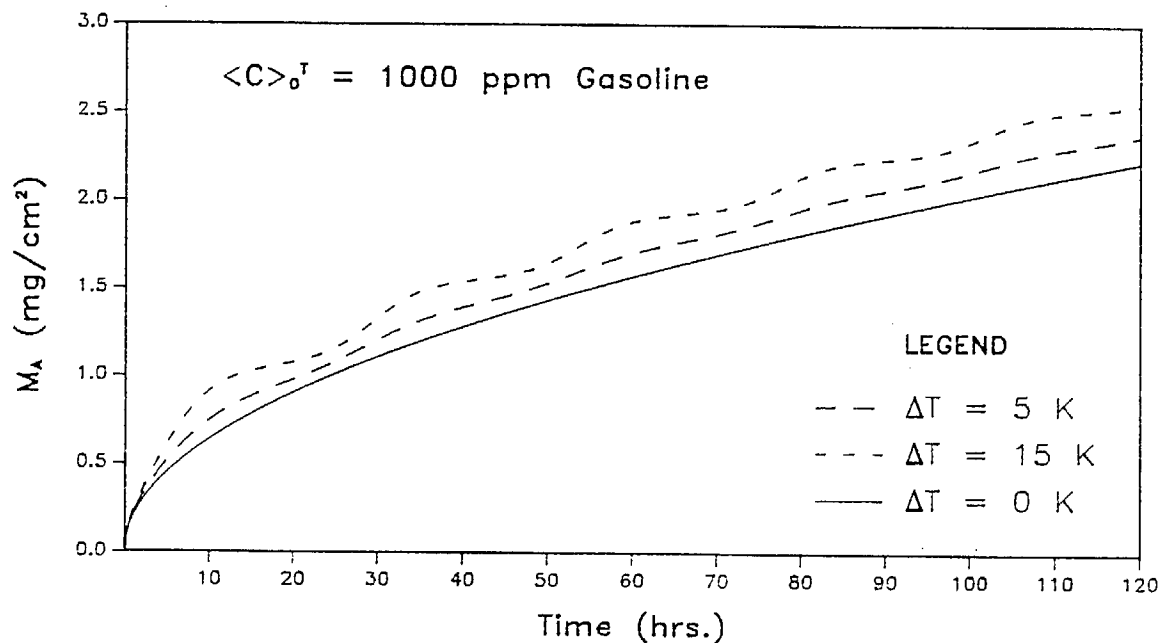


Figure 22. Effect of a diurnal soil temperature cycle on M_A using a penetration model starting at sunrise. $\bar{T} = 298^{\circ}\text{K}$.

temperature cycle resulting in an increase in total emissions over time. This enhancement can be easily explained by considering the equation for the equilibrium adsorption constant given by equation 6. This expression for K_H is highly non-linear and is the source of the enhanced emission rates. The magnitude of the enhanced total emissions is between 10 and 20% for most of the time between time equal to zero and 5 days.

When the computer simulation is started at sunset, the emission rates are initially less than those predicted for $\Delta T = 0$ K (isothermal soil column). These results are shown graphically on Figures 23 and 24. It is of interest to note that an enhancement in the total emissions of component A occurs in this case also. The conclusion to be drawn is that enhanced emission totals occur from soil subjected to a diurnal fluctuation in temperature regardless of the initial state of the system and that at long times the accumulated emissions of A approaches the same level of enhancement.

Another conclusion from this study is that the level of enhanced emission totals due to soil temperature fluctuations is a small fraction of the total loss though it is perceptible. For instance, if a 10% error in emission totals estimates is acceptable, and a penetration model is valid, then the evaluation of the loss can be greatly simplified by utilizing the analytical solutions for N_A and M_A evaluated at the mean soil temperature. This approach is particularly useful and valid at long times where a computer simulation can be very expensive. However, for very short time estimates it is observed that the analytical solution will deviate greatly ($\sim 100\%$) from actual emission totals. Under these conditions, it is recommended to evaluate the emissions numerically under non-isothermal soil conditions.

Gasoline Emissions from Dry Soil vs. Time

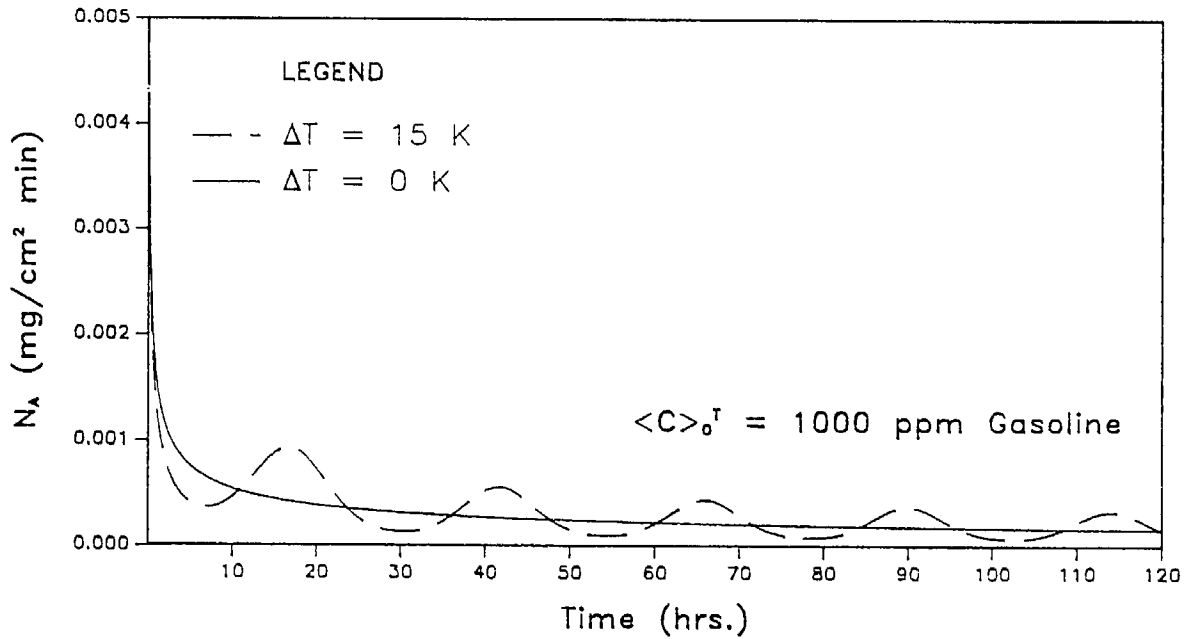


Figure 23. Effect of a diurnal soil temperature cycle on N_A using a penetration model starting at sunset. $\bar{T} = 298 \text{ K}$.

Total Gasoline Emissions from Dry Soil

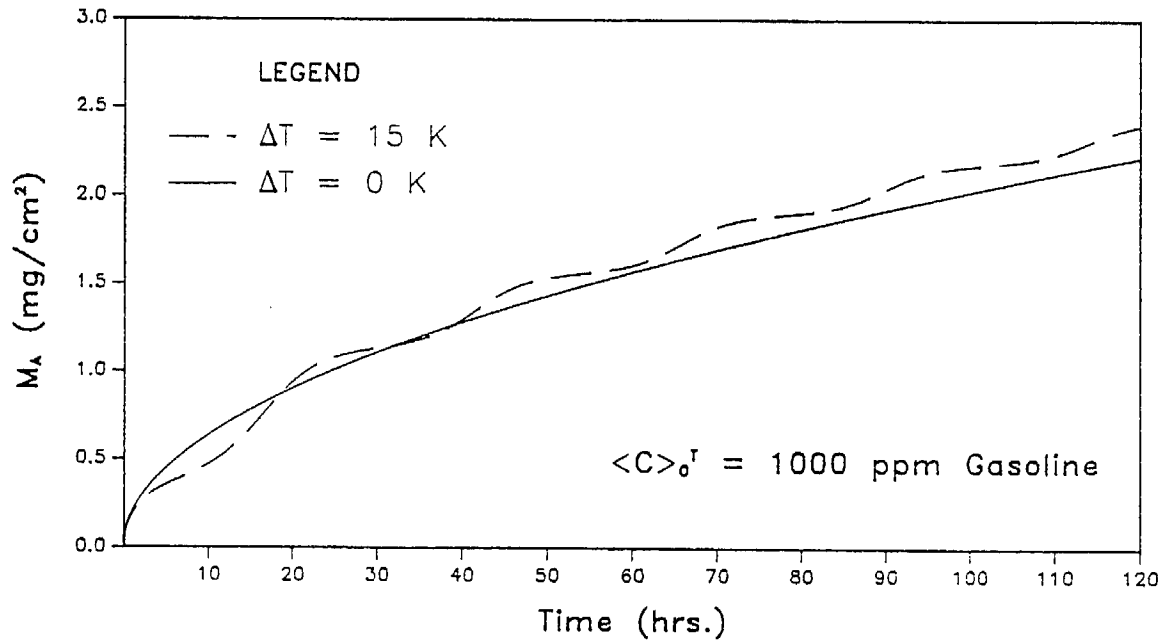


Figure 24. Effect of a diurnal soil temperature cycle on M_A using a penetration model starting at sunset. $\bar{T} = 298 \text{ K}$.

As stated previously, emission totals were shown to be enhanced for a soil column undergoing diurnal temperature fluctuations when compared to an isothermal soil column. A penetration model was chosen for this modeling application due to its simplicity even though the predictions do not agree very well with our own laboratory data. However, the effect of temperature fluctuations in the soil on the emission totals is expected to be similar for even widely differing models simply due to the overwhelming effect of temperature fluctuations on adsorption. And indeed we will investigate different modeling strategies in the future in order to predict more exactly our laboratory data.

5.1-6. Multicomponent Emission Rate Predictions

In order to more simply determine the emission rates and totals from a multicomponent mixture of VOC's, such as gasoline for example, the assumption of dilute concentration of each species must be made. The term dilute means that the concentration of each component in the mixture is very much less than the air concentration through which it diffuses. Not only must the above restriction on the analysis be made, but also that the sum of the individual concentrations of each component in the mixture must be much smaller than the air concentration.

When these restrictions apply, each component can be modeled as a diffusion process that is decoupled from the diffusion of the other species in the mixture (25, p.20). This decoupling is also expected to apply to the adsorption processes in the soil for sufficiently dilute concentrations. At this point, we do not know the restrictions required of the adsorption process, however, this topic is of future interest.

The emission rates for each component in the mixture are independently obtained. Using the penetration model for simplicity and to illustrate the method, the emission rates for each component is given as

$$N_i = (C_i)_0^Y \cdot D_{\text{eff},i} \sqrt{1/(D_{\text{app},i} \pi t)}$$

where

i = the i ,th component in the mixture

When a component analysis of the soil contaminant is performed, as it was shown for gasoline in section 4.3, the initial concentration of each relevant species can be obtained. In that section, five representative gasoline components were chosen in order to model multicomponent emission rates from gasoline contaminated soils. To be sure, more accuracy would dictate an increase in the number of components chosen. For an illustration of the method, only five will be considered. The initial concentration for each component is given by

$$\langle C_i \rangle_0 = \langle C \rangle_0 \cdot w_i$$

where

$$w_i = \text{the mass fraction of } i = x_i \frac{MW_i}{\sum x_i MW_i}$$

$\langle C \rangle_0$ = the initial concentration of gasoline in the soil (mg/cc soil)

x_i = measured mole fraction of i from GCMS

MW_i = the molecular weight of i (g/mole)

The emission rate for the entire mixture is simply the sum of the component emission rates

$$N_T = \sum_{i=1}^5 N_i$$

5.2 CONCLUSIONS.

1. A laboratory apparatus has been constructed so that atmospheric emission rates of VOC from gasoline contaminated soil can be obtained. A 2 in. deep by 2 in. diameter column was filled with a Yolo Loam soil and uniformly contaminated with unleaded gasoline to the level of 1 mg per gram of soil. Initial measurements indicate that emission rates increase by approximately a factor of 6 when soil moisture is present at a level of 30-35% over the emission rate from an air-dry soil. When soil temperature was changed for an air-dry soil column, emission rates increased by a factor of 3-4 for a 15°C increase in soil temperature.
2. After 12 hours, the contaminated soil columns emitted from between .38 to 2.31 mg gasoline/cm² soil surface. Each soil column was initially contaminated with 1 mg gasoline per gram of dry soil. The reported range in emitted gasoline is due to soil temperature and moisture content. For a 1000 m² area of contaminated soil, these emissions correspond to between 3.8 kg (8.4 lb.) and 23.10 kg (50.9 lb.) for the first 12 hour period.
3. An analytical solution to the equation of continuity for a single gasoline component was obtained. Diffusion and adsorption of the component was considered. The assumptions inherent in this derivation are outlined in Appendix I. The trend in the experimental data in terms of emission rate vs. time were adequately predicted by this analytical solution (Penetration model) even though agreement over the entire range of the data set was poor.
4. Using the Penetration model, a method for determining the transport coefficient, D_{app} , was outlined in Appendix II. From this analysis, an estimate of the equilibrium adsorption coefficient, K_H , was obtained and showed reasonably good agreement with literature values. The Penetration model is not required in this analysis of D_{app} and K_H and was used only to illustrate the method.

5. A method was outlined for evaluating the effect of soil moisture on the diffusivity of a component of gasoline through soil. This method was a summary of published literature.
6. Multicomponent diffusion and adsorption in soils was analyzed using the Penetration model and a GCMS analysis of the gasoline. The Penetration model was used only to illustrate the method.
7. Diurnal soil temperature fluctuations were analyzed theoretically and the numerical results indicate that emission rates of a gasoline component are enhanced when compared to an isothermal soil column at the mean soil temperature. However, a relatively small error results (~ 10% error) if the soil column is assumed to be isothermal at the mean soil temperature. For quick emission rate estimates, an isothermal soil column is justified, particularly at long times (> 1 day) when the highly non-linear effects of the soil temperature fluctuations do not influence the total emissions as much as at earlier times.

5.3 FUTURE CONSIDERATIONS FOR MODELS

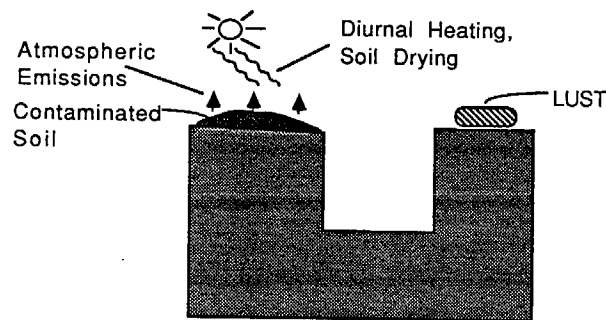
Further developments in modeling gasoline emissions from soils will include several objectives:

1. Include the multicomponent nature of gasoline in the model.
2. Incorporate soil moisture in the model.
3. Evaluate the importance of water evaporation on the emission rates of gasoline components.
4. Incorporate a heat transfer model to the soil to more realistically express the temperature distribution in a newly excavated gasoline contaminated soil.
5. Include non-linear adsorption isotherms.
6. Investigate the influence of soil micropore diffusional resistance on the emission rate model.

Appendix I. Derivation of the Continuity Eqn for a Gasoline Component in Dry Soil.

The schematic representation of the problem of gasoline emissions from dry soil is shown below.

Leaky Underground Storage Tanks (LUST)



It is assumed that soil physical and chemical properties of ϵ_γ , ρ_B , D_{eff} , κ are known a priori and that only solid and vapor phases are present. The initial concentration of gasoline in soil is low enough such that no gasoline phase is present and that a linear adsorption isotherm applies for the partitioning of the gasoline component of interest between the vapor and solid phases. The gas phase mass transfer resistance at the soil surface is very much less than the soil phase mass transfer resistance. This allows that the surface concentration of the gasoline component can be set to zero with negligible error. It is also assumed that the component diffuses primarily in one direction, that is up to the soil surface.

The derivation of the continuity eqn for the γ phase average concentration of gasoline component A starts from the point continuity eqn for component A.

$$\frac{\partial C_A}{\partial t} = - \nabla \cdot \underline{N}_A + R_A \quad (1)$$

Also, accumulation of A at the soil particle surfaces is governed by

$$\frac{d\hat{C}_A}{dt} = - \rho_{\gamma\alpha} \cdot \underline{N}_A \quad (2)$$

and

$$\hat{C}_A = K_H^{-1} C_A \quad (3)$$

at the interface of the vapor and solid surface. $R_A = 0$ in the vapor phase. In order to obtain an eqn for the γ phase average concentration of A, $\langle C_A \rangle^\gamma$, eqn 1 is integrated over a suitable small γ phase volume in the soil, V_γ .

$$\frac{1}{V_\gamma} \int_{V_\gamma} \frac{\partial C_A}{\partial t} dV = \frac{1}{V_\gamma} \int_{V_\gamma} -\nabla \cdot \underline{N}_A dV \quad (4)$$

The γ phase average concentration of A is defined as:

$$\langle C_A \rangle^\gamma = \frac{1}{V_\gamma} \int_{V_\gamma} C_A dV \quad (5)$$

and since the derivative operator and integration over V_γ are independent, the first term in 4 can be expressed as

$$\frac{1}{V_\gamma} \int_{V_\gamma} \frac{\partial C_A}{\partial t} dV = \frac{\partial}{\partial t} \frac{1}{V_\gamma} \int_{V_\gamma} C_A dV = \frac{\partial \langle C_A \rangle^\gamma}{\partial t} \quad (6)$$

By applying the Divergence theorem to the second term in 4 the volume integral can be converted to an integral over the surfaces in the volume of interest.

$$\frac{1}{V_\gamma} \int_{V_\gamma} -\nabla \cdot \underline{N}_A dV = \frac{1}{V_\gamma} \int_A -\underline{n} \cdot \underline{N}_A dA \quad (7)$$

The surfaces in the volume of interest are composed of "free" surfaces at entrances and exits, A_f , and solid/vapor interfaces $A_{\gamma\alpha}$.

$$\frac{1}{V_Y} \int_A -\underline{n} \cdot \underline{N}_A \, dA = \frac{1}{V_Y} \int_{A_{Y\alpha}} -\underline{n}_{Y\alpha} \cdot \underline{N}_A \, dA + \frac{1}{V_Y} \int_{A_f} -\underline{n}_f \cdot \underline{N}_A \, dA \quad (8)$$

The flux of A at the solid/vapor interface and on the free surface is respectively,

$$-\underline{n}_{Y\alpha} \cdot \underline{N}_A = \frac{\partial \hat{C}_A}{\partial t} \quad (9)$$

$$\underline{n}_f \cdot \underline{N}_A = -\underline{n}_f \cdot D_{AB} \nabla C_A \quad (10)$$

assuming dilute concentration of A and no convective flow. If a one dimensional diffusion problem is considered then the integration of the last term in 8 will cancel except at z and at z + Δz. If the assumption that

$$\frac{1}{V_Y} \int_{A_{f,z}} -\underline{n}_f \cdot \underline{N}_A \, dA \sim \frac{1}{\Delta z} D_{\text{eff}} \left. \frac{\partial \langle C_A \rangle^Y}{\partial z} \right|_z \quad (11)$$

and the definition of $\langle \hat{C}_A \rangle$ is used in conjunction with eqn 9, then 8 can be replaced by

$$\begin{aligned} \frac{1}{V_Y} \int_A -\underline{n} \cdot \underline{N}_A \, dA = & -\frac{a_V}{\epsilon_Y} \frac{\partial \langle \hat{C}_A \rangle}{\partial t} + \frac{1}{\Delta z} \left[D_{\text{eff}} \left. \frac{\partial \langle C_A \rangle^Y}{\partial z} \right|_{z+\Delta z} \right. \\ & \left. - D_{\text{eff}} \left. \frac{\partial \langle C_A \rangle^Y}{\partial z} \right|_z \right] \end{aligned} \quad (12)$$

Substituting 12 and 6 into 4 and letting $\Delta z \rightarrow 0$

$$\frac{\partial \langle C_A \rangle^Y}{\partial t} = -\frac{a_V}{\epsilon_Y} \frac{\partial \langle \hat{C}_A \rangle}{\partial t} + \frac{\partial}{\partial z} \left(D_{\text{eff}} \frac{\partial \langle C_A \rangle^Y}{\partial z} \right) \quad (13)$$

When Henry's Law applies to average concentrations, 3 can be restated as

$$\langle \hat{C}_A \rangle = K_H^{-1} \langle C_A \rangle^Y$$

and 13 becomes

$$\frac{\partial \langle C_A \rangle^Y}{\partial t} + \left(\frac{a_V}{\epsilon_Y K_H} \right) \frac{\partial \langle C_A \rangle^Y}{\partial t} = \frac{\partial}{\partial z} \left(D_{\text{eff}} \frac{\partial \langle C_A \rangle^Y}{\partial z} \right) \quad (14)$$

Simplifying 14

$$\frac{\partial \langle C_A \rangle^Y}{\partial t} = \frac{1}{\left(1 + \frac{a_V}{\epsilon_Y K_H} \right)} \frac{\partial}{\partial z} \left(D_{\text{eff}} \frac{\partial \langle C_A \rangle^Y}{\partial z} \right) \quad (15)$$

APPENDIX II. D_{app} and Henry's Law Constant for Adsorption of Gasoline Component A onto Soil.

Adsorption of gasoline components from the vapor phase onto soil particles can be described by Henry's Law in the limit of dilute solutions (19). The form of Henry's Law for adsorption and the temperature dependence of the coefficient are

$$\hat{C}_A = K_H^{-1} C_A \quad (1)$$

$$K_H(T) = RT K_{Ho} \exp \left[- \frac{\Delta H_a}{RT} \right] \quad (\text{cm}^{-1}) \quad (2)$$

where

ΔH_a = Heat of adsorption ~ 8.0 kcal/mol.

R = Ideal gas constant = 1.987×10^{-3} kcal/mol.

T = Temperature (K)

The value for ΔH_a was obtained from typical values for hydrocarbon adsorption onto Zeolite (19).

The value of the pre exponential factor, K_{Ho} , can be obtained from experimental data collected from dry soil emission studies using gasoline contaminated soils. One such study was carried out at 25°C (298 K) with an initial soil concentration of 1.257 mg gasoline/cc dry soil. From a regression fit of the emissions data to the penetration model, the emission rate of gasoline vs. $1/\sqrt{\text{time}}$ showed that

$$N_A = \langle C_A \rangle_0^Y D_{eff} \sqrt{1/(D_{app} \pi t \cdot 60)} \cdot 60 = \frac{.012611}{\sqrt{t}} \quad (\text{mg}/(\text{cm}^2 \text{ min})); t \text{ in min} \quad (4)$$

where

$$D_{app} = \frac{D_{eff}}{(1 + a_v/\epsilon_Y K_H)} \quad (\text{cm}^2/\text{sec}) \quad (5)$$

and

$$D_{eff} = D_{AB} \epsilon_Y^2$$

By assuming $\epsilon_V = .5$ and $a_V = 10^4 \text{ cm}^{-1}$ (reasonable values for dry soils),

D_{app} can be solved for from 4

$$D_{app} = \frac{\epsilon_V^2 \pi (.012611)^2}{(\langle C_A \rangle_0^I)^2 \cdot 60} \quad (6)$$

Substituting these values into 6, the result for D_{app} is

$$\begin{aligned} D_{app} &= \frac{(.5)^2 (.012611 \text{ mg}/(\text{cm}^2 \cdot \text{min}^{1/2}))^2 \pi}{(1.257 \text{ mg}/\text{cm}^3)^2 (60 \text{ sec}/\text{min})} \quad (7) \\ &= 1.32 \times 10^{-6} \text{ cm}^2/\text{sec} \quad @ 298 \text{ K} \end{aligned}$$

The value for $K_H(298 \text{ K})$ can be obtained from 7 and 5 by using the definition for

$$D_{eff} = \epsilon^2 D_{AB} = (.5)^2 (.08 \text{ cm}^2/\text{sec}) = .02 \text{ cm}^2/\text{sec}.$$

$$K_H = \left(\frac{\epsilon_V D_{eff}}{a_V D_{app}} - \frac{\epsilon_V}{a_V} \right)^{-1} = \left(\frac{\epsilon_V}{a_V} \left(\frac{D_{eff}}{D_{app}} - 1 \right) \right)^{-1}$$

$$\begin{aligned} K_H &\sim \left(\frac{\epsilon_V D_{eff}}{a_V D_{app}} \right)^{-1} = \left[\frac{(.5) (.02 \text{ cm}^2/\text{sec})}{(10^4 \text{ cm}^{-1}) (1.32 \times 10^{-6} \text{ cm}^2/\text{sec})} \right]^{-1} \\ &= 1.32 \text{ cm}^{-1} \quad @ 298 \text{ K} \end{aligned}$$

From 2, $K_{H0} = 1.6434 \times 10^6 \text{ cm}^{-1}$. By substituting the above calculated values in eqn 2 we can determine the variation of K_A with temperature and TABLE II-1 is a summary of these results.

TABLE II-1. TEMPERATURE DEPENDENCE OF K_A

<u>T(K)</u>	<u>$K_H(\text{cm}^{-1})$</u>
285	.682
300	1.454
315	2.893

REFERENCES

1. California State Water Resources Control Board, Report on Unauthorized Releases of Hazardous Substances From Underground Storage Tanks, January, 1987.
2. Campbell, G.S., An Introduction to Environmental Biophysics, pg. 14-17, Springer-Verlag, New York.
3. Curry, J.A., "Gaseous diffusion in porous media. Part 2. - Dry granular material", *Brit. J. of Appl. Phys.*, 11:314 (1960).
4. de Vries, D.A., "Heat Transfer in Soils", In Heat and Mass Transfer in the Biosphere Part I Transfer Processes in the Plant Environment. D.A. de Vries and N.H. Afgan, Eds. pgs. 6-28. Scripta Book Co., 1975.
5. Farmer, W.J., Igue, K., Spencer, W.F., and Martin, J.P., "Volatility of organochlorine insecticides from soil: I. Effect of concentration, temperature, air flow rate, and vapor pressure", *Soil Sci. Soc. Am., Proc.*, 36:447 (1972).
6. Farmer, W.J., Yang, M.S., Letey, J., and W.F. Spencer, Hexachlorobenzene: Its vapor pressure and vapor phase diffusion in soil. *Soil Sci. Soc. Amer. J.* 44:676-680 (1980).
7. Goring, C.A.I., Theory and principles of soil fumigation. *Adv. Pest Control Res.* 5:47-84 (1962).
8. Igue, K., Farmer, W.J., Spencer, W.F., and Martin, J.P., "Volatility of organochlorine insecticides from soil: II. Effect of relative humidity and soil water content on Dieldrin volatility", *Soil Sci. Soc. Am., Proc.*, 36: 443 (1972).
9. Jury, W.A., Spencer, W.F., and Farmer, W.J.; "Behavior Assessment Model for Trace Organics in Soil: I. Model Description", *J. Environ. Qual.*, Vol. 12, No. 4, 1983, pp. 558-564.
10. Jury, W.A., Spencer, W.F., and Farmer, W.J.; "Behavior Assessment Model for Trace Organics in Soil: II. Chemical Classification and Parameter Sensitivity", *J. Environ. Qual.*, Vol. 13, No. 4, 1984, pp. 567-572.
11. Jury, W.A., Spencer, W.F., and Farmer, W.J.; "Behavior Assessment Model for Trace Organics in Soil: III. Application of Screening Model", *J. Environ. Qual.*, Vol. 13, No. 4, 1984, pp. 573-579.
12. Jury, W.A. Spencer, W.F., and Farmer, W.J.; "Behavior Assessment Model for Trace Organics in Soil: IV. Review of Experimental Evidence", *J. Environ. Qual.*, Vol. 13, No. 4, 1984, pp. 580-585.
13. Karimi, A.A., Farmer, W.J., and Cliath, M.M., Vapor Phase Diffusion of Benzene in Soils, submitted to *J. Envir. Qual.*

14. Letey, J. and Farmer, W.J., Movement of pesticides in soil pp. 67-97 In Pesticides in Soil and Water, W.D. Guenzi (ed.) Soil Sci. Soc. Amer., Madison WI. (1974).
15. Lyman, W.J., Reehl, W.F., and Rosenblatt, D.H., Handbook of Chemical Property Estimation Methods; Environmental Behavior of Organic Compounds, McGraw-Hill, New York, 1982, Chpt. 16.
16. Millington, R.J. and Quirk, J.P., Permeability of porous solids. Trans. Faraday. Soc. 57:1200-1207 (1961).
17. Monteith, J.L., Principles of Environmental Physics, pg. 128-133, Edward Arnold.
18. Perry, R.H., and D.W. Green, Eds., Perry's Chemical Engineers' Handbook, 6th Edition, pg. 3-285, McGraw-Hill Book Co., 1984.
19. Ruthven, D.M., Principles of Adsorption and Adsorption Processes, pp. 43-44, John Wiley & Sons, 1984.
20. Sellers, W.D., Physical Climatology, The University of Chicago Press, Chicago.
21. Spencer, W.F., Cliath, M.M., and Farmer, W.J., "Vapor density of soil-applied Dieldrin as related to soil-water content, temperature, and Dieldrin concentration", Soil Sci. Soc. Am., Proc., 33:509 (1969).
22. Spencer, W.F., and Cliath, M.M., "Pesticide volatilization as related to water loss from soil", J. Environ. Quality, 2 (2): 284 (1973).
23. Spencer, W.F., Farmer, W.J., and Cliath, M.M., "Pesticide Volatilization", in Residue Reviews, F.A. Gunther (ed.), vol. 49, 1973.
24. Spencer, W.F. and Cliath, M.M., "Factors affecting vapor loss of Trifluralin from soil", J. Agric. Food Chem., 22 (6): 987 (1974).
25. Whitaker, S., "Transport Processes with Heterogeneous Reaction", in: Concepts and Design of Chemical Reactors, S. Whitaker and A.E. Cassano; eds. pg. 41 Gordon and Breach Science Publishers, New York (1986).

Nomenclature: Section

- A_f - the "free" surface of the vapor phase representing areas of entrances and exits from a small volume of soil (cm^2).
- $A_{Y\alpha}$ - the surface area of the solid/vapor interface represented inside a small volume of soil (cm^2).
- a_v - the surface area of solid per unit volume of soil. (cm^{-1}).
- $\langle C \rangle_0$ - the initial gasoline concentration in the soil (mg/cm^3 soil).
- C_A - the point concentration of A in the vapor phase (mg/cc).
- \hat{C}_A - the point concentration of A on the soil surface (mg/cm^2).
- $\langle C_A \rangle$ - the total average soil conc. of A = $\epsilon_Y \langle C_A \rangle^Y + a_v \langle \hat{C}_A \rangle$.
- $\langle \hat{C}_A \rangle$ - the average surface concentration of A in a small volume of soil

$$(\text{mg}/\text{cm}^2) = \frac{1}{A_{Y\alpha}} \int_{A_{Y\alpha}} C_A dA$$

- $\langle C_A \rangle^Y$ - the intrinsic vapor phase avg. soil conc. of A (mg/cc) = $\frac{1}{V_Y} \int C_A dv$.

- $\langle C_A \rangle_0^Y$ - the initial $\langle C_A \rangle^Y$.

- D_{AB} - the vapor or liquid phase diffusivity of component A through phase B.

- D_{app} - the apparent diffusivity of a component in dry soil = $\epsilon_Y D_{eff} / (\epsilon_Y + \frac{a_v}{K_H})$

- D_{eff} - the effective diffusivity of a component in the vapor phase of a soil (cm^2/sec).

- ΔH_a - the heat of adsorption of component A onto soil (kcal/mol).

- ΔP - the pressure drop causing convection in the vapor phase.

- ΔT - the amplitude of the fluctuation in $\langle T_s \rangle$ (K).

- K_D - the linear distribution coefficient of a component between the aqueous phase and the solid surface (cm^{-1}).
- k_g - mass transfer coefficient for a component in the gas phase above the surface of the soil. (cm/sec).
- K_H - Henry's Law constant for adsorption of a component between the vapor phase and the solid phase. $\hat{C}_A = K_H^{-1} C_A$
- k_s - mass transfer coefficient for a component in the soil. (cm/sec).
- M_A - the accumulative loss of A from dry soil into the atmosphere (mg/cm^2).
- MW_i - the molecular weight of species i.
- N_A - the instantaneous flux of A through the soil surface into the atmosphere ($\text{mg}/(\text{cm}^2 \text{ min})$).
- \underline{n}_f - the unit normal vector from the free surface.
- $\underline{n}_{\gamma\alpha}$ - the unit normal vector pointing from the soil surface, α , into the vapor phase, γ .
- P_a - the air-filled porosity ($\text{cm}^3 \text{ air}/\text{cm}^3 \text{ soil}$).
- P_T - the total porosity = ϵ_γ .
- P_w - the porosity of water in soil ($\text{cm}^3 \text{ water}/\text{cm}^3 \text{ soil}$).
- Q - volumetric flow rate of air through the diffusion cell headspace (cc/sec).
- R - the ideal gas constant = $1.987 \times 10^{-3} \text{ kcal}/(\text{mol K})$
- R_A - the reaction rate of A ($\text{moles}/\text{cm}^3 \text{ sec}$).
- t - time (sec).
- \bar{T} - the mean temperature of a soil column (time average) undergoing a diurnal temperature fluctuation. (K).
- $\langle T_s \rangle$ - the volume average soil temperature (K).
- V - volume of the diffusion cell headspace (cc).
- V_E - the aqueous average velocity through soil caused by evaporation (cm/sec).
- V_γ - the volume of vapor phase, γ , in a small volume of dry soil (cm^3).
- w_i - the mass fraction of a component in gasoline.
- x_i - the mole fraction of a component in gasoline.
- z - depth in the soil (cm).

Greek

- ϵ_{γ} - void fraction in the soil.
- κ - the thermal diffusivity of the soil (cm^2/sec).
- μ - the biodegradation linear rate constant (sec^{-1}).
- ω - the diurnal frequency = $2\pi/1$ day (sec^{-1}).
- ρ_B - the bulk density of dry soil (g/cm^3).
- ρ_p - the density of soil particles (g/cm^3).
- τ - characteristic time for flow through the diffusion cell headspace = V/Q (sec).
- θ - the soil moisture content.

Subscripts - Superscripts

- A - species A.
- AB - species A and B.
- α - the solid phase in soil.
- f - free surface (entrances and exits into a small volume).
- γ - the vapor phase in soil.
- g - gas.
- i - species i.
- o - initial state.
- s - soil.

Abbreviations

- erf - error function.
- FID - flame ionization detector.
- GCMS - gas chromatography - mass spectroscopy.
- ppm - parts per million.
- RH - relative humidity.
- RPM - revolutions per minute.
- SMC - soil moisture content.
- VOC - volatile organic compound.